I.O.S.

SWANSEA BAY (SKER) PROJECT
TOPIC REPORT : 4

A D HEATHERSHAW AND F D C HAMMOND

Tidal currents : Observed tidal and residual circulations and their response to meteorological conditions

Report No 92

1979

NATURAL ENVIRONMENT RESEARCH COUNCIL

INSTITUTE OF OCEANOGRAPHIC SCIENCES

INSTITUTE OF OCEANOGRAPHIC SCIENCES

Wormley, Godalming,
Surrey, GU8 5UB.
(0428 - 79 - 4141)

(Director: Dr. A.S. Laughton)

Bidston Observatory,
Birkenhead,
Merseyside, L43 7RA.
(051 - 653 - 8633)

(Assistant Director: Dr. D.E. Cartwright)

Crossway,
Taunton,
Somerset, TA1 2DW.
(0823 - 86211)

(Assistant Director: M.J. Tucker

On citing this report in a bibliography the reference should be followed by the words UNPUBLISHED MANUSCRIPT.

Institute of Oceanographic Sciences Report No 92/1979

Addendum

Page 68, add to Figure 8 caption:

The directions of the currents shown in (a) correspond to the peak flood tide and the phase of the given constituent. In (b) the figures in brackets correspond to mid-depth current measurements.

SWANSEA BAY (SKER) PROJECT

TOPIC REPORT : 4

A D HEATHERSHAW AND F D C HAMMOND

Tidal currents : Observed tidal and residual circulations and their response to meteorological conditions

Report No 92

1979

This project was supported financially by the Department of the Environment

Institute of Oceanographic Sciences
Crossway
Taunton
Somerset

1. INTRODUCTION

Sediment is moved by tidal currents and to a lesser extent by the oscillatory currents and mass transport effects due to surface gravity waves. The object of this report is to describe the tidal and residual current circulation patterns in Swansea Bay (see Figure 1) and in particular to determine the role they play in transporting sediment towards or away from the foreshore on the E side of the Bay. However a complete description of the current system in the area should include a consideration of wind driven currents, surge currents and density currents. Therefore the effects of meteorological forcing and salinity and temperature on the water circulation are also evaluated.

The tidal dynamics of Swansea Bay are essentially those of the Bristol Channel with flow patterns and magnitudes being influenced by bathymetry and coastline geometry. It is beyond the scope of this report to review in full the physical oceanography of the Bristol Channel and reference should therefore be made to the review articles by Cooper (1967), Pugh et al (1971/72) and NERC (1972). More detailed accounts of recent work are given in Heaps (1968), Abdullah et al (1973), Hamilton (1973), Bennett (1975) and Robinson (1978).

The area being studied is characterized by a high tidal range (9.5m) and maximum surface currents of the order of 1.5m s^{-1}. The bottom is gently sloping, the depth increasing over a distance of 15km in an offshore direction to only 25m below Chart Datum on the outer edge of the study area. The sediments are generally fine sands (100 - 200μm) interspersed with muds and silts.

2. THEORETICAL CONSIDERATIONS

2.1 Tidal dynamics

Tidal oscillations in the Bristol Channel are usually considered (eg Defant (1961); Proudman (1953) to be co-oscillations of the tides in the Celtic and Irish Seas. Thus in the Channel the tidal oscillations may be represented by standing wave solutions to the equations of motion leading to the times of High Water in the area being synchronous. However, co-tidal and co-range data (see Figure 2) show that in general this is not the case, except for an area on the N side of the Channel in the vicinity of Swansea and Carmarthen Bays. On the S shore of the Channel, between Hartland Point and Portishead there is a

progression in the times of HW, with HW at Portishead lagging that at Hartland Point by about 90 minutes. Therefore tidal oscillations in the Bristol Channel may be viewed as a mixture of standing and progressive wave components. The phase relationship between surface elevations and currents in each of these cases is different.

The earliest theoretical treatment of the tides in the Bristol Channel was carried out by G I Taylor in 1921. Noting that the breadth (b) and depth (h) of the channel varied linearly with distance (x) along its axis (see Figure 2), Taylor obtained a solution of the linearized equations of continuity and motion

$$\frac{\partial}{\partial x}(bh\hat{u}) = -b\frac{\partial \zeta}{\partial t}, \qquad (1)$$

$$\frac{\partial \hat{u}}{\partial t} = -g\frac{\partial \zeta}{\partial x}, \qquad (2)$$

where in this case $\hat{u}$ is the cross sectionally averaged flow at the particular harmonic which is being modelled, and

$$\left.\begin{aligned} b &= \frac{b_0}{x_0}.x, \\ h &= \frac{h_0}{x_0}.x. \end{aligned}\right] \qquad (3)$$

Here ζ is the height of the sea surface above its undisturbed level, g is the acceleration due to gravity and b_0 and h_0 are the breadth and depth a distance x_0 from the head of the Channel. Thus friction was neglected as were the non-linear terms in the equations of motion and continuity (see equations (1) and (2)). Additionally, Coriolis forces were not considered in (2). By a rearrangement of terms, Taylor obtained a solution for (2) of the form

$$\zeta = KJ_1\{2(kx)^{1/2}\}/(kx)^{1/2} \qquad (4)$$

where K is a constant, J_1 represents a Bessel function of the first order and the

wavenumber k is given by

$$k = \omega^2 x_0 / h_0 g , \qquad (5)$$

ω being the tidal frequency.

It is important to note that the solution (2) obtained by Taylor represents a standing wave with no net flow of energy into or out of the estuary and with the phase everywhere the same. However, while Taylor's work gave good agreement between predicted and observed amplitudes along the Channel it left unexplained the observed progression in the times of HW (see Figure 3).

As we have already seen, the immediate effect of neglecting friction is to make the times of HW everywhere the same. Grace (1936) using observed amplitude and phase relationships, estimated the effects of friction in terms of a friction coefficient. However Heaps (1968), in an analytical study of the tides in the Channel appears to have been the first to include friction in the equations of motion and to compare both amplitude and phase with tidal observations along the coasts. By numerically integrating the equations of continuity and motion Heaps obtained good agreement between the predicted and observed harmonic constants for the M_2 tidal elevations. Therefore friction should be considered as important in modifying the phase of the tide in the Channel. In many respects Heaps' (1968) results confirm an earlier finding of Hunt (1964) from a study of tidal oscillations in the Thames Estuary, that the effect of friction on the tidal oscillations in a wedge shaped estuary is to introduce a progression in the times of HW along the estuary, while maintaining the phase difference between currents and elevations as that of a standing wave. Hunt used the linearised equations of continuity and motion (1) and (2) with the addition of a frictional term. Thus (2) becomes

$$\frac{d\hat{u}}{dt} = -g\frac{d\zeta}{dx} - c\hat{u} , \qquad (6)$$

where C is a linear friction coefficient given by

$$C = \frac{8}{3\pi}\cdot\frac{C_0}{h}|\hat{u}_0| , \quad \hat{u} = \hat{u}_0(x)e^{i\omega t} , \qquad (7)$$

and C_0 is a quadratic friction coefficient of order .002 - .003. In this case the usual quadratic friction term $C_0\hat{u}|\hat{u}|/h$ has been linearized. Hunt (1964)

examined the solutions of (1) and (6) for various estuary configurations and obtained solutions for the elevation (ζ) and the current ($\hat{u}$) which are important in as much that they indicate a motion which resembles a standing wave with amplitude and phase varying slowly along the estuary and show clearly that there is a $\pi/2$ phase difference between the elevation and currents.

In contrast to this approach Bennett (1975) has more recently used a non-standing wave solution to examine tides in the Bristol Channel. Whereas the classical standing wave solutions are energy conserving with no energy dissipation, a non-standing wave solution permits an energy flux to be transmitted into the estuary. Thus by taking a solution to the linearized and frictionless equations of motion (1) and (3) of the form

$$\zeta = \left[\left\{ A_1 J_1 [2(kx)^{1/2}]/(kx)^{1/2} + A_2 Y_1 [2(kx)^{1/2}]/(kx)^{1/2} \right\} \cos \omega t + \left\{ A_3 J_1 [2(kx)^{1/2}]/(kx)^{1/2} + A_4 Y_1 [2(kx)^{1/2}]/(kx)^{1/2} \right\} \sin \omega t \right] \quad (8)$$

where J_1 and Y_1 are Bessel functions of the first and second kinds of order 1 and by matching the solution for ζ at two places Bennett was able to obtain the coefficients A_1, A_2, A_3 and A_4. Good agreement was obtained with the observed amplitudes and phases of the elevations between the calibration sections at Minehead and Worms Head. However, above Minehead and towards Newport the agreement was not so good. It is interesting to note however that Bennett's solution (8) represents a partly progressive and partly standing wave.

More recently Robinson (1978) has reverted to the use of a linearized and frictionless analytical model to study the effects of a barrage on the tides in the Bristol Channel and found that while the predicted elevation of the tides gives reasonable agreement with observation there is a considerable disparity between observed and predicted currents. This model can of course only reproduce a standing wave oscillation and is thus unable to reproduce the observed progression in times of HW along the Channel.

In many respects Robinson's work serves to highlight one of the major shortcomings of both analytical and numerical models; that is their poor predictive ability when the amplitudes of tidal streams and residual currents are considered. Consequently we are still heavily dependent upon observation.

Therefore, although the observed tides in the Channel (see Figure 2) exhibit both standing and progressive wave characteristics, theoretical

considerations, particularly those of Hunt (1964), lead us to believe that in this area the tides are correctly described by standing wave oscillations with the inclusion of friction leading to the observed progression in the times of HW but at the same time maintaining the correct phase relationship between the elevation and currents.

2.2 Meteorological forcing

Meteorological factors may affect the water circulation in two ways:

(a) directly by the application of wind stress to the sea surface, leading to a surface drift;

(b) indirectly from changes in sea level which may occur as a result of the wind piling up water against a coast or as a result of changes in atmospheric pressure (the 'inverted barometer' effect).

2.2.1 Wind driven currents

In the ocean, wind driven currents, or surface drifts, consist of two components. These are:

(a) a wind-induced shear current, and

(b) a wave-induced mass transport.

Since surface waves are nearly always present on the sea's surface, even for moderate wind speeds, it is likely that a contribution from (b) will always be present in the total drift.

The first detailed theoretical treatment of wind driven currents was that carried out by Ekman (1905). Since the results of Ekman's theory are referred to extensively in this report and used as the basis of order of magnitude comparisons, salient features of the theory have been summarised in Appendix A. The wave-induced mass transport effect however predates Ekman's theory quite considerably and was first predicted by Stokes in 1847. The contributions that each mechanism may make to the total drift current are now dealt with separately:

2.2.1.1 Ekman drift

Two factors emerge from Ekman's theory (see Appendix A) which are of some practical use in making a qualitative assessment of the response of the water column to meteorological forcing. These are:

(a) the depth of frictional influence given by

$$D = \pi\left(\frac{2N_z}{f}\right)^{1/2}, \qquad (9)$$

where N_z is the vertical eddy viscosity and f is the Coriolis parameter; and (b) the ratio of h/D where h is the water depth.

The depth of frictional influence (D) (see Appendix A for derivation) is that depth at which for most practical purposes the wind driven shear current has fallen to an insignificant level. The ratio h/D is important in determining the vertical structure of the wind driven current in various types of simple current systems which may be applied to the open ocean and to shallow coastal seas.

For values of $h/D > 1$, which approximates the infinite depth case (see Appendix A) the wind driven surface current flows at 45° to the right of the wind in the Northern Hemisphere, and with increasing depth rotates clockwise and decreases in amplitude until at a depth equal to D it is flowing in the opposite direction to the surface current and with strength $e^{-\pi}$ of its value at the surface. The vertical distribution of these currents is described by equations (A5) and is the well known Ekman spiral.

For values of $h/D < 1$ which approximates the finite depth case (see Appendix A) the current structure changes progressively as h/D decreases, the surface current decreasing in strength and becoming more nearly aligned with the wind for small values of h/D. The vertical distribution of these currents is described by equations (A8).

Values of the ratio h/D are shown in Table 1. These suggest that the depth of frictional influence does not become equal to the total water depth until a wind speed of 8 - 10 m s^{-1} is reached. However at wind speeds lower than this the depth of frictional influence (D) may still comprise a significant proportion of the total flow depth.

Estimates of the wind driven current in a shallow coastal sea (depth 20m) typical of Swansea Bay, have been calculated using Ekman's theory (equations A8) and are shown in Table 2 for wind speeds (W) up to 20m s^{-1}. The vertical eddy viscosity N_z was calculated using Thorade's (1914) relationship (equations A12 and A13) and then halved for the calculation in equations A8. This corresponds in practice to taking the depth mean value of a vertical distribution of N_z which varies linearly from a maximum value at the surface, given by equations A12 and A13, to zero at the sea-bed. This value was then combined

linearly with a tidal shear flow value of $N_z = 100\text{cm}^2\text{s}^{-1}$ (calculated from equation A14 in Appendix A) which corresponds to a tidal current of about 20cm s^{-1}.

2.2.1.2 Stokes Drift

The slow but continuous forward motion of the particles in a progressive water wave was first predicted by Stokes (1847). For small amplitude waves in an infinitely deep frictionless fluid Stokes showed that the water particles do in fact possess a steady second order drift velocity superimposed upon their orbital motion. This drift velocity is always in the direction of wave propagation, is known as the Stokes drift velocity and is given by

$$u_s(z) = k^2 a^2 e^{-2kz} c . \qquad (10)$$

Here k is the wave number given by $k = 2\pi/\lambda$ where λ is the wavelength, a the amplitude of the wave and c is its phase velocity given by

$$c^2 = g/k , \qquad (11)$$

where g is the acceleration due to gravity. At the surface $z = 0$ and the Stokes drift velocity is given by

$$u_s\big|_{z=0} = k^2 a^2 c . \qquad (12)$$

For progressive irrotational waves in a finite depth fluid we would expect the steady forward drift, at various depths, given by equation (10), to be modified on the grounds of continuity to give a near-bottom return flow. However, experimental observations have shown that the situation is considerably more complex than this due to the irrotationality assumption involved in deriving equation (10). By including the effects of viscosity in a laminar flow model (see Appendix B) Longuet-Higgins (1953) obtained better agreement with the observations. In particular in the interior of the fluid Longuet-Higgins obtained a solution for the drift velocity of the form given in equation B1 of Appendix B. This theory also predicts a drift velocity near the bed given by

$$u_s\big|_{z=d} = \frac{5}{4} \frac{a^2 \sigma k}{2\nu k^2 h} \qquad (13)$$

and furthermore, following observations by Russell and Osario (1957), Longuet-Higgins (1957) has shown that this laminar case (equation 13) may be extended to the case of a turbulent boundary layer in which the coefficient of eddy viscosity is independent of depth.

Table 3 gives values of the wave-induced Stokes drift velocities at different depths for a wave period and heights which are typical of Swansea Bay. These values have been calculated using equation (B1), and may be compared with the wind induced shear currents shown in Table 2. From Table 3 it is apparent that the Stokes drift will be in a forward direction, ie the direction of wave propogation at the surface and at the sea-bed, with a return flow at mid-depths. In the event of an extreme wave height of 2m (only exceeded for about 20% of the year - see Fortnum and Hardcastle (1979)) the drift velocities may be of the order 2 - 4cm s^{-1}. However, a wave height of 1m is more representative and this would give drift velocities of up to 1cm s^{-1} throughout the water column which we would consider typical for the area. These would be about 10% of the largest wind driven currents (see Table 2).

Strictly speaking estimates of u_s from the interior of the fluid, obtained from equation (B1), are only valid for wave amplitudes (a) much less than the thickness of the boundary layer under the wave. Since the latter is likely to be of the order of 10cm and less, this condition will hardly ever be fulfilled in practice. This may in turn explain why the drift velocities given in Table 3 do not appear to exhibit continuity, particularly at large wave heights.

2.2.2 Surge currents

It is beyond the scope of this report to consider in full the very extensive work which has been carried out on surge generation and propagation. An excellent review may be found in Heaps (1967) with recent theoretical developments described for example by Davies and Flather (1977).

Strictly speaking the term 'storm surge' applies to a raising or lowering of sea level produced by the wind and by changes in the atmospheric pressure over the sea associated with a storm. The precise combination of meteorological conditions which leads to the occurence of storm surges in British waters have been described by Lennon (1963) and Heaps (1965) and are reviewed in Heaps (1967). Suffice it to say that in general when a depression moves over a sea area there is usually a rise in sea level followed by a fall. However a change in sea level at any one location may be considered as due partly to changes in atmospheric pressure and partly due to the action of the wind on the sea's surface.

The change in sea level Δz due to a change in pressure is given by the statical law

$$\Delta z = \frac{\Delta p_a}{\rho g} \quad , \tag{14}$$

where Δp_a is the increase in atmospheric pressure p_a over and above some ambient level, ρ the fluid density and g the acceleration due to gravity. A decrease in atmospheric pressure of one millibar leads to an increase in sea level of approximately one centimetre (this effect being known as the "inverted barometer effect").

Unless a depression is particularly small, deep and fast moving, changes in sea level due to the pressure effect (equation 14) are generally small when compared with those changes which are brought about by action of the wind on the sea's surface. We have shown already from Ekman's theory in Section 2.2.1.1 and Appendix A of this report that in the northern hemisphere, dependent upon the ratio of the water depth h to the depth of frictional influence D, this leads to a wind driven shear current in the general direction of the wind, or to its right in deeper water. Where the motion of the water thus established is intercepted by a coastline this may lead to a piling up of water against the coast which for an onshore wind will lead to a positive surge or set-up, and which for an offshore wind will lead to a negative surge or set-down.

The sea surface gradient which is thus established by an applied wind stress will set up a horizontal pressure gradient in the water column leading to a combined current system consisting of the onshore wind driven flow at the surface, and a compensatory or return flow at or near the sea bed.

To calculate the strength of these currents it is necessary to know the gradient of the sea surface which is set up in the direction of the wind. This is given (see, for example, Neumann and Pierson (1966)) by

$$\beta = \frac{m\tau}{\rho g h} \tag{15}$$

where β is the slope of the sea surface, m is a coefficient which decreases with increasing depth from the value 3/2 to 1 and τ is the wind stress. Equation (15) is Ekman's equation for a stationary slope in an enclosed sea and is the simplest and most basic equation for storm surge prediction.

If the depth of water is sufficiently great and dependent upon the direction of the wind relative to the coast, a layer of frictional influence, analogous

to that at the sea-surface, may form near the sea-bed. The thickness of this layer is given by D^* (see Appendix A). The current system may therefore consist of up to three components. For $h > D + D^*$ Ekman's elementary current system is obtained consisting of a surface current, a deep or geostrophic current and a bottom current. For a surface current, consisting of a pure drift current, the flow is described by equation (A5) and for a pure slope current in the bottom layer by equation (A10). Between these layers a geostrophic current given by

$$u_g \simeq \frac{\tau}{f\rho h} \qquad (16)$$

will be established.

Since D^* is the same order as D and we have already shown (see Table 2) that D, for wind speeds of the order 20m s^{-1}, is about 5 times larger than the mean water depth in Swansea Bay, it seems likely that with prevailing SW winds, the resultant current system would consist simply of a wind driven onshore component at the surface, and possibly a bottom return flow. We have already estimated the magnitude of the surface current from equations (A8)(see Table 2) and the slope current has been estimated (see Table 4) for corresponding wind speeds using equation (A10).

These two sets of values have been included here as order of magnitude estimates <u>only</u> and should not be combined since there are no constraints on continuity implicit in the two derivations given in equations (A8) and (A10).

There are very few observations of current surges in shallow coastal waters to compare with the predictions given in Table 4. However Howarth (1975) has observed current surges in the St George's Channel, of about 20 - 30cm s^{-1} in a water depth of approximately 90m. One might therefore expect surge currents to be of a larger magnitude in shallow coastal waters. Actual measurements of currents which occurred during a storm surge in Swansea Bay are described in a later section of this report.

From Tables 2 and 4 we see that the wind driven currents at extreme wind speeds of 20m s^{-1} are of the order 12cm s^{-1} whereas the slope currents, which would result from a wind induced set-up, are about a half of this and of the order of 6cm s^{-1}. Since no constraints on continuity have been applied these two estimates are not necessarily equal.

To summarise this section of the report therefore, we would conclude on a theoretical basis that meteorological forcing, for typical conditions of wind speed, wave height and wave period and in a water depth of 20m, is likely to

make the following contributions to the tidal and tidally-induced residual circulation in Swansea Bay:

(a) wind driven currents of order 10cm s^{-1}

(b) slope (or surge) currents of order 5cm s^{-1}

(c) Stokes Drift of order 1cm s^{-1}

3. METHODS AND OBSERVATIONS

Between October 1975 and November 1977 the Institute carried out recording current meter observations at a number of locations in the Swansea Bay area (see Figure 3). These were chosen on the basis that they would provide as much useful information on the water circulation pattern as possible and ultimately enable some conclusions to be drawn concerning the directions and rates of sediment transport. Since we have been concerned here with sediment transport processes preference was given to making synoptic sets of observations of the near bottom velocity field. However, where the depth of water was sufficiently great, observations were also made at about the mean mid-water depth.

The bulk of the measurements described here were made with Plessey M021 recording current meters (see Figure 4) mounted on conventional U-shape moorings (see Figure 5) although a number of observations were made with Aanderaa RCM4 current meters. Early attempts to make near bottom current measurements with current meters mounted in frames were not successful.

At most locations bottom current measurements were made at a height of 2m above the sea bed with mid-depth measurements being made at 10 or 12m above the sea bed. Details of the locations, instrument types, elevations and record dates and durations are given in Table 5.

The general strategy during these measurements was to operate one current meter mooring, in a central position, on a long term basis (as a 'control') and to make synoptic sets of observations at the other locations under 'summer' and 'winter' conditions. In this way it was hoped to be able to monitor transient phenomena (eg storm surges) as well as being able to describe the circulation under relatively quiescent conditions. Thus observations were made at Station A over very nearly the full 2-year period, the meter being changed every 2 months, and observations were also made for up to 3 periods of approximately 2 months at Stations B - K. In all cases current speed and direction were recorded every 10 minutes.

Approximately 39,620 hours of useful recording current meter data have been

collected and analysed and this, together with meteorological data collected over the 2-year period (by the Meteorological Office), forms the basis of this report.

4. TIDAL CURRENTS

4.1 Harmonic analysis

In order to examine the tidal dynamics of the Swansea Bay area, in particular the phase relationship between currents and elevation, current meter records were harmonically analysed using the IOS Bidston computer program TIRA (Tidal Institute Recursive Analysis). This program, which employs a least squares regression technique, was used to analyse 29 day data sets, the optimum length for separating the tidal constituents (see Doodson, 1928), to produce information on the amplitude and phase of the tidal constituents in current meter records.

A total of 32 records from Stns A - K have been analysed, using TIRA, for 27 major plus 8 related constituents (see Table 6). The related constituents are those that cannot be separated in a 29 day record. These are listed in Table 7. Insufficient tidal data were available from Swansea to use measured ratios for the related constituents and we have instead used values taken from the equilibrium tide (see Doodson, 1928).

Edited current meter records with timing adjusted to GMT were corrected for any timing errors. These in general were of the order $\pm$ 5 - $\pm$ 15 s day^{-1} and therefore close to the manufacturer's stated tolerance of $\pm$ 10 s day^{-1} (for the Plessey MO21 meter). However some large values did occur and these are indicated, together with timing errors for all the current meter records, in Table 5. For records being analysed with TIRA, timing error corrections were made by a linear interpolation procedure which amounts to stretching or contracting the record to fit the optimum 29 day period.

The results of the harmonic analyses of the current meter data are shown in Tables 8 - 10. At Stn A (see Figure 3), the long term mooring where some 15 records, suitable for analysis with TIRA were obtained, it has been possible to examine the variability of the amplitude and phase estimates. Thus in Tables 8 and 9 the means (μ), standard deviations (σ) and standard errors ($\sigma/N^{\frac{1}{2}}$) of the amplitude and phase values are given for the principal tidal constituents in the resolved components U and V of the currents. At Stns B - K where fewer records were available at each Staion, the amplitude and phase values for the

principal semi-diurnal constituents (M_2 and S_2) only are given. These results are given in Table 10.

The amplitudes and phases of the same constituents in the elevations at Swansea are also shown in Table 11. These were obtained from an analysis of 1 year's tidal records (carried out by IOS Bidston).

Comparisons of the amplitudes and phases of the M_2 tidal constituents, shown in Tables 8 - 11, indicate an 80 - 90° phase difference between elevations and currents which is the required relationship for a standing wave tidal oscillation.

4.2 Rotary analysis

Current meter data have been used to construct tidal ellipses for the constituents of interest using a rotary analysis method (Gonella, 1972; Godin, 1972). This method is described in full in Appendix C.

Current meter records, of an optimum 29 days' duration and corrected for timing errors, were first resolved into east-west (U) and north-south (V) components and then harmonically analysed using TIRA for 8 related and 27 given constituents (see Table 7) and using the equilibrium tide for the related constituents (this assumes that currents behave in the same way as elevations - see Robinson, 1979 for discussion of this problem). From the harmonic analyses of the U and V time series we have obtained sets of amplitudes H_u and H_v and phases g_u and g_v and from this information constructed the tidal ellipses using the method outlined in Appendix C.

Records from Stations A - K have been routinely analysed in this manner and typical tidal ellipse characteristics from Station A are shown in Figures 6 and 7. These show the semi- and quarter-diurnal constituents M_2, S_2, N_2 and K_2 and M_4 and MS_4 respectively, in simultaneous records of the current at 2 m and 10 m above the sea-bed at Station A. These diagrams give a good indication of the degree of rectilinearity of the currents with M_2 ellipticities, that is the ratio b/a expressed as a percentage, being of the order of 10% and less. Figure 8 summises the M_2 tidal ellipse data for the mid-depth and near-bottom currents in the area. In particular the ellipse orientation, tidal current phase and ellipticities (see Appendix C) are shown. It is interesting to note that the ellipticity of the near bottom currents has been found to be larger than that at mid-depth and that the sense of rotation of the currents is different. In fact over the area as a whole we have found that the mid-depth ellipses rotate clockwise whereas the near bottom ellipses rotate

anticlockwise. This feature has been observed consistently at Station A, in the long term current measurements, and over the area as a whole.

4.3 Non-linear effects

From the tidal ellipse data it has been possible to map out the distributions of the M_2 and S_2 bottom currents in the area and these are shown in Figure 9. Broadly speaking the dynamics of the M_2 and S_2 currents are similar with ratio S_2/M_2 not varying by more than about 10% from a mean value for the area of .39 which compares with a figure of .36 for the same ratio in the elevations (see Table 11). The M_2 and S_2 contours do, however, illustrate the horizontal non-uniformity of the flow. From the ellipse orientation and amplitude data shown in Figures 8 and 9 we can see that currents flowing into and out of the area undergo considerable acceleration and deceleration on the W and E sides of the Bay respectively. These spatial accelerations lead to important non-linear effects in the currents which in turn have special implications for sediment transport.

The depth integrated equations of motion and continuity, including the effects of friction and Coriolis forces may be written (see Heaps, 1978) as

$$\left.\begin{aligned} \frac{\partial \hat{u}}{\partial t} + \hat{u}\frac{\partial \hat{u}}{\partial x} + \hat{v}\frac{\partial \hat{u}}{\partial y} - f\hat{v} &= -g\frac{\partial \zeta}{\partial x} - c_0\frac{\hat{u}(\hat{u}^2+\hat{v}^2)^{1/2}}{\lambda+\zeta} \\ &\quad + \nu_H\left(\frac{\partial^2 \hat{u}}{\partial x^2} + \frac{\partial^2 \hat{u}}{\partial y^2}\right) \\ \frac{\partial \hat{v}}{\partial t} + \hat{u}\frac{\partial \hat{v}}{\partial x} + \hat{v}\frac{\partial \hat{v}}{\partial y} + f\hat{u} &= -g\frac{\partial \zeta}{\partial y} - c_0\frac{\hat{v}(\hat{u}^2+\hat{v}^2)^{1/2}}{\lambda+\zeta} \\ &\quad + \nu_H\left(\frac{\partial^2 \hat{v}}{\partial x^2} + \frac{\partial^2 \hat{v}}{\partial y^2}\right) \end{aligned}\right\} \qquad (17)$$

and

$$\frac{\partial \zeta}{\partial t} + \frac{\partial}{\partial x}\{(\lambda+\zeta)\hat{u}\} + \frac{\partial}{\partial y}\{(\lambda+\zeta)\hat{v}\} = 0 . \qquad (18)$$

$\hat{u}$ and $\hat{v}$ are now depth mean currents and in equations (17) and (18) wind stress and atmospheric pressure gradient effects have been neglected.

It is a relatively simple matter to show that the equations of motion and continuity contain three sets of non-linear terms which generate tidal harmonics, M_4, M_6, M_8, ...etc in the currents. These are

the advective terms	$\hat{u}\frac{\partial \hat{u}}{\partial x}$	etc	
the frictional terms	$C_0 \frac{\hat{u}(\hat{u}^2+\hat{v}^2)^{1/2}}{\lambda+\zeta}$	etc	(19)
the shallow water terms	$\frac{\partial}{\partial x}(\lambda+\zeta)\hat{u}$	etc	

In particular in shallow shelf seas the M_4 tidal component is likely to be large and to play an important role in determining the direction of sediment movement (see Pingree and Griffiths, 1979; Hunter, 1979).

An order of magnitude analysis of these terms, assuming a purely one dimensional flow on the E side of the Bay (a region showing marked spatial accelerations) shows (see Table 12) that the friction term is likely to be the most effective non-linear term in the equations of motion. These calculations were based on the co-tidal and co-range data shown in Figure 2 and the M_2 and S_2 tidal current amplitudes shown in Figure 9.

The distribution of M_4 tidal currents (Figure 10) shows that these are largest in areas where the advective or spatial acceleration terms and the friction terms are likely to be greatest. In general, Figure 10 shows that the M_4/M_2 ratio in the currents increases to a maximum of about .15 in the shallower water nearer the coast. This is about an order of magnitude larger than the same ratio in the elevations which is about .017 (see Table 11). These differences serve to illustrate the importance of the non-linear terms in the flow of tidal currents near coasts, particularly in bays and in the vicinity of headlands.

From the tidal ellipse information we may also examine the distribution of currents over the Neap-Spring cycle. However, since sediment transport varies at high transport rates as u_*^3 and since tidal mixing varies as u_0^3/h (see Robinson, 1979), where u_* is the friction velocity and u_0 the tidal stream amplitude, it is instructive to look at the distributions of the currents as

$$(M_2 - S_2)^3 \quad \text{Neaps} \qquad (20)$$

$$(M_2 + S_2)^3 \quad \text{Springs} \qquad (21)$$

In general, the M_2 and S_2 tidal ellipses have very nearly the same orientations and we therefore carry out an arithmetic addition of the M_2 and S_2 tidal currents. Figure 11 shows that at any one location in the Bay we may expect tidal mixing or sediment transport to undergo an order of magnitude variation over the Neap-Spring cycle. Furthermore, since the dissipation of tidal energy by friction is proportional to u_*^3, we may expect the dissipation of tidal energy to undergo a similar variation.

5. RESIDUAL CURRENTS

The tidally induced Lagrangian residual velocity, $\bar{u}_L$ will consist of two components given (see Longuet-Higgins, 1969) by

$$\bar{u}_L = \bar{u} + u_s \qquad (22)$$

where $\bar{u}$ is the Eulerian residual, ie the residual current which we measure at a fixed point, and u_s the Stokes velocity given by

$$u_s = \overline{\int u\,dt \cdot \frac{\partial u}{\partial x}}\ , \qquad (23)$$

where the integration is taken over a tidal period and the overbar denotes a time average over one or more tidal cycles.

Longuet-Higgins (1969) has shown that this term is of order $\bar{u}^2(\tau/\ell)$ where τ and ℓ are time and length scales associated with the current. By taking the time and distance between co-tidal lines in Figure 2 it is possible to estimate τ/ℓ in the area of interest. Taking τ = 600s and ℓ = 15km gives $O(\tau/\ell) \simeq .0004\text{s cm}^{-1}$. Thus with $u \simeq 50$ cm s^{-1} we have $O(u_s) \simeq .01\text{cm s}^{-1}$ which as we shall see is generally much smaller than the measured Eularian residuals. This result is confirmed by investigations of the residual circulation in this area using numerical models (Owen, 1979) which show little or no difference between the Eularian and Lagrangian residuals.

5.1 Residual circulation

To obtain the Eularian residuals we have applied a digital filter to the current meter data to eliminate the tidal currents. Doodson's (see, for example Groves, 1955 and Appendix D of this report) X_0 filter was chosen for this purpose. Similarly to Hill and Ramster (1972) we have found (see Figures

12 and 13) that this yields similar residual flow estimates to those obtained from a 24hr 50min average. However we have used Doodson's X_0 filter in preference since its tidal suppression characteristics are well determined (see Pugh and Vassie, 1976). Therefore vector time series of current speed and direction were resolved into E and N flowing components, u and v respectively, and the X_0 filter applied to hourly arithmetic averages of u and v to yield filtered estimates every 24 hours. The component values were combined to yield daily residual flow estimates centered on 1200 GMT each day.

The magnitudes and directions of the measured residuals are summarised in Figure 14 and Tables 13 and 14. It is emphasised that these are Eularian residuals and that they relate only to the net flow of water through the point at which the current was measured. Tables 13 and 14 show that the measured residuals vary from about 8cm s^{-1} offshore to about .5cm s^{-1} close inshore.

Four interesting features emerge from the residual circulation pattern shown in Figure 14. These are:

(a) the area of low residual currents in the area between Port Talbot and the river Neath;

(b) the area of divergence in the residual velocity field between Port Talbot and Sker Point;

(c) the presence of a large clockwise eddy in the mean circulation over the Scarweather Sands with near bottom convergence and mid-depth divergence to the N and S of the Bank; and

(d) the reversal with depth of the mean circulation near Mumbles Head which, as we shall see later, is possibly related to the presence of density currents.

All four features have important implications for sediment transport in the area. In particular the large eddy, having a horizontal extent of about 10km and occuring in a region of high tidal energy, may be responsible for maintaining the Scarweather Sands and related Banks in their present positions and is therefore an area in which relatively coarse material accumulates. However the area of divergence off Port Talbot is an area of low tidal energy (see Figure 9) and low net transport and therefore an area in which fine material is likely to accumulate.

While the observations shown in Figure 14 confirm the presence of the gross features predicted by numerical models of the residual circulation in this area (see Owen, 1979), there are important differences in both the magnitude and direction of observed and predicted residuals at some locations.

Furthermore, depth averaged numerical models are unable to account for the vertical structure of the mean currents. Figure 14 shows quite clearly that at some locations the near bottom residuals can be in quite different directions to those at the mid-depth level. In fact at Station A, the long term mooring, they are in almost completely opposite directions. This behaviour has been consistently observed in the measurements taken at this location (see Table 13 and Figure 15) over the 2-year period with different instruments and is therefore considered to be a genuine feature of the flow. Indeed, the only occasions when this behaviour has not been observed seems to be during periods of strong SW winds or storm surge activity. This aspect of the circulation is discussed in a later section of this report.

As previously mentioned, the observed veering in the mean circulation at Stations A and D (N and S of the Scarweather Sands) occurs as a result of the large eddy shown in Figure 14. Such a feature requires a source of vorticity (Tee, 1976), and Pingree (1978) has recently shown that tidal stream curvature past headlands is capable of generating the required vorticity, and furthermore by comparisons with purely circular motion, in which the effects of the earth's rotation and bottom friction are included, leads to convergence and divergence effects near the sea bed and at the surface. The current meter observations from Swansea Bay support this finding, but this aspect of the work is considered beyond the scope of this report and is not discussed further.

5.2 Variability in measured residual currents

Good estimates of the residual current may be obtained (see Hill and Ramster, 1972; Howarth, 1975) by applying 24hr 50min running means to the 10 minute values of current speed and direction to produce smoothed progressive vector plots. Examples are shown in Figures 15 and 16 and E1 to E11 inclusive. However, it is apparent from some of these measurements that there is considerable variability in both the strength and the direction of the residual flow (for example the residual flow at Stn B shown in Figure E2.2 of Appendix E). Under these circumstances we need to consider the significance of the residual flow speed and direction estimates. It is obvious that a greater reliability may be placed on residual currents derived in this manner when the residual flow is consistently in one direction and large, for example Station E shown in Figures E5.1 - E5.3, where the residual flow is of the order 8cm s^{-1}. However where the residuals are low, eg 1cm s^{-1} and less, we may expect the uncertainty in direction and speed to be greater. In this study we have

examined the variability of residual currents as follows: daily estimates of the residual current were calculated using Doodson's X_0 filter and the variability in the direction and speed of the residual flow estimates examined separately.

5.2.1 Variability in direction

We have used a steadiness factor ($\mathcal{B}$) (for discussions see Ramster et al, 1978) to evaluate the variability of the residual currents illustrated in Figures 15 and 16 and Figures E1 - E11. The steadiness factor is simply the ratio of the vector mean to the scalar mean, expressed as a percentage, in a progressive vector plot. Expressed mathematically

$$\mathcal{B} = \frac{|\bar{\underset{\sim}{u}}|}{\overline{|\underset{\sim}{u}|}} \cdot 100\ \%, \qquad (24)$$

where $\bar{\underset{\sim}{u}}$ is the vector mean residual current.

Values of $\mathcal{B}$ are given for each residual flow measurement shown in Tables 13 and 14. Examples of typical progressive vector plots with their associated $\mathcal{B}$ values are shown in Figures E1 - E11. These show that where the residual flow is always in the same direction, without deviation, $|\bar{\underset{\sim}{u}}| = \overline{|\underset{\sim}{u}|}$ and $\mathcal{B}$ = 100%. However where the direction varies the value of $\mathcal{B}$ will decrease and in this case less confidence can be placed on the direction estimates.

5.2.2 Variability in speed

This has been assessed by examining the resolved components of the residual currents and expressing the variability in terms of the standard errors

$$\sigma_{\langle\bar{u}\rangle} = \frac{\sigma_{\bar{u}}}{N^{1/2}} \quad \text{and} \quad \sigma_{\langle\bar{v}\rangle} = \frac{\sigma_{\bar{v}}}{N^{1/2}} \qquad (25)$$

of the north-south east-west components of flow, where N is the number of independent samples entering into the overall mean for a record. Values of $\sigma_{\langle\bar{u}\rangle}$ and $\sigma_{\langle\bar{v}\rangle}$ are tabulated in Table 15 and show clearly that less confidence can be placed on the low residual flow estimates (eg Stations B and G) where the standard errors (25) may be as much as 50% of the mean. The brackets $\langle\ \rangle$ indicate the means of the N daily mean residual flow estimates in each estimate of $\bar{u}$ or $\bar{v}$.

Tables 13, 14 and 15 may be used to estimate the variability in the mean circulation pattern which is summarised in Figure 14. From these data it is apparent that the tidally induced residuals off headlands and in the vicinity of

the offshore banks (eg Stations A, C, D, E and F) are fairly consistent features of the mean circulation, whereas close inshore, for example Stations B and G, there is likely to be considerable variability in both the speed and the direction of the residual flow estimates (see Figures E2.2 and E7.1 for Stations B and G, much of which may be due to meteorological effects and/or the effect of density currents (see later).

6. METEOROLOGICAL FORCING

As mentioned previously in this report the water circulation in shallow coastal waters is likely to be influenced by meteorological forcing, that is by the action of the wind on the sea's surface and by changes in atmospheric pressure.

The information that may be gained about these motions from shallow water current measurements is ostensibly limited by the uncertain response of conventional rotor-vane current meters to surface wave activity (see for example Hammond and Collins, 1979). However we will show later that this is not as serious a problem as it might appear at first sight, and that it is possible to make a number of general deductions from observation and theory which indicate how the mean circulation in Swansea Bay might vary with differing meteorological inputs.

As we have already seen in Section 2 the action of a wind blowing towards a coast across shallow water is to pile up water against the coast (wind set-up). This will set up horizontal pressure gradients leading to a seaward flowing or slope current at or near the sea-bed which, dependent upon the depth and the wind speed, will be in some kind of geostrophic balance (see Appendix A). In the case of Swansea Bay, prevailing winds are from the SW and we would thus anticipate a wind set-up effect during these periods. It is possible to determine the order of magnitude of the components in the resulting current system although, as previously noted (see Appendix A), precise estimates are made difficult by the uncertain nature of the eddy viscosity coefficient (N_z) in the wind mixed surface layer and in the tidal current. Using Ekman's theory (described in Neumann and Pierson, 1966) we have already estimated the wind driven surface currents and the slope currents for wind speeds of up to an extreme value of 20 m s^{-1}.(This value was exceeded during a storm surge in November 1977.) These results are summarised in Tables 2 and 4 and show that for moderate wind speeds (about 10 m s^{-1}) the shoreward flowing surface currents are likely to be of order 10 cm s^{-1}, with predicted slope currents of about

5 cm s^{-1}. Clearly no attempt has been made here to preserve continuity since this would require precise specification of the bathymetry and coastline geometry and such calculations are beyond the scope of this report. However the estimates do enable an order of magnitude comparison to be made between the current system induced by the wind and the tidally induced residual currents. This shows, for example, that for an extreme wind speed of 20 m s^{-1} the current system consists almost entirely of a shoreward flowing current of the order of 12 cm s^{-1} (see Table 2) which must turn along the coast at the shore to maintain continuity. This estimate gives a reasonable upper bound to the effect of meteorological forcing.

We have already seen that in a general way we may examine the effect of an applied wind stress at the sea-surface in terms of the ratio of the water depth (h) to the thickness of the layer of frictional influence (D) which, notionally at least, is that depth below which the wind has little or no effect. D may be calculated from Ekman's theory. Table 1 shows how this ratio varies with wind speed (N_z varying with wind speed also) and that for a water depth (h) of 20 m (typical of the centre of the Bay) D becomes equal to h at a wind speed between 8 and 10 m s^{-1} and that above this range of values the ratio h/D falls off rapidly indicating that the wind's effect is increased throughout the water column.

6.1 Storm surge of 11 November 1977

Observations show that the situation may be considerably more complex than that which has been described previously. During 1977 it was possible to make current measurements during a particularly severe storm surge which occurred on 11 November 1977. Daily filtered residual flow estimates, obtained using Doodson's X_0 filter, have been compared with daily mean wind speeds, residual tidal elevations and atmospheric pressure data. Figure 17 shows a 90 day set of these variables, wind speed ($\bar{W}$) having been plotted as $\bar{W}|\bar{W}|$ to parameterize wind stress. Current measurements and wind speed data have been resolved into a frame of reference (see Figure 18) giving alongshore and onshore-offshore components of the residual current and daily mean wind speed $\bar{u}_x$, $\bar{u}_y$, $\bar{W}_x$ and $\bar{W}_y$ respectively. The storm surge of 11 November 1977 is clearly indicated in Figure 17. This followed the usual pattern for surges on the W coast of the British Isles (see Graff, 1978) leading to a 1.4 m surge being recorded at Port Talbot. Figure 17 shows that during the storm surge and for the 10 days or so preceding it there is a progressive change in the residual flow pattern

culminating in a peak residual flow of the order of 10 cm s^{-1}, at 2 m above the sea-bed, which is nearly three times larger than the quiescent flow value (see Table 13). The peak occurs about one day later than the surge.

The effect of the storm surge is perhaps best illustrated in the progressive vector diagrams for this period which are shown in Figures 19 and 20 and which show a pronounced change in the direction of the residual flow, at both depths, at the time of the surge. The result is unusual in as much that the flow in this new direction persists for some time after the surge. However we should note that although the wind from the SW gradually diminished after the surge there was a relatively prolonged period of strong NW winds following it, and we will show later that it is these winds have the most pronounced effect on the circulation.

6.2 Regression analysis

The data set shown in Figure 17 was subjected to a multi-regression analysis, the results of which are summarised in Table 16. This has shown that the only significant correlation over the entire period occurs between the residual elevations ($\bar{\zeta}_R$) and atmospheric pressure ($\bar{P}_R$) which were significantly correlated at the 5% level with a negative correlation coefficient of -.74. Figure 17 illustrates this effect (the "inverted barometer effect") clearly, with the observed tides being about .2 m higher than predicted at times of low pressure and about .2 m lower at times of high pressure. It is also worth noting in Table 16 and Figure 17 the high degree of correlation which exists between the residual currents at different depths.

During periods of strong SW winds the "inverted barometer effect" is likely to be complicated by the effects of wind set-up and Figure 17 does indeed show that during storm surge there is a much less clear correlation with atmospheric pressure and in fact during the 2 - 4 days following the surge the observed tides were lower than predicted even though the atmospheric pressure was low. This is due, we believe, to a wind induced set-down as a result of the prolonged period of NW winds following the surge (see Figure 17). In fact the residual elevations shown in Figure 17 indicate that a period of wind set-up is followed very rapidly by a period of set-down which appears to generate the large residual currents of order 5 - 10 cm s^{-1}. Multi-regression analysis on the last 18 days' data (day 60 onwards) isolates this effect. These results are summarised in Table 17 and show significant negative correlations between the residual currents and the wind stress and residual elevations. The presence of the negative

correlations in Table 17 would suggest that the residual circulation in Swansea Bay is influenced by wind induced set-up or set-down, but that following the storm surge of November 1977 the prolonged period of NW winds lead to a set-down in the head of the Bay which in turn generated the strong shoreward flowing residuals shown in Figures 19 and 20.

If this is the case the observed residual currents are in reasonable agreement with the theoretical predictions for slope currents described previously in this report (see Table 4) and in Appendix A.

It is worth noting that no significant correlations were found between the residual currents and wave height which was included as an independent variable in the multi-regression analysis (see Tables 16 and 17). However this does not exclude entirely the possibility of waves having influenced the current measurements.

7. SALINITY AND TEMPERATURE

7.1 Surface salinity distribution measurements

Surface salinity (data supplied by the Welsh National Water Development Authority) (see Figure 21), indicate that there are appreciable horizontal gradients of salinity (see Figures 22 and 23) arising from the freshwater discharges into the Bay and these gradients persist throughout the year. Furthermore, the summer and winter patterns are consistent with the seasonal variations in the outer Channel and Celtic Sea reported by Bowden (1955) and Hamilton (1973). These show an intrusion of the more saline and oceanic water into the Channel during the winter possibly as a result of an increase in the wind driven currents. In fact the 33‰ isohaline is almost completely absent from the summer distributions shown in Figure 22 but appears prominently in the winter pattern shown in Figure 23.

It is also apparent from the salinity and temperature data that there is considerable vertical stratification at the head of the Bay which persists throughout the tidal cycle (maximum temperature differences between surface and bottom being of the order .5°C). The salinity data in Figure 24 shows that even at Station A where the peak mid-depth tidal currents are of the order 50 cm s^{-1} there is still evidence to suggest that weak vertical stratification persists over the tidal cycle.

7.2 Density currents

On the basis of the salinity distributions shown in Figures 22, 23 and 24, we would expect density currents to play some part in the non-tidal circulation of the Bay. To estimate their effect we have used the analytical solution obtained by Heaps (1972) to investigate density currents in Liverpool Bay, and later by Hamilton (1973) to study the circulation in the Bristol Channel. Full details of these calculations are given in Appendix F.

In order to calculate the density currents, it is necessary to know:
(a) the isopycnal (lines of constant density) spacing;
(b) the freshwater discharges into the Bay.
Using the tidally and depth averaged data from Stations A, B and G (see Figure 24) it is possible to estimate the isopycnal spacing and their approximate orientation. Figure 25 shows that these are orientated towards the head of the Bay, that is towards the source of the freshwater discharge. However, we should note that these conditions do not appear to entirely agree with those implicit in the solution of the dynamical equations given by Heaps, which requires that the isopycnals be parallel to the coast and that there be no lateral constraints on the resulting flow. However, despite this reservation, we feel that the isopycnal spacing gives a representative estimate of the density currents flowing on section $X_1 X_2$ in Figures 25 and 26.

The solution of the dynamical equations for a steady state (that is neglecting tides and all other variations with time), and now taking u and v to be the density current components, gives (see Appendix F)

$$u = g\frac{(h+\zeta)}{f}\frac{1}{\rho}\frac{\partial \rho}{\partial x}.F_1 + \frac{fq}{C}.F_2 \qquad (26)$$

$$v = g\frac{(h+\zeta)}{f}\frac{1}{\rho}\frac{\partial \rho}{\partial x}.F_3 + \frac{fq}{C}.F_4 \; . \qquad (27)$$

F_1, F_2, F_3 and F_4 are all functions of depth z, total depth h, the Coriolis parameter f, eddy viscosity N_z and friction coefficient C as given by Heaps (1972) and shown in Appendix C. Here u and v are defined in a left handed system of co-ordinates with z positive downwards (see Figures 25 and 26).

Equations (26) and (27) thus contain two terms which influence the velocity field; these are $\frac{1}{\rho}\frac{\partial \rho}{\partial x}$ which represents the effect of the modified density field on the nearshore velocity field, and $\frac{fq}{C}$ which represents the direct effect

of the freshwater discharges on the nearshore velocity field.

$1/\rho . (\partial\rho/\partial x)$ may be evaluated from the isopycnal spacing shown in Figure 25. q is evaluated by dividing the freshwater discharge rate to the Bay by a representative length of coastline. The bulk of the discharge from all the rivers between Mumbles Head and Sker Point (see Stoner, 1977) is provided by the Rivers Tawe, Neath and Afan which together discharge about 30 $m^3\ s^{-1}$ over a 20 km length of coastline. In Appendix F it is shown that q is small and of the order 10^{-2} cm s^{-1}, a value similar to that obtained by Heaps (1972) for Liverpool Bay.

In order to evaluate u and v from equations (26) and (27) it is necessary to parameterize the variations of the eddy viscosity N_z along the section shown in Figures 25 and 26. The procedure adopted by Heaps (1972) and Hamilton (1973) and which has been followed here is to hold the ratio Ch/N_z as a constant, that is

$$\Lambda = Ch/N_z = \text{constant}, \tag{28}$$

where C is a linear friction coefficient.

This is not an unreasonable assumption in view of the evidence presented by Heaps (1972) which shows that the depth integrated and tidally averaged values of the eddy viscosity N_z may be given on dimensional grounds by

$$N_z = M u_0 h , \tag{29}$$

where M is a constant, u_0 is the tidal stream amplitude and h is the depth. Note: this relationship has already been used in connection with wind driven currents (see equation A14 in Appendix A)). Bowden et al (1959) found that M varied between 1.49×10^{-3} and 2.83×10^{-3}. From current measurements at Stations A and G on section $X_1 X_2$ (see Figure 26) a representative value of u_0 may be taken as 25 cm s^{-1} and taking a mean value of $M = 2.16 \times 10^{-3}$ and $C = .2$ cms $^{-1}$ gives

$$\Lambda = \frac{Ch}{N_z} = \frac{C}{M u_0} \simeq 4 . \tag{30}$$

This value of M is slightly lower than that given by Bowden (1953) but is perhaps more representative of changes over the tidal cycle in the area as a whole. Similarly to Heaps (1972) we have calculated u and v, see Appendix F and Table 18, for values of n = 1, 2 and 4. In a water depth of 14 m these values of n would correspond to N_z values of 280, 140 and 70 $cm^2\ s^{-1}$ respectively. Similarly to Heaps (1972) we find that this range of n values is realistic and probably accounts for most of the variation in tidally averaged N_z values along the section.

Figure 27 shows the speeds and directions of the resultant surface and bottom currents V_s and V_B respectively, along the section for different values of n and Figure 28 shows the u and v profiles at a position midway along the section for a value of n = 4. The salient features of the density current field are:

(1) the strong alongshore component of the surface current, towards the W (ie towards Mumbles Head), of order 2 cm s^{-1};

(2) the onshore component of the bottom current, towards the N (ie towards the coast) of order 1 cm s^{-1}. These values increase in deeper water as shown in Figure 27.

We can conclude from this analysis that the density currents are of the order 1 - 2 cm s^{-1} and are thus comparable with, if not greater than, the observed tidal residuals in the N of the Bay.

8. SUMMARY AND CONCLUSIONS

Observations of tidal and residual currents in Swansea Bay show that the area exhibits a diverse range of flow features. Foremost amongst these is the horizontal non-uniformity of the M_2 and S_2 tidal currents leading, via the non-linear terms in the equation of motion, to large quarter diurnal (M_4) currents, particularly in the vicinity of Porthcawl (see Figures 3 and 10). These play a significant role in sediment transport (see Pingree and Griffiths, 1979). Furthermore, the area is characterized by an order of magnitude variation in tidal mixing and sediment transport over the Neap-Spring cycle. The north of the Bay is an area of low tidal energy and therefore likely to be an area of net fine sediment deposition.

Residual current observations, summarised in Tables 13 and 14 and Figure 14 and schematically in Figure 29, confirm the presence of a large clockwise gyre situated over the Scarweather Sand and associated with this the presence of

convergent flow near the sea-bed and divergent flow at mid-depth on the flanks of the sandbank. The area to the S of Port Talbot appears to be an area of divergence in the mean tidal circulation.

The measured phases of the currents and elevations (see Tables 8 - 11) indicate a standing wave tidal oscillation with the M_2 tidal current phase being of the order of 90° within the Bay but showing a variation from S to N of about 10°, with the currents in the Bay apparently reaching a maximum about 20 minutes later than those in the deeper flow of the Bristol Channel to the S of the Scarweather Sands.

Theory and observation suggest that the circulation in the Bay is likely to be influenced by meteorological forcing, particularly during periods of storm surge activity. The response is complex but the results indicate that wind set-up or set-down may be the most likely mechanism affecting the residual circulation. In particular during a storm surge wind induced set-down would appear to have the greatest effect on the residual circulation.

During these periods residual currents may reach speeds of about 10 cm s^{-1} which is about five times the value during quiescent flow conditions. During quiescent periods residual tidal elevations show the expected inverse correlation with atmospheric pressure ("inverted barometer effect") with the tides being over or under estimated by about .2 m.

In the shallow area to the N of the Bay, salinity and temperature measurements indicate that the freshwater discharges from the Rivers Neath, Tawe and Afan significantly modify the density field giving rise to density currents of the order of 1 - 2 cm s^{-1} which are comparable with, if not greater than, the tidal residuals. It is not improbable that in the N of the Bay, the mean circulation is entirely controlled by the density field.

9. ACKNOWLEDGEMENTS

We would like to acknowledge the support and co-operation of our colleagues at the Institute of Oceanographic Sciences, Taunton. Salinity and temperature data were supplied by the Welsh National Water Development Authority, and Mrs A J Williams of the Department of Oceanography, University College, Swansea, kindly made her tidal elevation data available. This work was supported by the Department of the Environment.

REFERENCES

ABDULLAH M I, H M DUNLOP and D GARDNER (1973). Chemical and Hydrographic observations in the Bristol Channel during April and June 1971. J.Mar.biol.Ass.UK, 53, 299-319.

BENNETT A F (1975). Tides in the Bristol Channel. Geophys.J.R.astr.Soc., 40, 37-43.

BOOTH D A, M J HOWARTH, J A DURANCE and J H SIMPSON (1978). A comparison of Residual Currents Estimated with Current Meters and a Parachute Drogue in a Shallow Sea. Dt.hydrogr.Z., 31, 237-248.

BOWDEN K F (1953). Note on wind drift in a channel in the presence of tidal currents. Proc.R.Soc. A, 219, 426-446.

BOWDEN K F (1955) Physical Oceanography of the Irish Sea, Fishery Invest., Lond. Ser 2, 18, pp 67.

BOWDEN K F, L A FAIRBAIRN, and P HUGHER (1959). The distribution of shearing stresses in a tidal current. Geophys.J.R.astr.Soc., 2, 288-305.

BRETSCHNEIDER C L (1968). On wind tides and longshore currents over the continental shelf due to winds blowing at an angle to the coast. Mitt.Inst.Meeresk.Univ. Hamburg, No 10. 96-102.

BYE J A T (1967). The wave-drift current. J.Mar.Res. 25, 95-102.

CARRUTHERS J N, A L LAWFORD and V F C Veley (1949). Studies of water movements and winds at various light v ssels in 1938, 1939 and 1940. Ann.biol. Copenh. 6, 115-120.

COOPER L H N (1967). The Physical Oceanography of the Centic Sea. Oceanogr.Mar. Biol.Ann.Rev., 5, 99-110.

CSANADY G T (1972). The coastal boundary layer in Lake Ontario. J.Phys. Oceanogr. 2, 168-176.

DAVIES A M and R A FLATHER (1977). Computation of the Storm Surge of 1 to 6 April 1973 using Numerical models of the North West European Continental Shelf and the North Sea. Dt.hydrogr.Z., 30, 139-162.

DEFANT A (1961). Physical Oceanography, Vol 1, Pergamon Press, Oxford. pp 729.

DOODSON A T (1928). The analysis of tidal observations. Phil.Trans.Roy.Soc. (London), Ser.A227, 223-279.

DOOLEY H D and J H STEELE (1969). Wind driven currents near a coast. Dt.hydrogr.Z., 22, 213-223.

DURST C S (1924). The relationship between currents and wind. Quart.J.R.Met.Soc. 50, 113-119.

EKMAN V W (1905). On the influence of the earth's rotation on ocean currents. Ark.f.Mat. Astron.och.Fysik, 2, 1-52.

FARMER D M (1976). The influence of Wind on the Surface Layer of a Stratified Inlet: Part II. Analysis. J.Phys.Oceanogr., 6, 941-952.

FORTNUM B S H and P J Hardcastle (1979). Waves recorded at the Scarweather Bank in the Bristol Channel. IOS Report No 79, pp 7.

GODIN G (197?). The Analysis of Tides. Liverpool University Press. 264 pp.

GONELLA J (1972). A rotary-component method for analysing meteorological and oceanographic vector time series. Deep-Sea Res., 19, 833-846.

GRACE S F (1936). Friction in the tidal currents of the Bristol Channel. Mon. Not.R.astr.Soc.geophys.Suppl., 3, 388-395.

GRAFF J (1978). Abnormal sea levels in the North West. Dock Harb.Auth., 58, 366-371.

GROVES G (1955). Numerical filters for discrimination against tidal periodicities. Trans.Amer.Geophys.Union, 36, 1073-1084.

HAMILTON P (1973). The Circulation of the Bristol Channel. Geophy.J.R.astr.Soc. 32, 409-422.

HAMMOND T M and M B COLLINS (1979). Flume Studies of the Response of Various Current Meter Rotor/Propellers to Combinations of Unidirectional and Oscillatory Flow. Dt.hydrog.Z., 32, 39-58.

HEAPS N S (1965). Storm surges on a continental shelf. Phil.Trans.R.Soc., Ser.A257, 351-383.

HEAPS N S (1967). Storm Surges. Oceanogr.Mar.Biol.Ann.Rev., 5, 11-47.

HEAPS N S (1968). Estimated effects of a barrage on tides in the Bristol Channel. Proc.Inst.Civ.Engrs., 40, 495-509.

HEAPS N S (197?). Estimation of Density Currents in the Liverpool Bay area of the Irish Sea. Geophys.J.R.astr.Soc., 80, 415-432.

HEAPS N S (1978). Linearized Verticallt-Integrated Equations for Residual Circulation in Coastal Seas. Dt.hydrogr.Z., 31, 147-169.

HEATHERSHAW A D (1977). Water Circulation in Swansea Bay. IOS Internal Document No 18, pp 11.

HILL H W and J W RAMSTER (197?). Variability in current meter records in the Irish Sea. Rapports et Proces-Verbaux des Reunions, Conseil Permanent International pour l'Exploration de la Mer, 162, 232-247.

HOWARTH M J (1975). Current Surges in the St George's Channel. Est.Coast.Mar.Sci. 3, 57-70.

HUNT J N (1964) Tidal Oscillations in Estuaries. Geophys.J.R.astr.Soc., 8, 440-455.

HUNTER J H (1979). On the Interaction of M_2 and M_{2n} Tidal Velocities in Relation to Quadratic and Higher Power Laws. Dt.hydrogr.Z. 32, 145-153.

JOHNS B (1969). Some consequences of an inertia of turbulence in a tidal estuary. Geophys.J.R.astr.Soc., 18, 65-72.

KENYON K E (1970). Stokes drift for random gravity waves. J.Geophys.Res., 74, 6991-6994.

KONDO J (1976). Parameterization of turbulent transport in the top metre of the ocean. J.Phys.Oceanogr., 6, 712-720.

LEE A and J W RAMSTER (1968). The hydrography of the North Sea. A review of our knowledge in relation to pollution problems. Helgolander wiss.Meeresunters. 17, 44-63.

LENNON G W (1963). The identification of weather conditions associated with the generation of major storm surges along the west coast of the British Isles. Quart. J.R.Met.Soc., 89, 381-394.

LONGUET-HIGGINS M S (1953). Mass transport in water waves. Phil.Trans.R.Soc. Lond., Series A245, 535-581.

LONGUET-HIGGINS M S (1957). The mechanics of the boundary-layer near the bottom in a progressive wave. Appendix to Russell and Osorio (1957).

LONGUET-HIGGINS M S (1969). On the transport of mass by time-varying ocean currents. Deep-Sea Res., 16, 431-447.

MADDOCK L and R D PINGREE (1978). Numerical Simulation of the Portland Tidal Eddies. Est.Coast,Mar.Sci., 6, 353-363.

MURRAY S P (1975). Trajectories and Speeds of Wind-Driven Currents Near the Coast. J.Phys.Oceanogr., 6, 347-360.

NERC (1972). The Severn Estuary and Bristol Channel. Natural Environment Research Council Publications Series C.No.9, pp 20.

NEUMANN G (1952). On the complex nature of ocean waves and the growth of the sea under the action of wind. Gravity Waves, National Bureau of Standards. Circular 521.

NEUMANN G and W J PIERSON (1966). Principles of Physical Oceanography, Prentice Hall, Inc.Englewood Cliffs. N.J. pp 545.

OWEN A (1979). The tidal regime of the Bristol Channel: a numerical modelling approach (in preparation).

PALMEN E (1931). Zur Bestimmung des Triftstromes aus Terminbeobachtungen. J.Cons.Internat., 6, 387-401.

PINGREE R D (1978). The formation of the Shambles and other Banks by tidal stirring of the Seas. J.Mar.Biol.Ass.UK. 58, 211-226

PINGREE R D and D K GRIFFITHS (1979). Sand Transport Paths around the British Isles resulting from M_2 and M_4 tidal interactions. J.Mar.Biol.Ass.UK. 59, 497-513.

PROUDMAN J (1953). Dynamical Oceanography. Methuen, London pp 409.

PUGH D T, M J HOWARTH and J R ROSSITER (1971/72). An assessment of the knowledge of the Phyaical Oceanography of Liverpool Bay, the Severn Estuary and Bristol Channel. ICOT Internal Report No 31, pp 20.

PUGH D T and J M VASSIE (1976). Tide and surge propagation offshore in the Dowsing Region of the North Sea. Dt.hydrogr.Z., 29, 163-213.

RAMSTER J W, D G HUGHES and G K FURNES (1978). A 'Steadiness' Factor for Estimating the Variability Residual Drift in Current Meter Records. Dt.hydrogr.Z., 31, 230-236.

ROBINSON I S (1978). Tidal response of a wedge-shaped estuary to the installation of a power barrage: a simplified analytical approach. Proc.Inst.Civ.Engrs., 65, 773-790.

ROBINSON I S (1979). The tidal dynamics of the Irish and Celtic Seas. Geophys. J.R.astr.Soc., 56, 159-197.

RUSSELL R C H and J D C OSORIO, (1957). An experimental investigation of drift profiles in a closed channel. Proc.6th Conf. on Coastal Eng., Miami, 171-193.

SHEMDIN O H (1972). Wind generated current and phase speed of wind waves. J.Phys.Oceanogr., 2, 411-419.

SPILLANE K T and G D HESS (1978). Wind-induced Drift in Contained Bodies of Water. J.Phys.Oceanogr., 8, 930-935.

STOKES G G (1847). On the theory of oscillatory waves. Trans.Camb.Phil.Soc., 8, 441-445.

STONER J H (1977). A Report on the first year of a programme to monitor inputs to Swansea Bay 1973-1974. Welsh National Water Development Authority Report No SS TW 77/2. pp 24.

TAYLOR G I (1921). Tides in the Bristol Channel. Proc.Camb.Phil.Soc., 20, 320-325.

TEE K T (1976). Tide-induced residual current, a 2-D nonlinear numerical tidal model. J.Mar.Res., 34, 603-628.

THORADE H (1914). Die Geschuindigkeit von Triftstromungen und die Ekman'sche Theorie. Ann.d.Hyd.u.Marit.Meteorology. 42, p 379.

WU J (1973). Prediction of near-surface drift currents from wind velocity. J.Hyd.Div.ASCE., 99, 1291-1302.

WU J (1975). Wind induced drift currents. J.Fluid Mech., 68, 49-70.

TABLE 1

Ratios of the water depth (h) to the depth of frictional influence (D) for various windspeeds (W) and for surface layer mixing only.

W ($m\ s^{-1}$)	h/D (h = 20m)
2	7 61
4	2.69
6	-
8	1.30
10	.33
12	.28
14	.24
16	.20
18	.18
20	.17

D has been calculated from Ekman's (1905) theory using equation (9) with a depth mean value of N_z based upon a maximum surface value of N_z, given by Thorade's (1914), relationship decreasing linearly to zero at the sea-bed (see Table 2).

TABLE 2

Estimates of wind driven surface currents as a function of windspeed in an unbounded sea of finite depth calculated from equations (A8).

W (m s^{-1})	N_z (m^2 s^{-1})	λ/D (λ = 20m)	u (cm s^{-1})	v (cm s^{-1})
2	.0100	7.61	.42	.43
4	.0103	2.69	1.73	1.79
6	-	-	-	-
8	.0235	1.30	3.35	5.72
10	.0310	.33	3.57	7.73
12	.0400	.28	3.45	9.41
14	.0510	.24	3.09	10.60
16	.0650	.20	2.60	11.25
18	.0800	.18	2.23	11.81
20	.0950	.17	1.98	12.44

Values of N_z are depth mean values based upon a surface maximum, given by Thorade's (1914) relationship (see Table A1), decreasing linearly to zero at the sea-bed with a linear supposition of a tidally averaged N_z value of .01m^2 s^{-1}.

Note that the wind is blowing in the v direction.

TABLE 3

Values of the Stokes drift u_s due to surface gravity waves as a function of depth for typical wave heights and periods in Swansea Bay calculated using equation (B1) for a total depth of 20m.

Depth z (m)	u_s (cm s^{-1})		
	H=.5m T= 8s	H=1m T= 8s	H=2m T= 8s
0	.22	.88	3.53
2	.03	.11	0.44
4	-.12	-.46	-1.84
6	-.21	-.85	-3.40
8	-.27	-1.08	-4.31
10	-.29	-1.15	-4.61
12	-.27	-1.09	-4.35
14	-.22	-0.89	-3.56
16	-.14	-0.56	-2.26
18	-.03	-0.11	-0.45
20	.12	.46	1.85

z depth (m)

H wave height (m)

T wave period (s)

u_s Stokes drift (cm s^{-1})

TABLE 4

Estimates of the maximum slope currents resulting from wind (W) induced set up calculated from equations (A10).

W ($m\ s^{-1}$)	N_z ($m^2\ s^{-1}$)	u $cm\ s^{-1}$	v $cm\ s^{-1}$
2	.0100	-.25	-.12
4	.0103	-1.02	-.51
6	-	-	-
8	.0235	-2.07	-2.51
10	.0310	-2.22	-3.58
12	.0400	-2.15	-4.49
14	.0510	-1.93	-5.15
16	.0650	-1.62	-5.53
18	.0800	-1.39	-5.84
20	.0950	-1.24	-6.17

Values of N_z are depth mean values based upon a surface maximum, given by Thorade's (1914) relationship (see TableA1), decreasing linearly to zero at the sea bed with a linear supposition of a tidally averaged N_z value of $.01 m^2\ s^{-1}$.

Note that the wind induced set up is in the v direction.

TABLE 5

Details of current meter records described in this report

Stn.A

Record	Station	Height (m)	Useful data (hrs	mins)	Timing error (s day^{-1})
237K5	A	10	218	30	*
244A6	A	10	415	20	*
237D6	A	10	117	30	*
232F6	A	10	1176	00	-0.29
244G6	A	10	500	40	*
237J6	A	10	938	50	*
667F7	A	10	1318	50	+201.20
669G7	A	10	1485	30	+4.82
667J7	A	10	1306	10	+232.83
238K5	A	3	1248	0	-10.77
238A6	A	2	261	10	*
560D6	A	2	1391	10	+5.17
629F6	A	2	932	10	+1.76
669G6	A	2	1463	10	+65.98
680M6	A	2	1050	00	-9.94
260B7	A	2	1203	50	-3.94
560D7	A	2	1077	20	+10.14
532F7	A	2	1320	10	0.00
594G7	A	2	1485	20	+0.97
532J7	A	2	1513	50	-10.46

* Timing error not known due to current meter stopping prior to recovery or having recorded a full magnetic tape

TABLE 5 (Continued)

Details of current meter records described in this report

Stations B — K

Record	Station	Height (m)	Useful data (hrs mins)	Timing error ($s\ day^{-1}$)
594F6	B	2	1317 10	+10.40
680K6	B	2	769 30	-14.96
667F6	C	2	1205 20	+16.09
594K6	C	2	857 10	-88.23
244K6	D	12	908 00	-12.09
877F6	D	2	1269 20	-124.50
269K6	E	12	834 00	- 10.27
878F6	E	2	1244 00	+0.10
667K6	E	2	909 10	+131.37
260K6	F	10	840 20	-8.83
885F6	F	2	1194 20	0.00
560K6	F	2	323 30	+13.10
573K5	G	1	1084 10	-53.71
626K5	H	1	613 00	*
267F6	H	2	1299 10	+6.54
534K6	H	2	319 30	*
269C7	H	2	706 40	*
534F6	I	2	1225 20	+61.95
532F6	J	2	766 50	-13.14
669C7	K	2	1511 10	+9.51

* Timing error not known due to current meter stopping prior to recovery or having recorded a full magnetic tape

TABLE 6

Summary of records harmonically analysed with TIRA

Station	Record	
	Bottom	Mid-depth
A	238K5	
	560D6	
	629F6	232F6
	669G6*	
		237J6
	680M6	
	260B7	
	560D7	
	532F7	667F7
	594G7	669G7
	532J7	667J7
B	594F6*	
	680K6	
C	667F6*	
	594K6	
D	877F6	
		244K6
E	878F6*	
	667K6	269K6
F	885F6	
		260K6
G	573K5	
H	267F6	
	269C7*	
I	534F6	
J	532F6	
K	669C7	

* Records not included in this report
Amplitude and Phase estimates given in Tables 8, 9 and 10

TABLE 7

Harmonic analysis of tidal currents

Constituents analysed using TIRA

Related	Major
P1	Z0
PI1	MM
PSI1	MSF
PHI1	Q1
K2	O1
T2	M1
NU2	K1
2N2	J1
	OO1
	MU2
	N2
	M2
	L2
	S2
	2SM2
	MO3
	M3
	MK3
	MN4
	M4
	SN4
	MS4
	2MN6
	M6
	MSN6
	2MS6
	2SM6

Related constituents were evaluated using equilibrium tide values.

TABLE 8

Amplitudes and phases of the principal tidal constituents in the currents at Stn A (Long-term mooring) at a height of 2m above the sea-bed.

		H_u, H_v (cm s^{-1})			g_u, g_v (°)		
		μ	σ	$\sigma/N^{1/2}$	μ	σ	$\sigma/N^{1/2}$
O_1	u	.29	.24	.08	237.45	63.28	20.01
	v	.11	.23	.07	32.76	170.44	53.90
K_1	u	.31	.32	.10	350.80	255.29	80.73
	v	.00	.48	.15	84.86	123.29	38.99
N_2	u	6.69	1.77	.56	78.62	16.65	5.27
	v	1.07	2.27	.72	200.49	63.89	20.21
M_2	u	37.91	1.73	.55	85.56	5.14	1.63
	v	4.10	2.85	.90	186.48	39.65	12.54
S_2	u	11.21	3.00	.95	145.50	44.08	13.94
	v	1.57	1.43	.45	262.43	58.33	18.45
M_4	u	3.46	.81	.26	328.31	9.41	2.98
	v	.83	.76	.24	246.69	159.90	50.57
MS_4	u	1.94	.46	.15	20.45	14.32	4.53
	v	.84	.54	.17	243.95	73.96	23.39
M_6	u	.12	.43	.14	267.99	130.67	41.32
	v	1.68	.85	.27	278.34	17.18	5.43

H_u, H_v = Amplitudes

g_u, g_v = Phases

μ = Mean

σ = Standard deviation

$\sigma/N^{1/2}$ = Standard error

N = Number of monthly analyses (= 10)

u east-west component of current in cm s^{-1}.

v north-south component of current in cm s^{-1}.

Phases are in degrees relative to the equilibrium tide at Greenwich.

Note: μ indicates a vector mean and the standard deviations, σ, are deviations from the vector mean estimates of H and g.

TABLE 9

Amplitudes and phases of the principal tidal constituents in the currents at Stn A (Long-term mooring) at a height of 10m above the sea bed.

		H_u, H_v (cm s^{-1})			g_u, g_v (°)		
		μ	σ	$\sigma/N^{\frac{1}{2}}$	μ	σ	$\sigma/N^{\frac{1}{2}}$
O_1	u	.40	.30	.14	259.11	92.86	41.53
	v	.21	.47	.21	180.22	68.86	30.79
K_1	u	.48	.22	.10	25.67	152.23	68.08
	v	.24	.28	.13	175 15	49.96	22.34
N_2	u	8.05	.78	.35	71.35	12.17	5.44
	v	.34	.37	.16	342.63	230.43	103.05
M_2	u	47.97	2.40	1.07	89.48	2.07	0.92
	v	2.61	1 97	.88	291.00	116.96	52.31
S_2	u	18.29	1.37	.61	143.09	4.00	1.79
	v	2.02	2.53	1.13	251.65	188.34	84.23
M_4	u	3.45	.33	.15	322.29	14.60	6.53
	v	1.43	.90	.40	264.89	175.07	78.29
MS_4	u	1.58	.18	.08	12.69	162.59	72.71
	v	1.20	.85	.38	253.64	114.98	51.42
M_6	u	1.24	.14	.06	225.60	3.93	1.76
	v	1.74	1.07	.48	286.89	45.61	20.40

H_u, H_v = Amplitudes

g_u, g_v = Phases

μ = Mean

σ = Standard deviation

$\sigma/N^{\frac{1}{2}}$ = Standard error

N = Number of monthly analyses (= 5)

u - east-west component of current in cm s^{-1}

v - north-south component of current in cm s^{-1}

Phases are in degrees relative to the equilibrium tide at Greenwich.

Note: μ indicates a vector mean and the standard deviations, σ, are deviations from the vector mean estimates of H and g.

TABLE 10

Amplitude and phases of the principal semi-diurnal constituents in the tidal currents at Stns B - K in Swansea Bay

Station			H_u, H_v (cm s^{-1}) Mid-depth	H_u, H_v (cm s^{-1}) Near bottom	g_u, g_v (°) Mid-depth	g_u, g_v (°) Near bottom
B	M_2	u		11.62		95.89
		v		11.75		266.70
	S_2	u		6.04		151.56
		v		3.94		321.80
C	M_2	u		38.00		93.09
		v		44.71		278.68
	S_2	u		16.84		159.07
		v		15.54		340.85
D	M_2	u	80.34	56.73	92.59	105.97
		v	12.65	17.03	283.41	284.82
	S_2	u	30.66	23.92	145.98	168.75
		v	4.01	6.45	332.69	357.12
E	M_2	u	62.29	47.75	84.96	80.88
		v	2.68	18.28	42.38	80.40
	S_2	u	22.84	17.31	135.43	132.25
		v	1.62	.47	70.47	9.73
F	M_2	u	69.25	45.55	81.68	86.57
		v	30.55	17.26	77.21	82.27
	S_2	u	23.14	17.07	128.84	141.92
		v	10.15	7.24	127.72	123.09
G	M_2	u		14.50		126.14
		v		4.48		143.15
	S_2	u		4.40		115.91
		v		2.20		120.94
H	M_2	u		10.70		82.05
		v		33.40		265.71
	S_2	u		6.38		163.88
		v		11.53		330.85

H_u, H_v = Amplitudes

g_u, g_v = Phases

u = east-west component of current in cm s^{-1}.

v = north-south component of current in cm s^{-1}.

Phases are in degrees relative to the equilibrium tide at Greenwich.

TABLE 10 (continued)

Amplitude and phases of the principal semi-diurnal constituents in the tidal currents at Stns B - K in Swansea Bay

Station			H_u, H_v (cm s^{-1}) Mid-depth	H_u, H_v (cm s^{-1}) Near bottom	g_u, g_v (°) Mid-depth	g_u, g_v (°) Near bottom
I	M_2	u	61.55			74.65
		v	10.68			77.99
	S_2	u	25.97			128.00
		v	4.48			110.13
J	M_2	u	55.31			199.65
		v	7.37			220.71
	S_2	u	22.80			257.31
		v	3.48			264.63
K	M_2	u	14.55			97.04
		v	21.63			269.52
	S_2	u	7.26			157.24
		v	7.44			325.08

H_u, H_v = Amplitudes

g_u, g_v = Phases

u = east-west component of current in cm s^{-1}

v = north-south component of current in cm s^{-1}

Phases are in degrees relative to the equilibrium tide at Greenwich.

APPENDIX B

STOKES DRIFT: MOTION IN THE INTERIOR OF THE FLUID

By including the effects of viscosity in Stokes' (1847) original solution for the drift velocity (see equation 10), Longuet-Higgins (1953) obtained an expression for the drift velocity in the interior of the fluid of the form

$$u_s\big|_{0<z<h} = \frac{a^2\sigma k}{4\sinh^2 kh}\Big[2\cosh\{2kh(\mu-1)+3 + kh\sinh 2kh(3\mu^2-4\mu+1) + 3\Big(\frac{\sinh 2kh}{2kh}+\frac{3}{2}\Big)(\mu^2-1)\Big]\Big] \qquad (B1)$$

where h is fluid depth and $\mu = z/h$. Here z is the distance measured positive downwards from the surface. This solution, which is essentially for laminar flow, reduces to the usual expression for the Stokes drift velocity near the bed which is given by equation (13). This may also be applied (see Longuet-Higgins, 1957) to a turbulent boundary layer. Equation B1 has been used here to calculate the Stokes drift velocities which are shown in Table 3.

Experimental observations (eg Russell and Osario, 1957) suggest that good estimates of the Stokes drift at the surface are probably given by Stokes' original irrotational flow solution (equation 10) but that in the interior of the fluid, and particularly at the bed, the effects of viscosity may well lead to Stokes drift velocity profiles of the form predicted by equation (B1).

In reality of course, the situation is far more complex than this with the total wave induced mass transport velocity being the resultant effect of a superposition of waves having a random distribution of heights, periods and phases.

It should be noted that considerable controversy still surrounds the relative magnitude of the wind driven shear current and the wave induced mass transport velocity. Wu (1975) has shown in laboratory experiments that the wave-induced Stokes transport may only be 3-15% of the surface dirft and this would not seem an unreasonable estimate in the light of our own calculations. However, as suggested by Wu (1975), the situation is far from being clear with, for example, Shemdin (1972) claiming, on the basis of laboratory data, that the surface drift is essentially a wind-induced shear current, whereas Bye (1967) and Kenyon (1972) concluded from a study of oceanic wave data that the surface drift is primarily a wave induced mass transport.

TABLE 12

Order of magnitude comparison of non-linear terms in equations of motion for Swansea Bay.

Comparative linear term ($cm\ s^{-2}$)	Non-linear terms ($cm\ s^{-2}$)
$O\left(\frac{\partial \hat{u}}{\partial t}\right) \simeq .007$	$O\left(\hat{u}\frac{\partial \hat{u}}{\partial x}\right) \simeq .004$
	$O\left(\frac{C_D \hat{u}(\hat{u}^2+\hat{v}^2)^{1/2}}{\lambda+\zeta}\right) \geq .004$

Calculated from tidal stream amplitude data shown in Figure 9 and for $\lambda \leq$ 20m on the E side of Swansea Bay with $C_D = .0025$.

TABLE 13

Summary of measured residual currents from current meter observations in Swansea Bay and variability in the direction of residual flow estimates from Doodson's X_o filter.

Station A - Long term mooring

Record	Station	Elevation	Residual current			
			Speed	Direction	Steadiness factor $\mathcal{B}$	Length of Record (days)
		(m)	(cm s^{-1})	(°)	(%)	
237K5	A	10	.91	54.97	64.78	8
244A6	A	10	1.93	16.80	58.87	16
237D6	A	10	2.14	297.11	95.74	3
232F6	A	10	1.62	323.58	84.64	48
244G6	A	10	1.55	30.34	87.89	20
237J6	A	10	1.11	336.52	52.61	38
667F7	A	10	1.21	70.22	70.28	54
669G7	A	10	1.28	23.60	73.01	61
667J7	A	10	1.83	85.99	68.08	53
238K5	A	3	.61	82.80	37.53	51
238A6	A	2	2.84	143.15	82.20	9
560D6	A	2	2.30	145.74	83.39	57
629F6	A	2	3.18	154.18	97.07	38
669G6	A	2	2.02	131.18	87.39	60
680M6	A	2	.95	122.47	35.86	43
260B7	A	2	2.37	105.82	53.36	49
560D7	A	2	1.97	143.88	70.22	44
532F7	A	2	2.91	143.78	95.08	54
594G7	A	2	3.12	157.82	95.14	61
532J7	A	2	1.40	97.55	47.28	62

TABLE 14

Summary of measured residual currents from current meter observations in Swansea Bay and variability in the direction of residual flow estimates from Doodson's X_0 filter.

Stations B - K

Record	Station	Elevation (m)	Residual current: Speed (cm s^{-1})	Direction (°)	Steadiness factor $\mathcal{S}$ (%)	Length of record (days)
594F6	B	2	.34	70.03	23.08	54
680K6		2	1.42	345.80	65.19	31
667F6	C	2	5.32	166.33	95.60	49
594K6		2	4.38	150.75	93.14	35
244K6	D	12	2.79	227.16	86.64	37
877F6		2	2.30	49.10	88.52	52
269K6	E	12	8.20	68.89	98.60	33
878F6		2	5.12	87.78	98.69	51
667K6		2	6.32	86.03	95.47	31
260K6	F	10	4.92	237.62	96.05	34
885F6		2	4.15	43.59	97.89	49
560L6		2	6.60	338.55	97.38	12
573K5	G	1	.55	316.64	20.63	39
626K5	H	2	1.60	144.30	78.58	24
267F6		2	3.63	134.70	93.90	53
534K6		2	3.98	135.42	92.20	12
269C7		2	4.91	136.71	84.50	28
534F6	I	2	.58	97.57	41.76	50
532F6	J	2	1.57	176.54	77.30	31
669C7	K	2	3.24	101.20	75.81	61

TABLE 15

Variability in the speed of residual flow estimates from Doodson's X_0 filter

Station A - Long term mooring

Record	Station	Elevation	Residual current			
			Speed ($cm\ s^{-1}$)	Direction ($^\circ$)	$\sigma_{\langle\bar{u}\rangle}$ ($cm\ s^{-1}$)	$\sigma_{\langle\bar{v}\rangle}$ ($cm\ s^{-1}$)
237K5	A	10	.91	54.97	.38	.24
244A6	A	10	1.93	16.80	.62	.43
237D6	A	10	2.14	197.11	.21	.33
232F6	A	10	1.62	323.58	.15	.14
244G6	A	10	1.55	30.34	.16	.18
237J6	A	10	1.11	336.52	.27	.24
667F7	A	10	1.21	70.22	.13	.15
669G7	A	10	1.28	23.60	.13	.14
667J7	A	10	1.83	85.99	.22	.26
238K5	A	3	.61	82.80	.18	.18
238A6	A	2	2.84	143.15	.57	.55
560D6	A	2	2.80	145.74	.18	.17
629F6	A	2	3.18	154.18	.17	.17
669G6	A	2	2.02	131.18	.13	.13
680M6	A	2	.95	122.47	.32	.30
260B7	A	2	2.37	105.82	.40	.51
560D7	A	2	1.97	143.88	.24	.26
532F7	A	2	2.91	143.78	.12	.17
594G7	A	2	3.12	157.82	.13	.15
532J7	A	2	1.40	97.55	.22	.33

$\sigma_{\langle\bar{u}\rangle}$ - standard error of E-W component of residual flow

$\sigma_{\langle\bar{v}\rangle}$ - standard error of N-S component of residual flow

TABLE 15 (continued)

Variability in the speed of residual flow estimates from Doodson's X_0 filter.

Stations B - K

Record	Station	Elevation	Residual current			
			Speed (cm s^{-1})	Direction (°)	$\sigma_{\langle\bar{u}\rangle}$ (cm s^{-1})	$\sigma_{\langle\bar{v}\rangle}$ (cm s^{-1})
594F6	B	2	.34	70.03	.17	.15
680K6		2	1.42	345.80	.25	.36
667F6	C	2	5.32	166.33	.22	22
594K6		2	4.38	150.75	.21	.36
244K6	C	12	2.79	227.16	.27	.28
877F6		2	2.80	49.10	.13	.15
269K6	E	12	8.20	68.89	.31	.26
878F6		2	5.12	87.78	.14	.12
667K6		2	6.32	86.03	.25	.31
260K6	F	10	4.92	237.62	.27	.25
885F6		2	4.15	43.59	.14	.10
580K6		2	6.60	338.55	.43	.65
573K5	G	1	.55	316.64	39	.27
626K5	H	2	1.60	144.30	.21	.22
267F6		2	3.63	134.70	.16	.13
534K6		2	3.98	135.42	.31	.69
269C7		2	4.91	136.71	.38	.62
534F6	I	2	.58	97.57	.19	.10
532F6	J	2	1.57	176.54	.20	.20
669C7	K	2	3.24	101.20	.29	.28

$\sigma_{\langle\bar{u}\rangle}$ - Standard error of E-W component of residual flow

$\sigma_{\langle\bar{v}\rangle}$ - Standard error of N-S component of residual flow

TABLE 16

Multi-regression analysis of 78 day meteorological forcing data set (Current measurements at Station A, 1/9/77-17/11/77)

Correlation Coefficient (r)

	$\bar{u}_{x_2}$	$\bar{u}_{y_2}$	$\bar{u}_{x_{10}}$	$\bar{u}_{y_{10}}$	$\bar{P}_R - 1000$	$\bar{w}_x\lvert\bar{w}_x\rvert$	$\bar{w}_y\lvert\bar{w}_y\rvert$	$\bar{H}_s$	$\bar{\zeta}_R$
$\bar{u}_{x_2}$		.98	.99	.98	- .08	- .07	- .08	.07	- .02
$\bar{u}_{y_2}$			.97	.97	- .15	.15	- .18	.15	.03
$\bar{u}_{x_{10}}$				.98	- .06	- .02	.04	- .03	- .04
$\bar{u}_{y_{10}}$					- .06	.06	- .08	.03	- .05
$\bar{P}_R - 1000$						- .21	.19	- .44	- .74
$\bar{w}_x\lvert\bar{w}_x\rvert$							- .35	.82	.42
$\bar{w}_y\lvert\bar{w}_y\rvert$								- .47	.14
$\bar{H}_s$									.47
$\bar{\zeta}_R$									

Values underlined significant at 5% level

x and y define frame of reference shown in Figure 18.

$\bar{u}_{x_2}, \bar{u}_{x_{10}}, \bar{u}_{y_2}, \bar{u}_{y_{10}}$: x and y components of daily residual flow at heights of 2 m and 10 m above sea-bed

$\bar{P}_R - 1000$: daily mean atmospheric pressure minus 1000 mb

$\bar{w}_x\lvert\bar{w}_x\rvert$, $\bar{w}_y\lvert\bar{w}_y\rvert$: square of x and y components of daily mean speed

$\bar{H}_s$ daily mean significant wave height measured at Scarweather Light Vessel

$\bar{\zeta}_R$ daily mean residual tidal elevation at Swansea (ie observed tide - predicted tide)

TABLE 17

Multiregression analysis of 18 day meteorological forcing data set (Current measurements at Station A, 31/10/77 - 17/11/77).

Correlation coefficient (r)

	$\bar{u}_{x_2}$	$\bar{\rho}_a - 1000$	$\bar{w}_x \lvert \bar{w}_x \rvert$	$\bar{w}_y \lvert \bar{w}_y \rvert$	$\bar{H}_s$	$\bar{T}_a$
$\bar{u}_{x_2}$		.11	.29	<u>-.75</u>	-.01	<u>-.69</u>
$\bar{\rho}_a - 1000$			.01	<u>.48</u>	-.23	.11
$\bar{w}_x \lvert \bar{w}_x \rvert$				.01	<u>.77</u>	<u>.79</u>
$\bar{w}_y \lvert \bar{w}_y \rvert$					.33	.43
$\bar{H}_s$						<u>.53</u>
$\bar{T}_a$						

	$\bar{u}_{y_2}$	$\bar{\rho}_a - 1000$	$\bar{w}_x \lvert \bar{w}_x \rvert$	$\bar{w}_y \lvert \bar{w}_y \rvert$	$\bar{H}_s$	$\bar{T}_a$
$\bar{u}_{y_2}$		-.19	.15	<u>-.77</u>	.41	-.31
$\bar{\rho} - 1000$			.01	<u>.48</u>	-.23	.11
$\bar{w}_x \lvert \bar{w}_x \rvert$				.01	<u>.77</u>	<u>.79</u>
$\bar{w}_y \lvert \bar{w}_y \rvert$					.33	.43
$\bar{H}_s$						<u>.53</u>
$\bar{T}_a$						

Values underlined significant at the 5% level

Terms defined in Table 17 and Figure 18 .

TABLE 17 (Continued)

Multiregression analysis of 18 day meteorological forcing data set
(Current measurements at Station A, 31/10/77 - 17/11/77)

Correlation coefficient (r)

	$\bar{u}_{x_{10}}$	$\bar{\rho}_a - 1000$	$\bar{w}_x \lvert\bar{w}_x\rvert$	$\bar{w}_y \lvert\bar{w}_y\rvert$	$\bar{H}_s$	$\bar{\tau}_a$
$\bar{u}_{x_{10}}$		.00	<u>-.58</u>	-.35	-.31	<u>-.72</u>
$\bar{\rho}_a - 1000$			.01	<u>.48</u>	-.23	.11
$\bar{w}_x \lvert\bar{w}_x\rvert$				.01	<u>.77</u>	<u>.79</u>
$\bar{w}_y \lvert\bar{w}_y\rvert$					.33	.43
$\bar{H}_s$						<u>.53</u>
$\bar{\tau}_a$						

	$\bar{u}_{y_{10}}$	$\bar{\rho}_a - 1000$	$\bar{w}_x \lvert\bar{w}_x\rvert$	$\bar{w}_y \lvert\bar{w}_y\rvert$	$\bar{H}_s$	$\bar{\tau}_a$
$\bar{u}_{y_{10}}$		-.02	.35	-.12	-.32	-.34
$\bar{\rho}_a - 1000$			.01	<u>.48</u>	-.23	.11
$\bar{w}_x \lvert\bar{w}_x\rvert$				.01	<u>.77</u>	<u>.79</u>
$\bar{w}_y \lvert\bar{w}_y\rvert$					.33	.43
$\bar{H}_s$						<u>.53</u>
$\bar{\tau}_a$						

Values underlined significant at the 5% level

Terms defined in Table 17 and Figure 18.

TABLE 18

Estimates of density currents flowing at a position midway along section X_1, X_2 in Figure 25.

n	z/λ	u (cm s^{-1})	v (cm s^{-1})
1	0	-.36	.15
	.2	-.28	.14
	.4	-.10	.10
	.6	.10	.06
	.8	.26	.02
	1.0	.29	.01
2	0	-.64	.53
	.2	-.50	.48
	.4	-.16	.34
	.6	.21	.18
	.8	.47	.06
	1.0	.46	.01
4	0	-1.08	2.04
	.2	.82	1.82
	.4	.23	1.82
	.6	.40	.65
	.8	.78	.17
	1.0	.64	.01

Total flow depth λ = 14m (midway along section)
Eddy viscosity (N_z) parameterization for λ = 14m

n	N_z (cm^2 s^{-1})
1	280
2	140
4	70

FIGURE 1

Location of study area

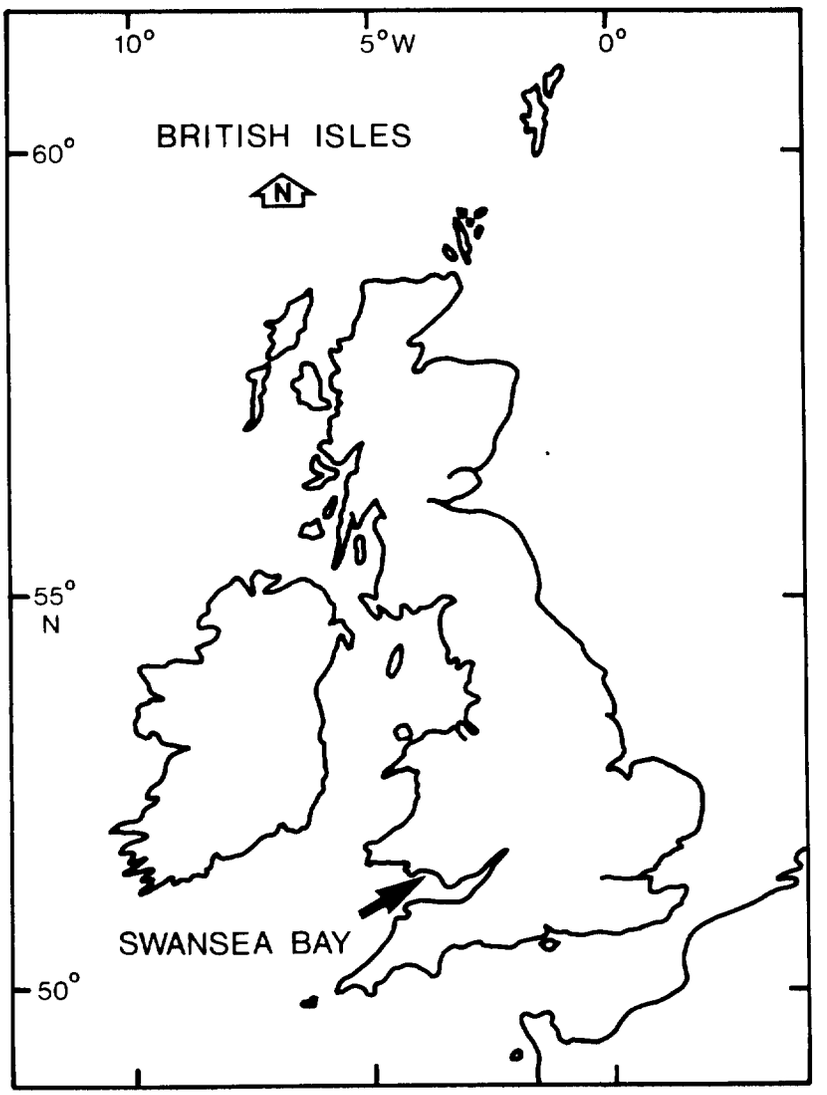

Fig.1

FIGURE 2

Co-tidal and co-range data for the Bristol Channel (Unpublished data reproduced courtesy of the Hydrographer of the Navy)

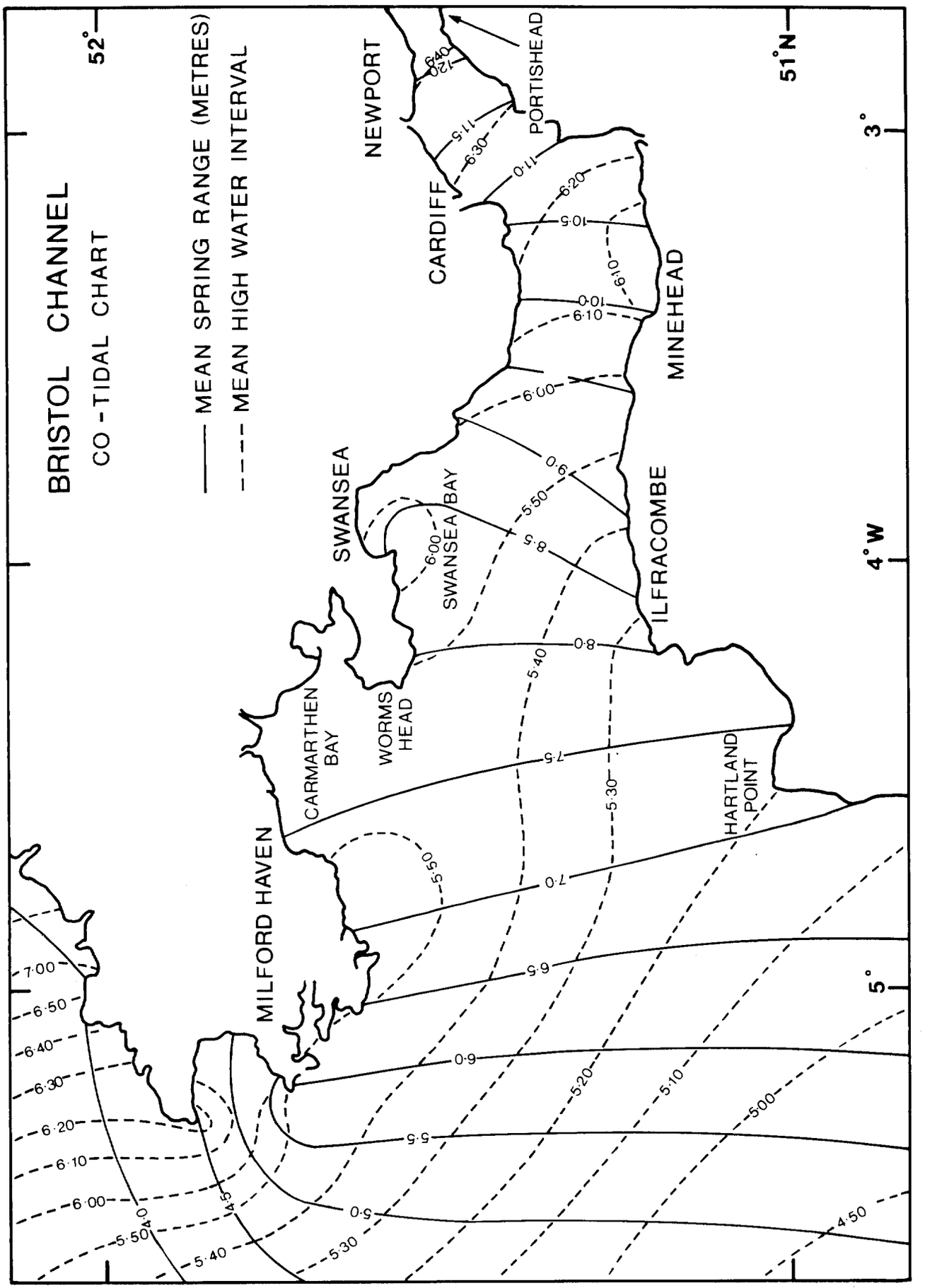
BRISTOL CHANNEL
CO-TIDAL CHART
MEAN SPRING RANGE (METRES)
MEAN HIGH WATER INTERVAL
52°
51°N
3°
4°W
5°
NEWPORT
CARDIFF
PORTISHEAD
SWANSEA
SWANSEA BAY
MINEHEAD
ILFRACOMBE
CARMARTHEN BAY
WORMS HEAD
MILFORD HAVEN
HARTLAND POINT
12.0
11.5
11.0
10.5
10.0
9.5
9.0
8.5
8.0
7.5
7.0
6.5
6.0
5.5
5.0
4.5
6.40
6.30
6.20
6.10
6.00
5.50
5.40
5.30
5.20
5.10
5.00
4.50
7.00
6.50
6.40
6.30
6.20
6.10
6.00
5.50
5.40

Fig. 2

FIGURE 3

Location of recording current meter moorings in Swansea Bay

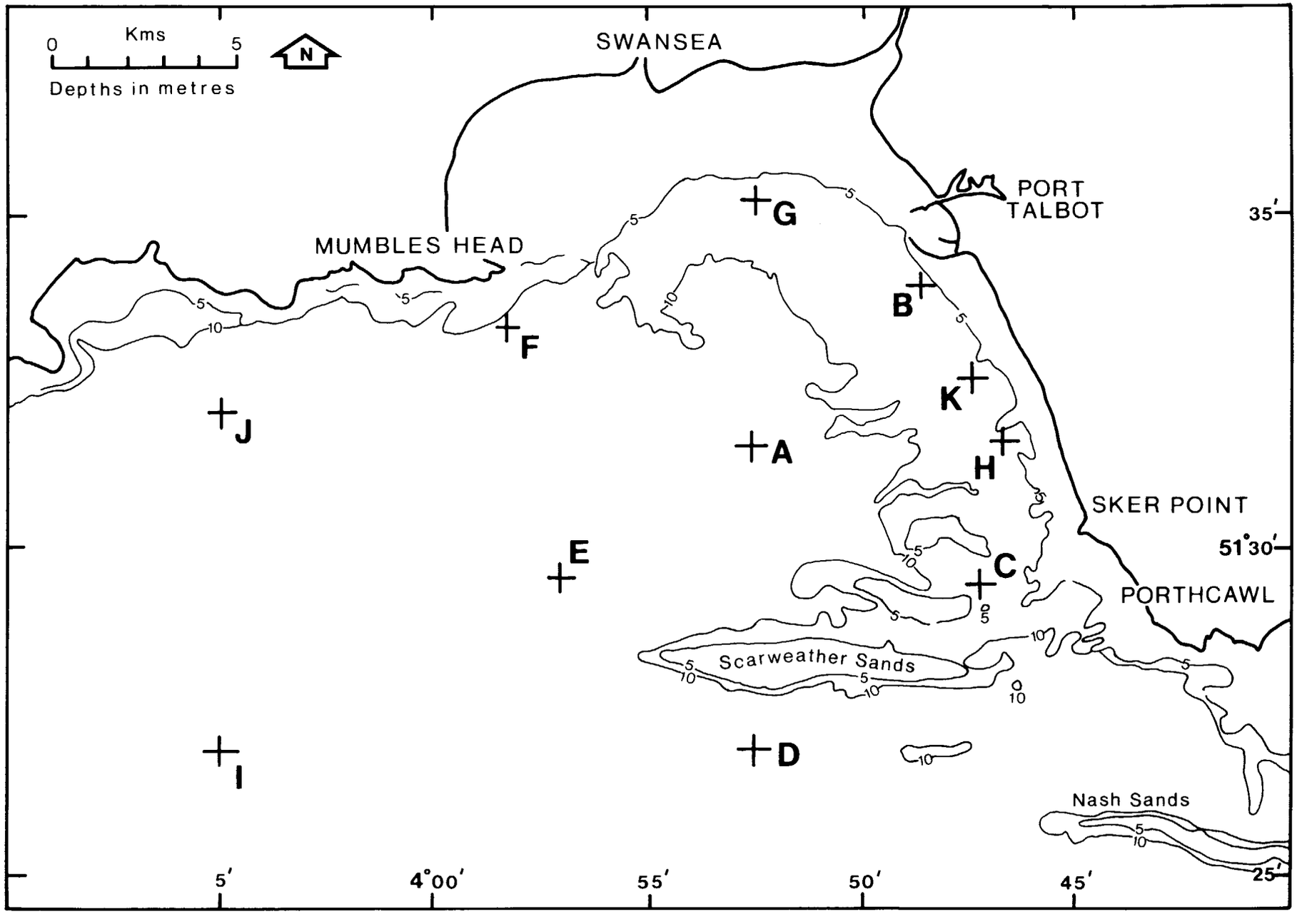
0
Kms
5
Depths in metres
N
SWANSEA
PORT
TALBOT
MUMBLES HEAD
G
B
F
K
J
A
H
SKER POINT
E
C
PORTHCAWL
Scarweather Sands
D
I
Nash Sands
35′
51°30′
25′
5′
4°00′
55′
50′
45′

Fig.3

FIGURE 4
The Plessey recording current meter

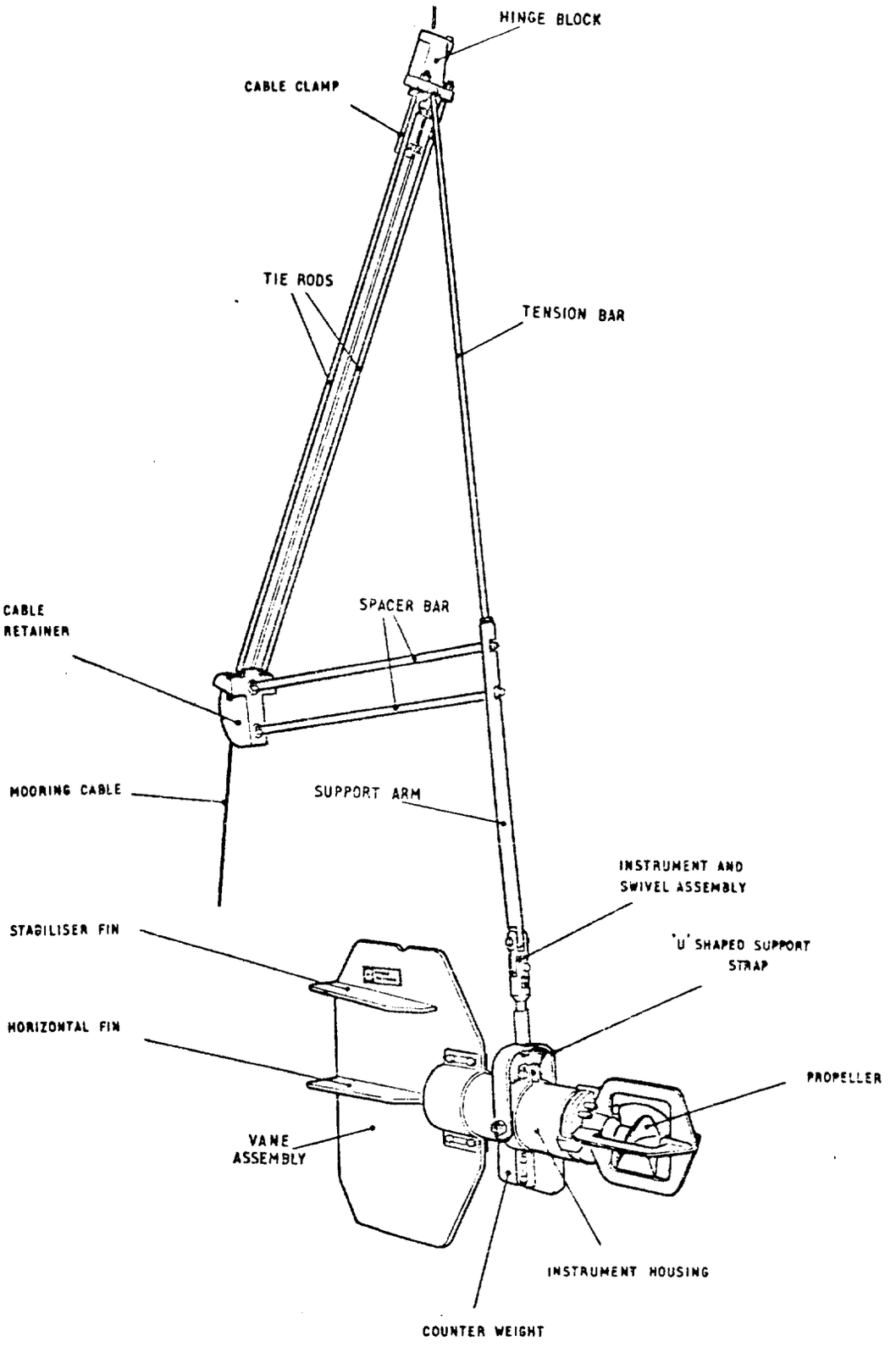

The Plessey recording current meter model M021

(Reproduced courtesy of the Plessey Company Ltd.)

Fig.4

FIGURE 5

Current meter mooring system

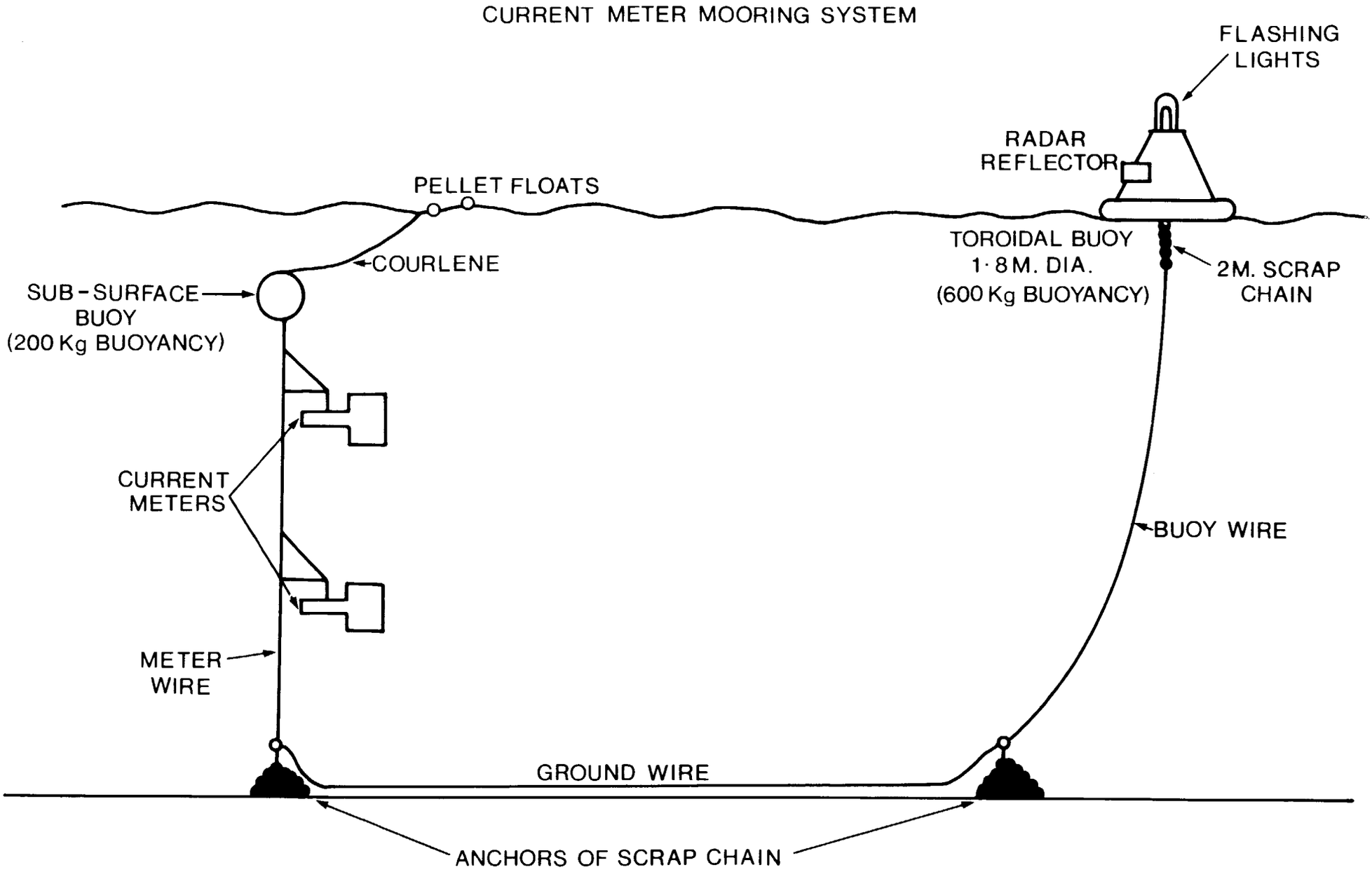
CURRENT METER MOORING SYSTEM
FLASHING LIGHTS
RADAR REFLECTOR
PELLET FLOATS
TOROIDAL BUOY 1·8M. DIA. (600 Kg BUOYANCY)
2M. SCRAP CHAIN
COURLENE
SUB-SURFACE BUOY (200 Kg BUOYANCY)
CURRENT METERS
BUOY WIRE
METER WIRE
GROUND WIRE
ANCHORS OF SCRAP CHAIN

Fig. 5

FIGURE 6

Tidal ellipses for the principal semi-diurnal (a) and quarter-diurnal (b) constituents in the mid-depth curr nts at Station A in Swansea Bay (record 232F6)

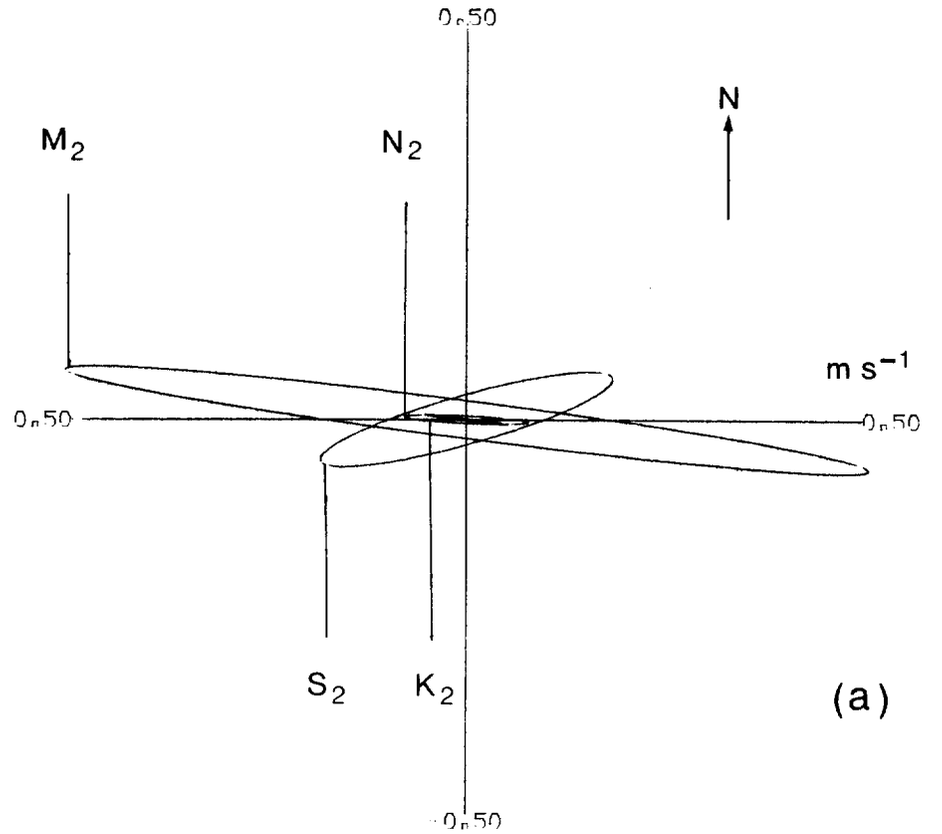

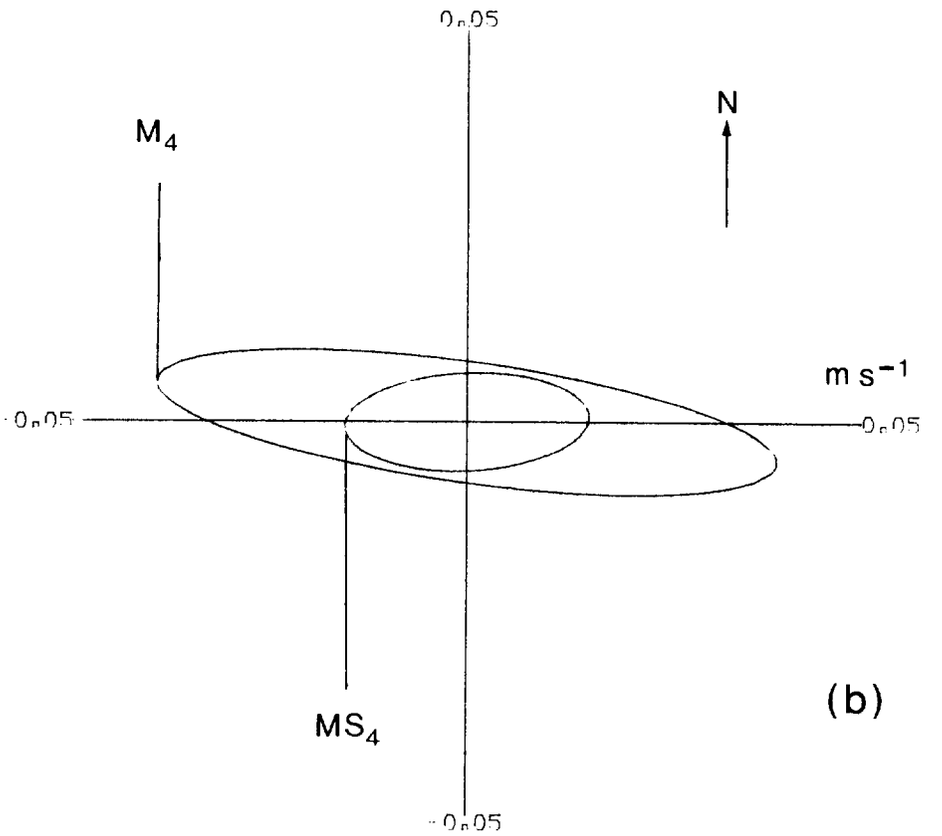

Fig.6

FIGURE 7

Tidal ellipses for the principal semi-diurnal (a) and quarter-diurnal (b) consituents in the near-bottom currents at Station A in Swansea Bay (record 629F6)

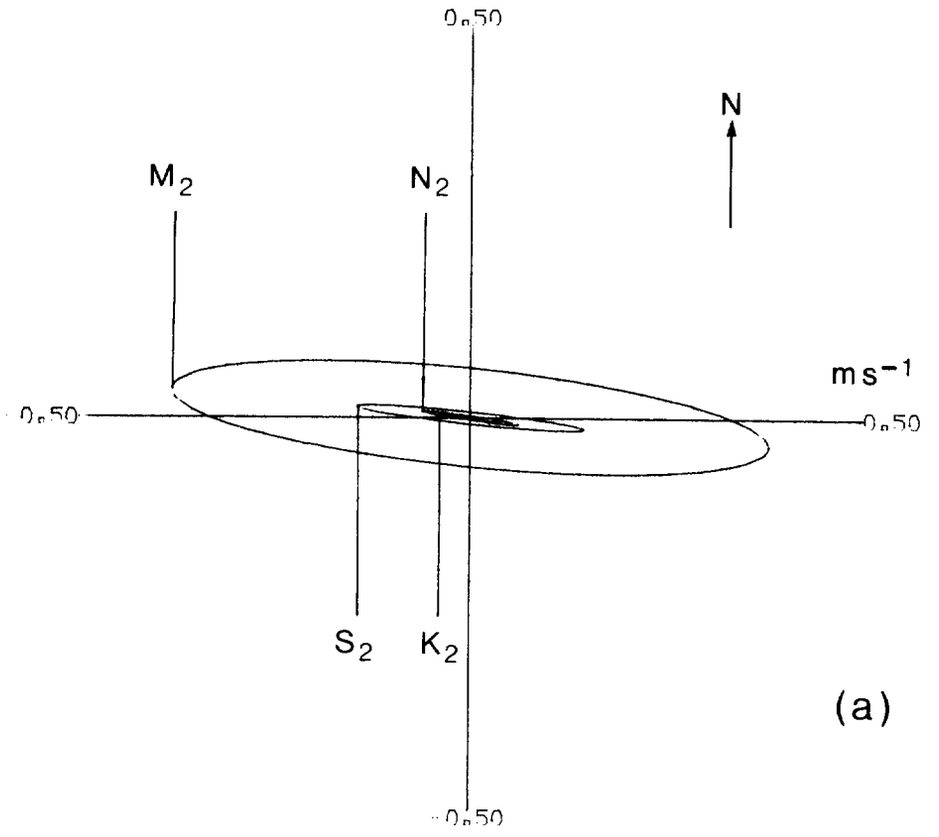

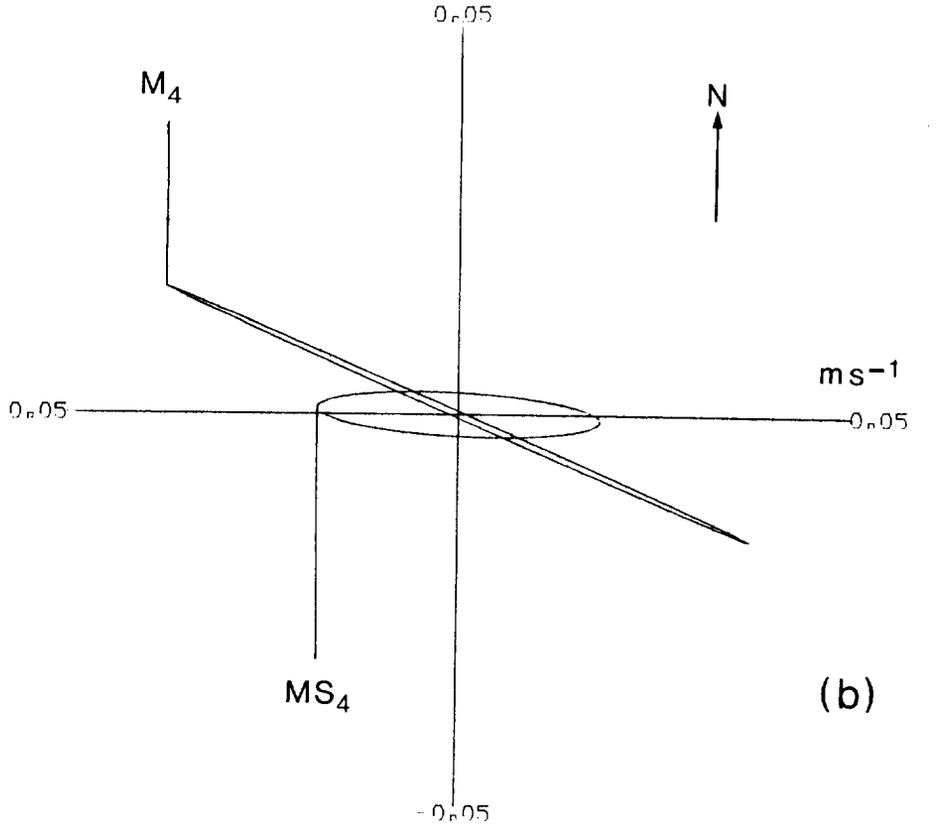

Fig.7

FIGURE 8

M_2 tidal current ellipse data:
(a) orientation ϕ_ω and phase g_ω (degrees),
(b) ellipticity as a percentage.
Negative and positive values indicate clockwise and anti-clockwise rotation respectively. Solid arrows indicate bottom currents, open arrows mid-depth currents

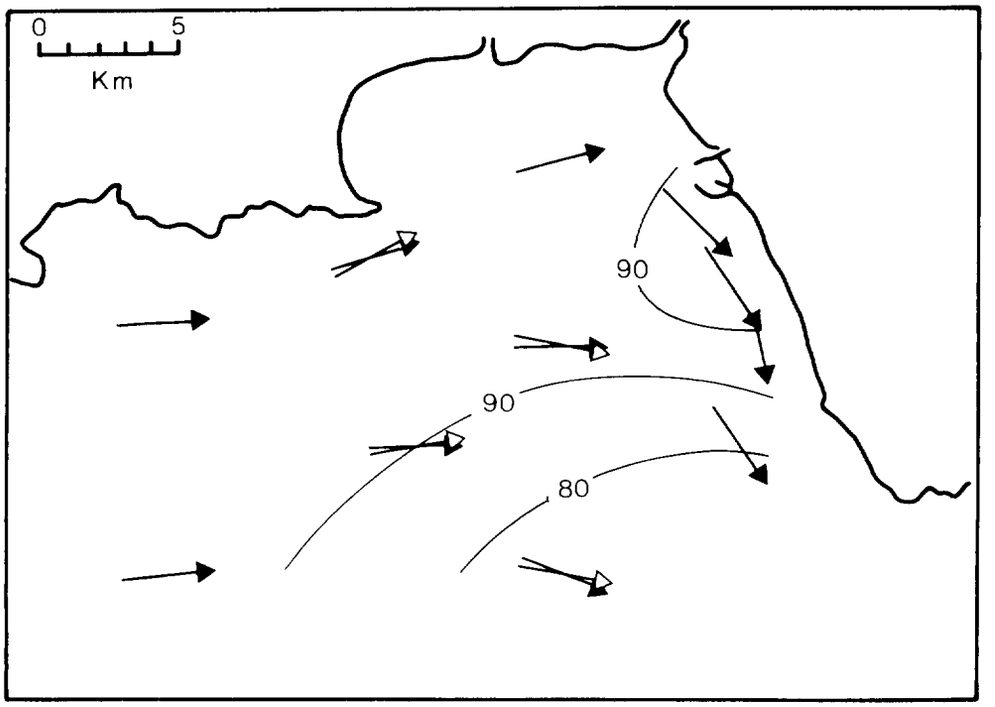

(a)

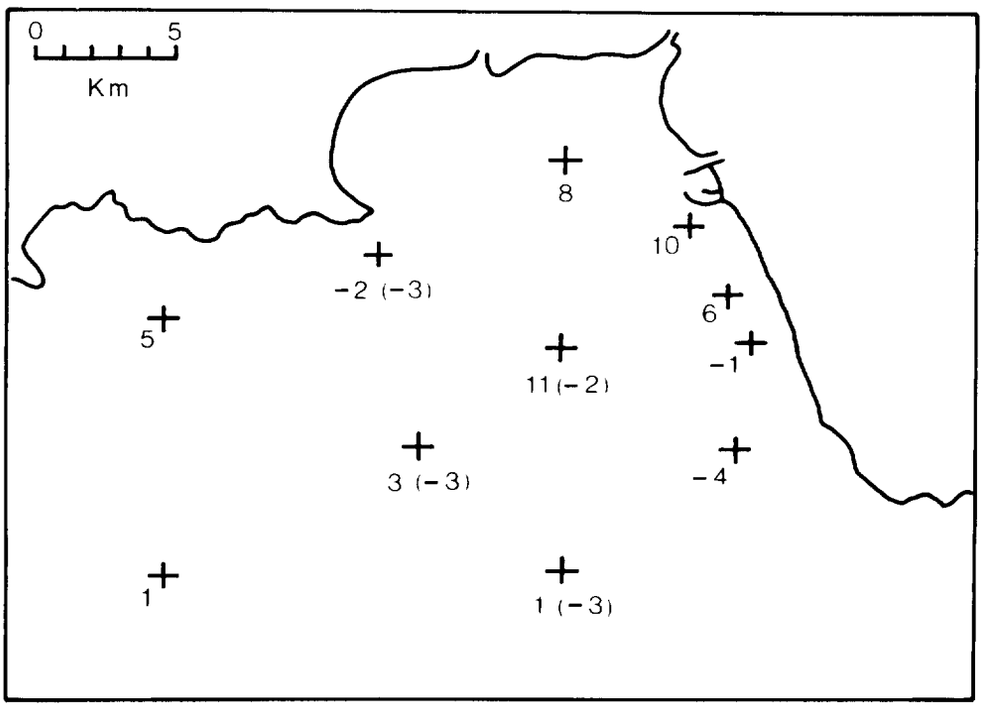

(b)

Fig. 8

FIGURE 9

Distribution of (a) M_2 and (b) S_2 tidal stream amplitudes (bottom currents only) in ms^{-1}

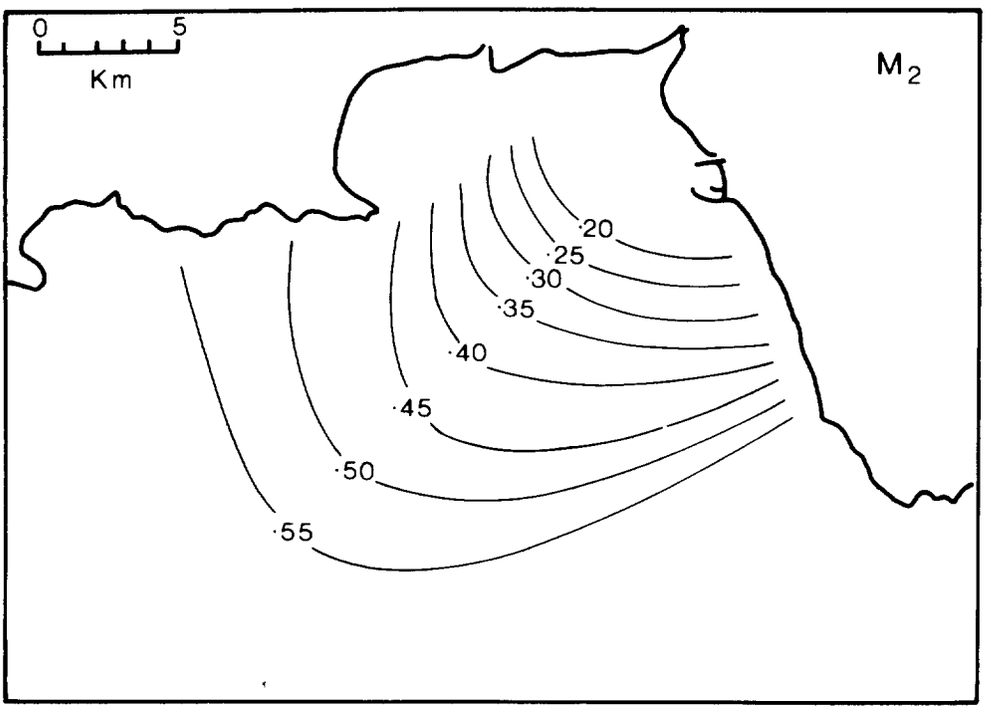

(a)

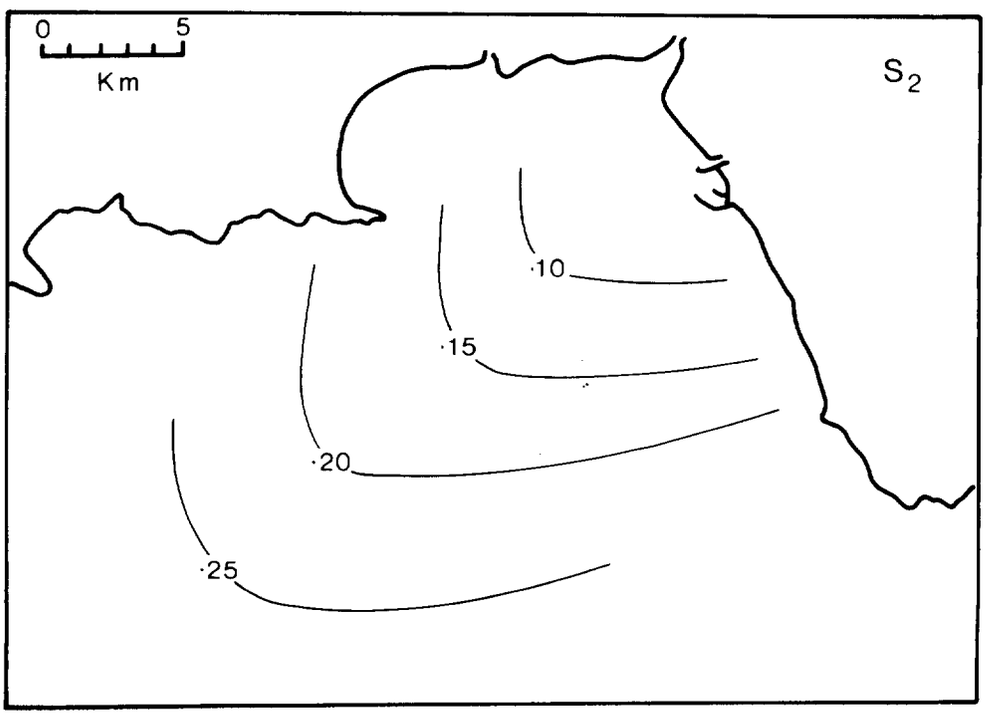

(b)

Fig. 9

FIGURE 10

Distribution of (a) M_4 tidal stream amplitude in ms^{-1} and (b) the ratio of M_4 to M_2 tidal stream amplitudes (bottom currents only)

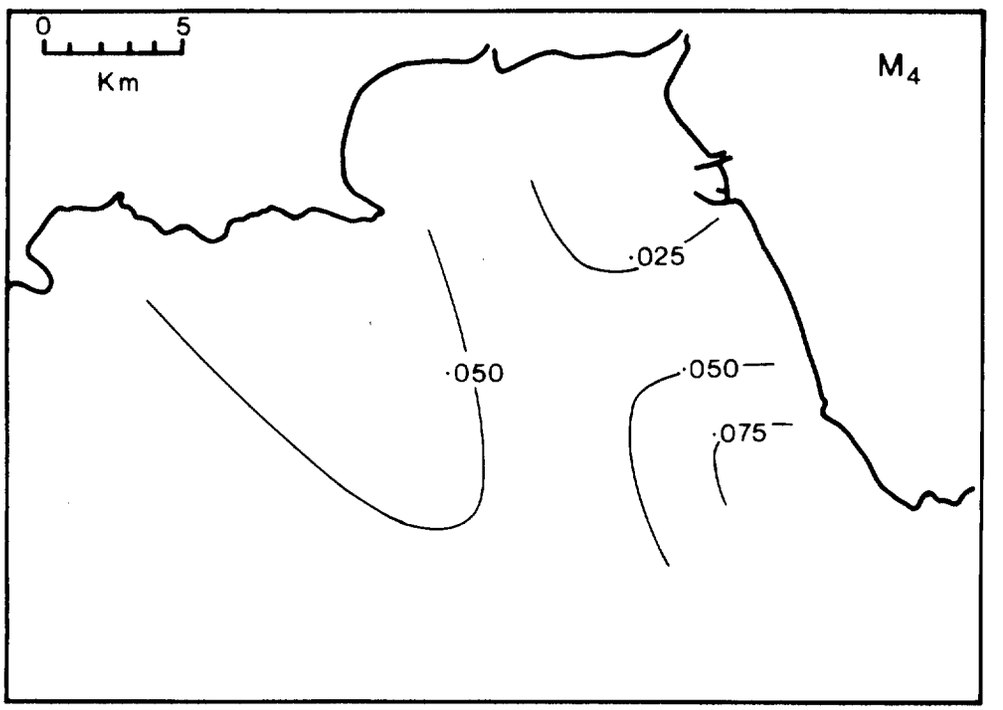

(a)

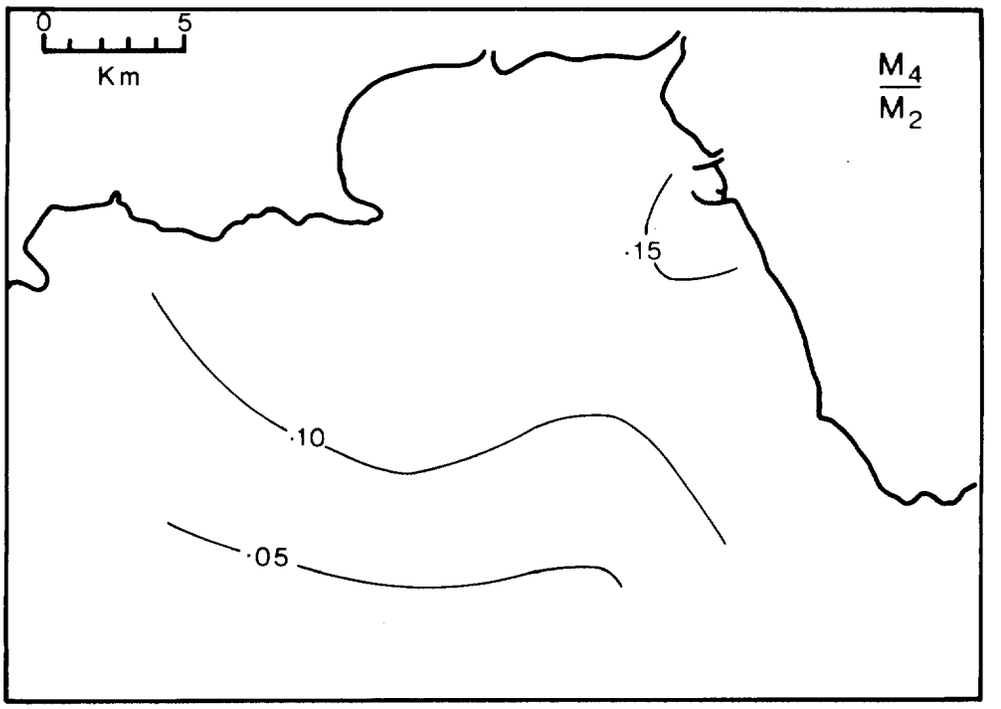

(b)

Fig.10

FIGURE 11

Distribution of (a) Spring tidal stream amplitude cubed and (b) Neap tidal stream amplitude cubed in m^2s^{-3} (bottom currents only)

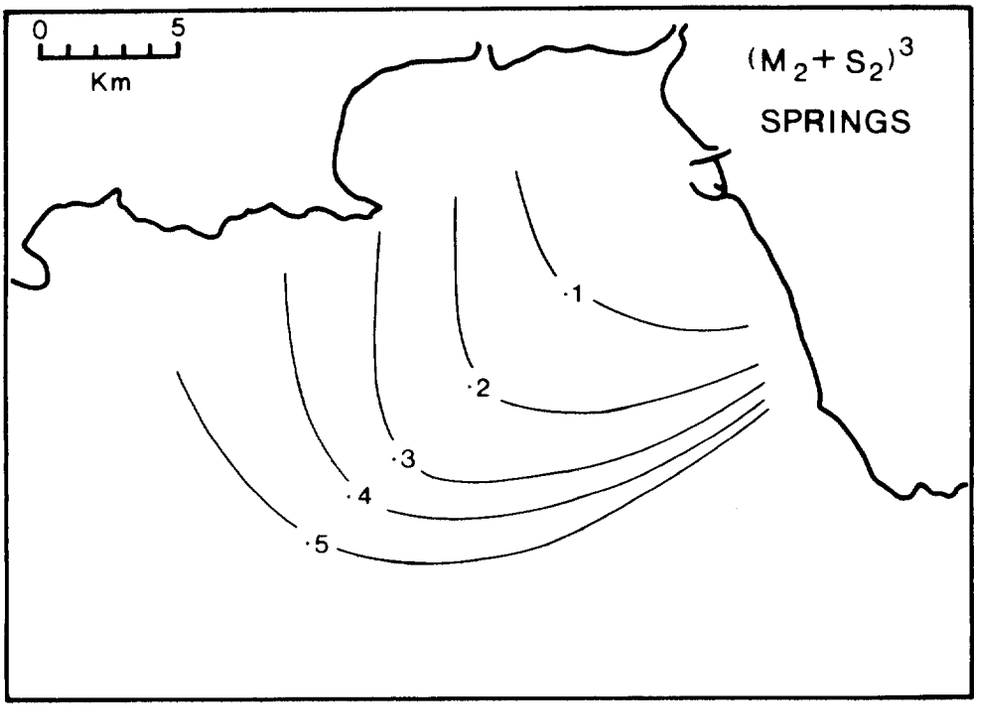

(a)

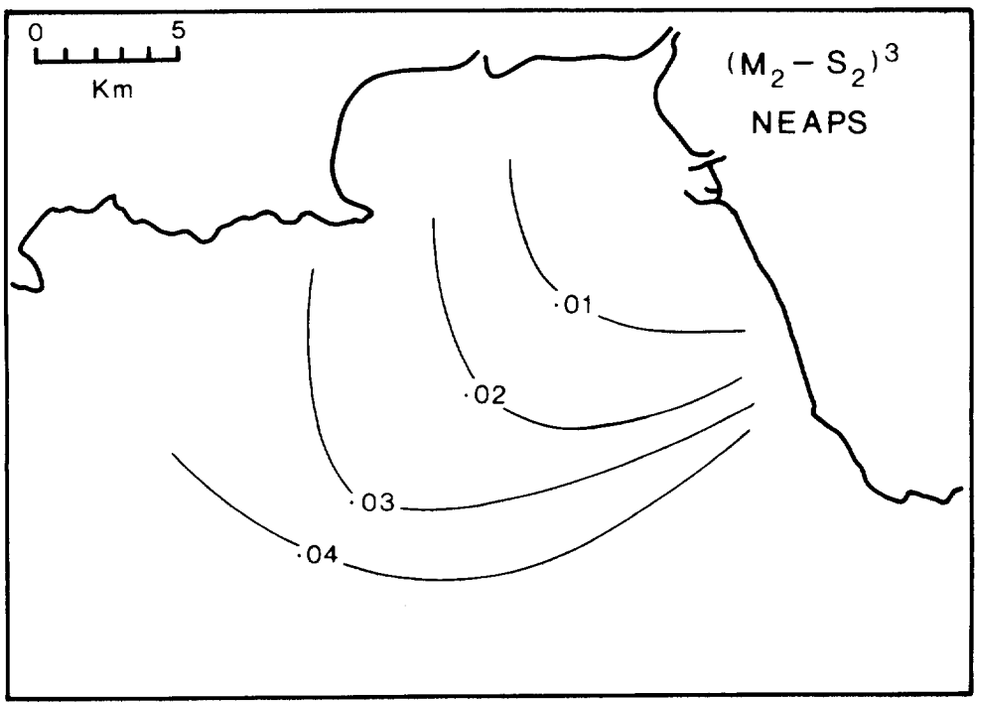

(b)

Fig.11

FIGURE 12

Scatter plot of residual flow estimates derived from 24 hour 50 minutes running means (y axis) and Doodson's X_0 filter (x axis). This figure shows high residual flows observed during the storm surge of 11 November 1977

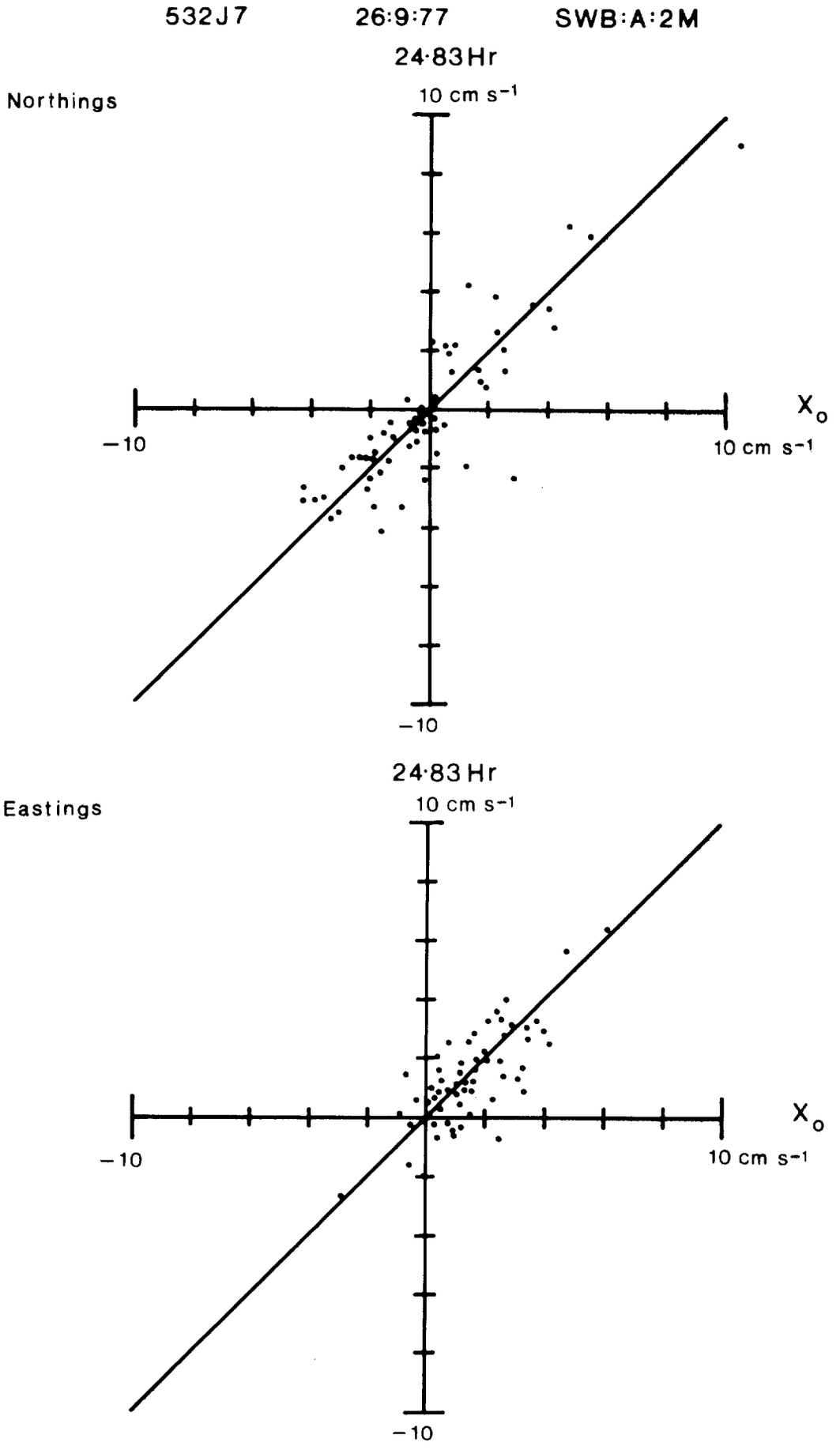
532J7 26:9:77 SWB:A:2M
24·83Hr
Northings
10 cm s⁻¹
−10
10 cm s⁻¹
X₀
−10
24·83Hr
Eastings
10 cm s⁻¹
−10
10 cm s⁻¹
X₀
−10

Fig.12

FIGURE 13

Scatter plot of residual flow estimates derived from 24 hour 50 minutes running means (y axis) and Doodson's X_0 filter (x axis). This figure shows quiescent residual flow values

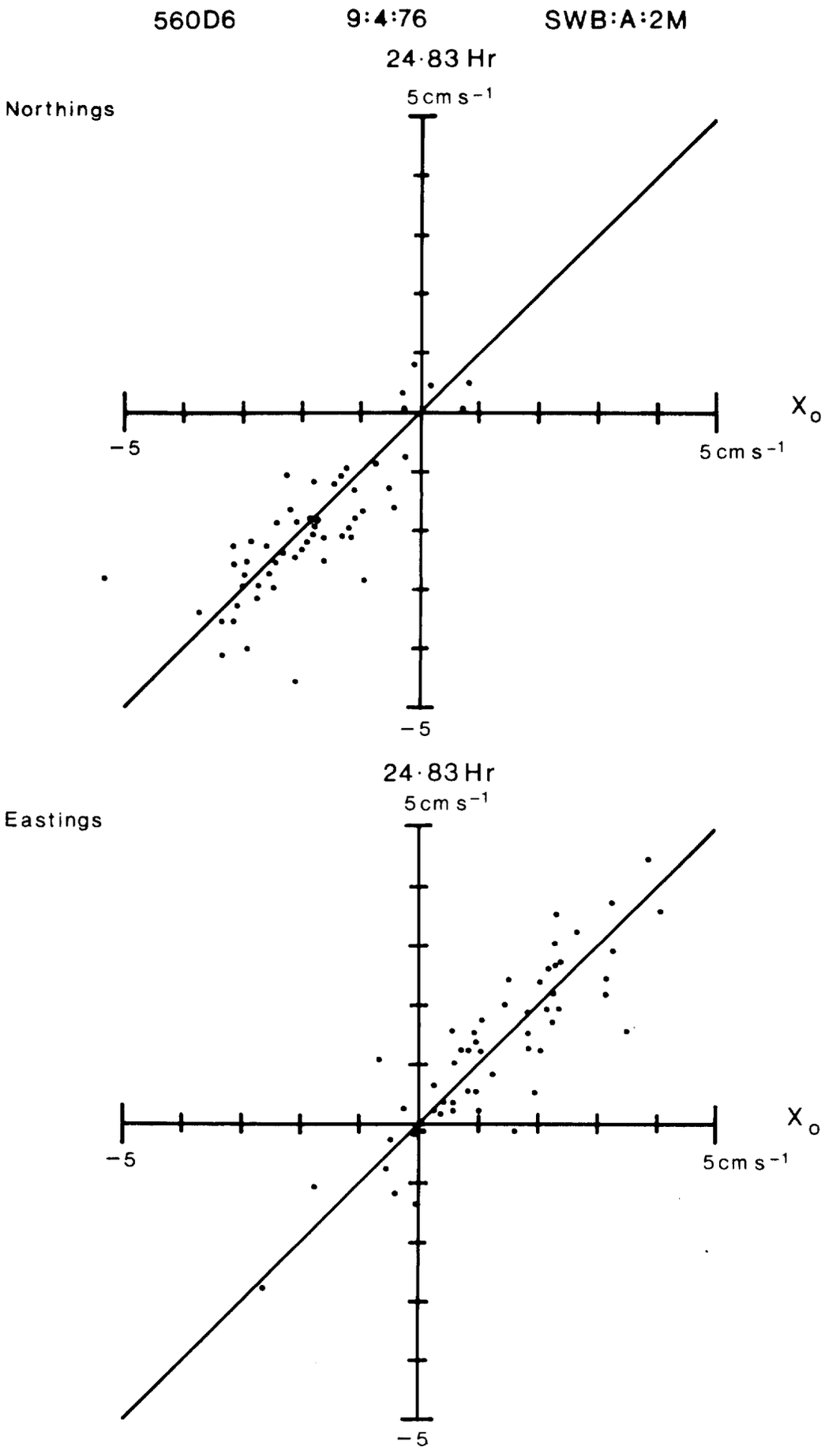
560D6 9:4:76 SWB:A:2M
24·83 Hr
Northings
5 cm s⁻¹
−5
5 cm s⁻¹
X_o
−5
24·83 Hr
Eastings
5 cm s⁻¹
−5
5 cm s⁻¹
X_o
−5

Fig.13

FIGURE 14

Summary of near-bottom (solid arrows) and mid-depth (open arrows) tidally induced residuals in Swansea Bay. Residual flow data have been presented in the manner suggested by Ramster et al (1978) and each measurement consists of a set of three figures indicating: the residual flow speed in cm s^{-1}, the steadiness factor $\mathcal{S}$ as a percentage and the length of the record in days (in that order)

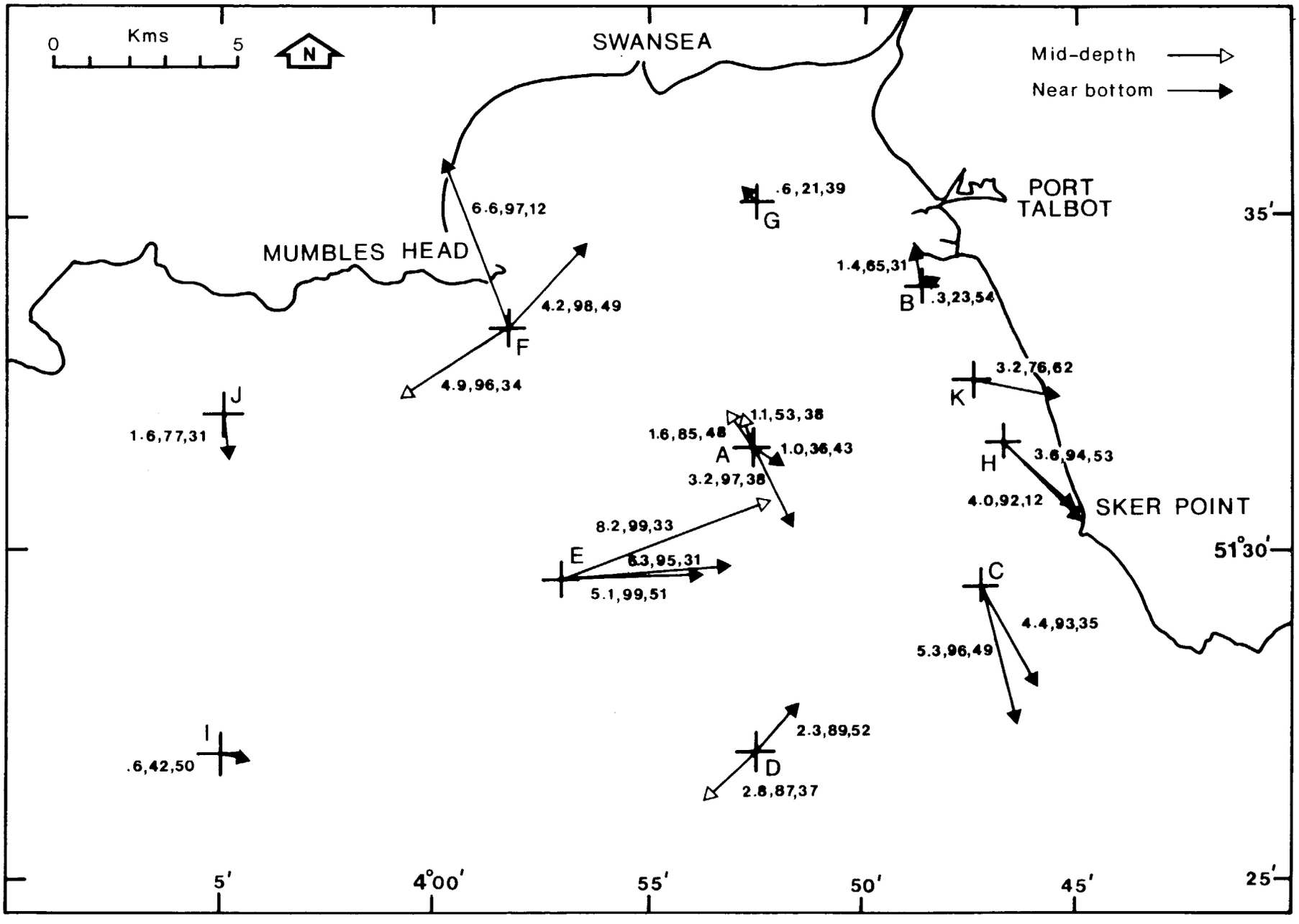
0 Kms 5
N
SWANSEA
Mid-depth
Near bottom
PORT TALBOT
MUMBLES HEAD
6.6,97,12
.6,21,39
G
1.4,65,31
B
.3,23,54
4.2,98,49
F
4.9,96,34
3.2,76,62
K
J
1.6,77,31
1.1,53,38
1.6,85,48
A
1.0,36,43
3.2,97,38
H
3.6,94,53
4.0,92,12
SKER POINT
8.2,99,33
E
8.3,95,31
5.1,99,51
C
4.4,93,35
5.3,96,49
I
.6,42,50
2.3,89,52
D
2.8,87,37
35'
51°30'
5'
4°00'
55'
50'
45'
25'

Fig.14

FIGURE 15

Progressive vector plot from Station A in Swansea Bay showing the residual flow at 10 m above the seabed in a NW direction. $\mathcal{B}$ is the steadiness factor expressed as a percentage

232F6 6:6:76 SWB:A:10M

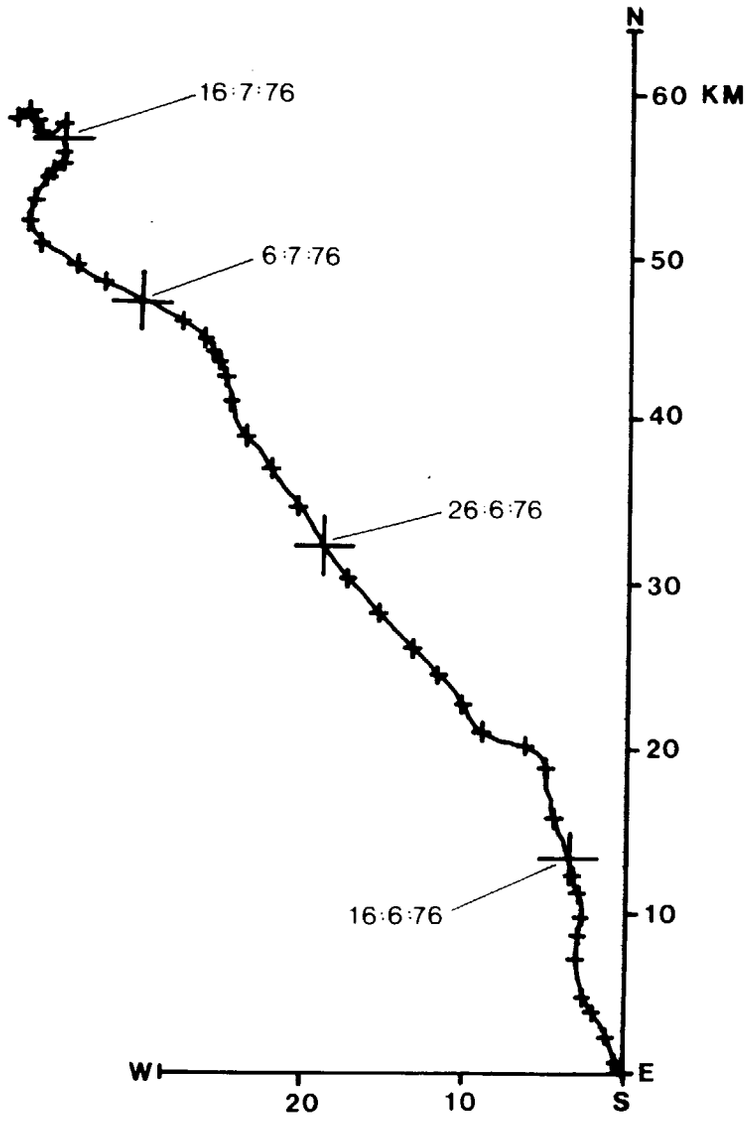

Fig.15

B = 84·64 %

FIGURE 16

Progressive vector plot from Station A in Swansea Bay showing the residual flow at 2 m above the seabed in a SE direction. This record was simultaneous with that shown in Figure 15. $\mathcal{B}$ is the steadiness factor expressed as a percentage.

629F6 6:6:76 SWB:A:2M

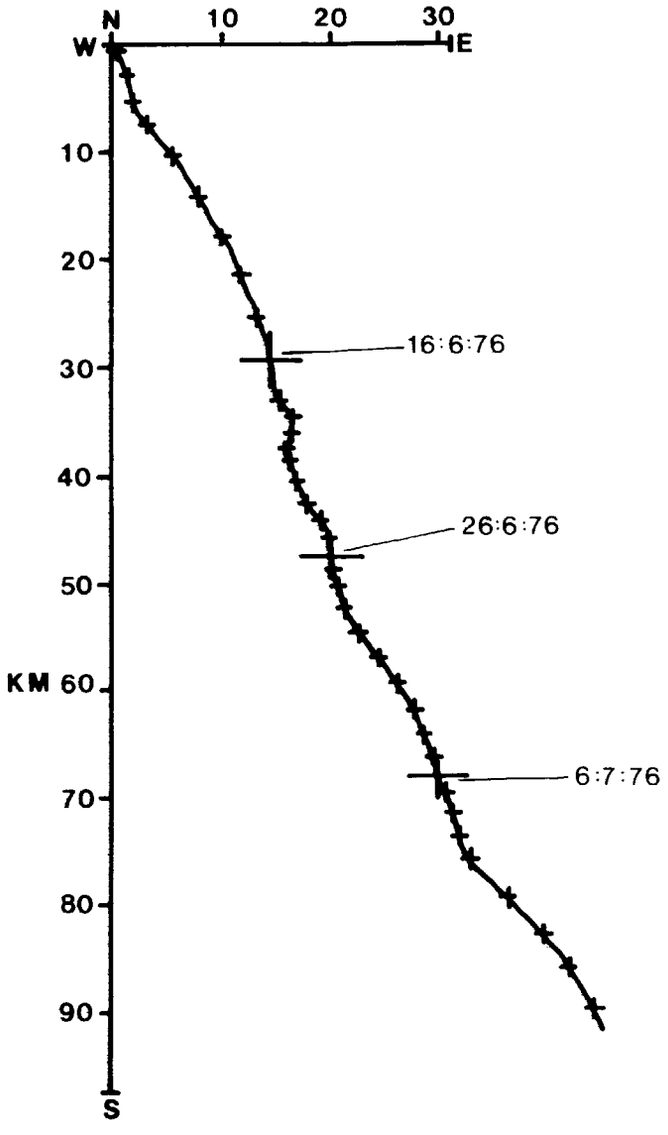

B = 97·07 %

Fig.16

FIGURE 17

A 90 day data set illustrating the effects of meteorological forcing on the residual circulation and tidal elevations in Swansea Bay and including the November 1977 storm surge. This Figure shows the onshore (55°) and alongshore (325°) components of the residual flow, $\bar{u}_x$ and $\bar{u}_y$ respectively, at heights of 2m and 10 m above the seabed; the mean wind speed squared as $\overline{W_x|W_x|}$ and $\overline{W_y|W_y|}$; the mean atmospheric pressure $\bar{p}_R$ at Rhoose and the mean residual tidal elevations $\bar{\zeta}_R$ at Swansea (see Figure 18 for definition of terms)

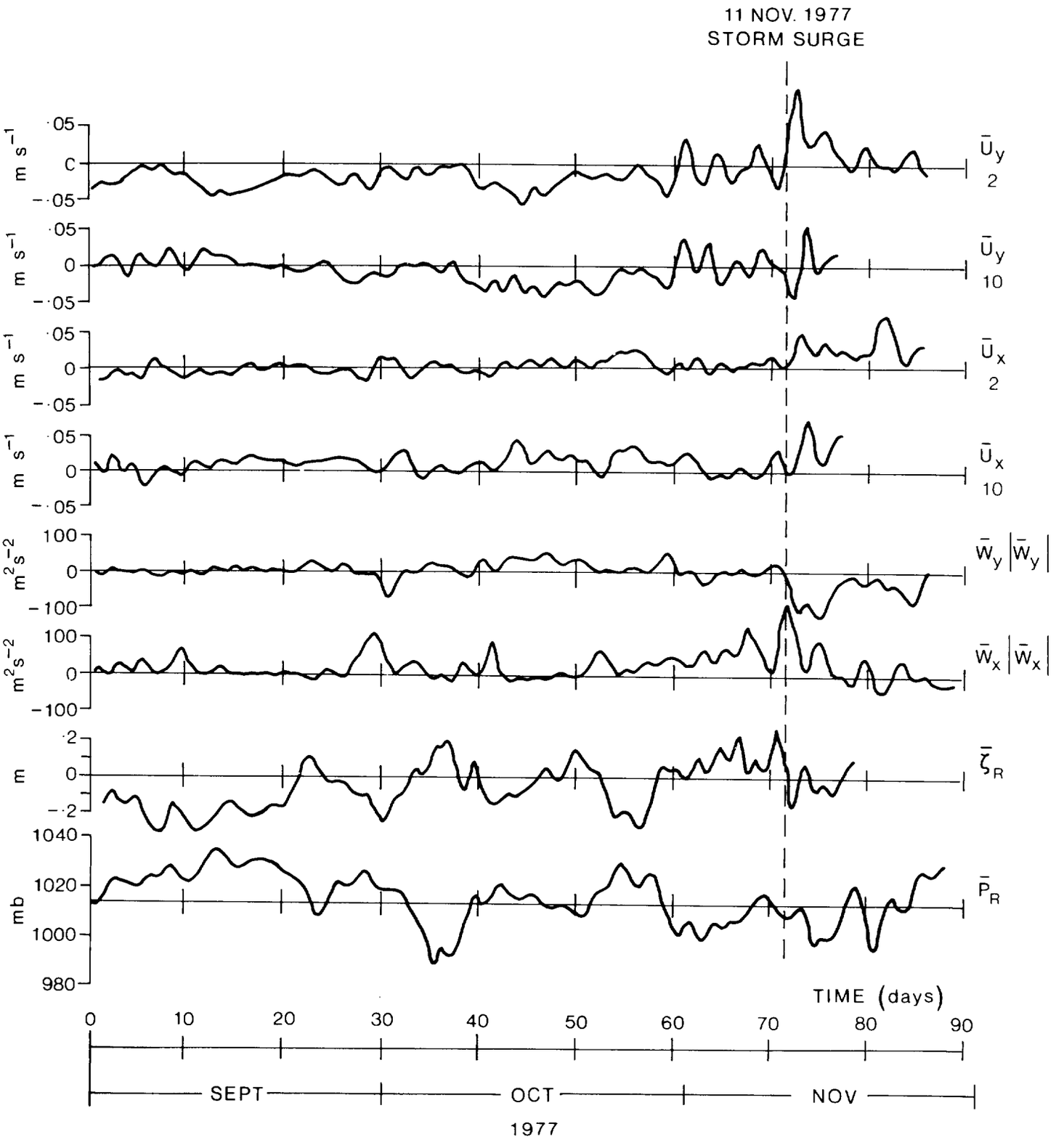
11 NOV. 1977
STORM SURGE
m s⁻¹
·05
0
-·05
$\bar{U}_y$ 2
$\bar{U}_y$ 10
$\bar{U}_x$ 2
$\bar{U}_x$ 10
m²s⁻²
100
-100
$\bar{W}_y|\bar{W}_y|$
$\bar{W}_x|\bar{W}_x|$
m
·2
-·2
$\bar{\zeta}_R$
mb
1040
1020
1000
980
$\bar{P}_R$
TIME (days)
0 10 20 30 40 50 60 70 80 90
SEPT
OCT
NOV
1977

Fig. 17

FIGURE 18

Definition of terms used in meteorological forcing studies; this Figure shows the onshore-offshore and alongshore components of the residual currents $\bar{u}_x$ and $\bar{u}_y$, the wind speed $\bar{w}_x$ and $\bar{w}_y$ and the atmospheric pressures at Aberporth, Hartland Point and Rhoose, p_A, p_H and p_R respectively. Only p_R has been used in this study

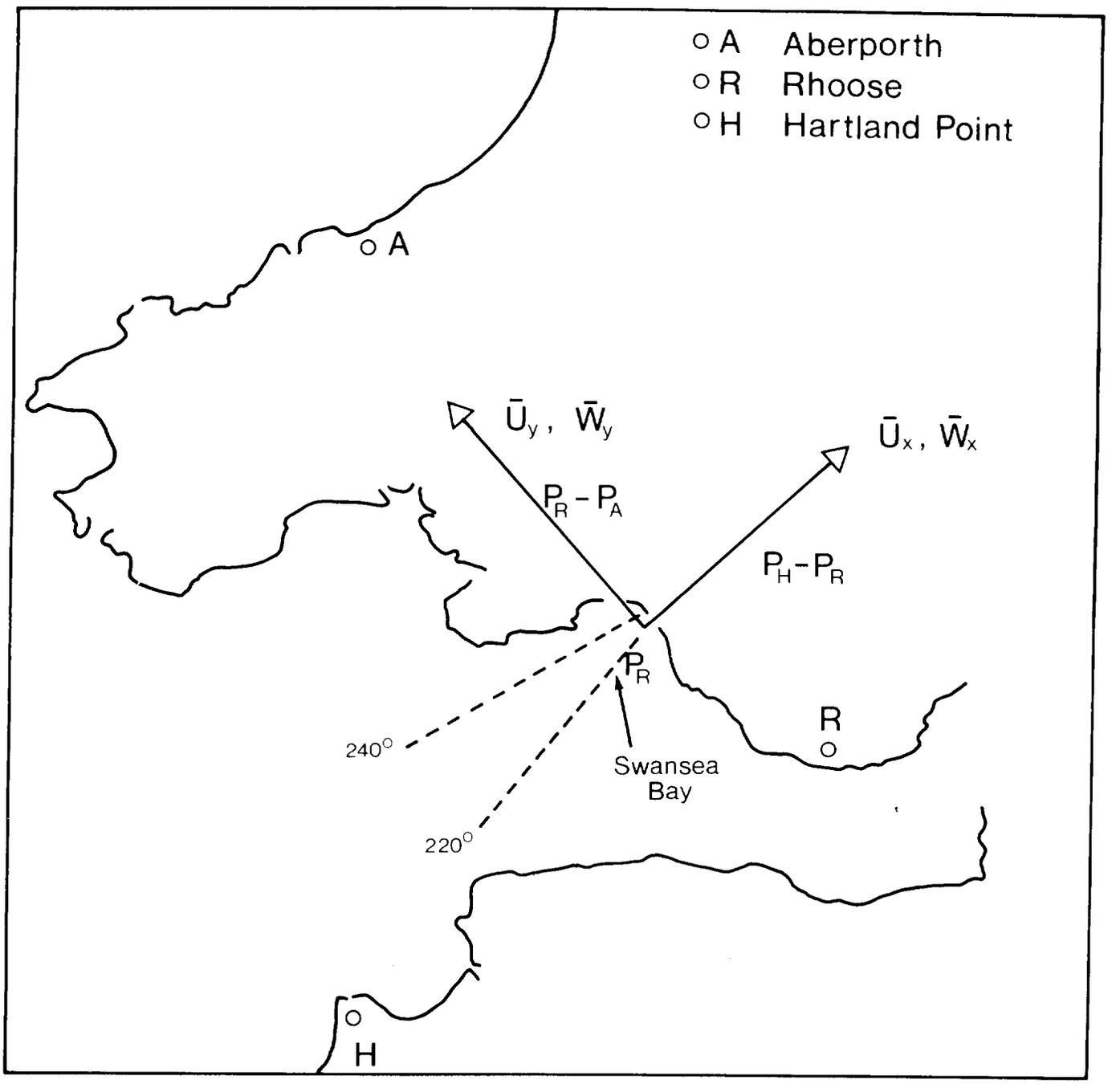
o A Aberporth
o R Rhoose
o H Hartland Point
o A
$\bar{U}_y$, $\bar{W}_y$
$\bar{U}_x$, $\bar{W}_x$
$P_R - P_A$
$P_H - P_R$
P_R
R
240°
220°
Swansea Bay
H

Fig.18

FIGURE 19

A progressive vector plot of the residual water movements at 10 m above the seabed, at Station A in Swansea Bay, before, during, and after the November 1977 storm surge

667J7 26:9:77 SWB:A:10M

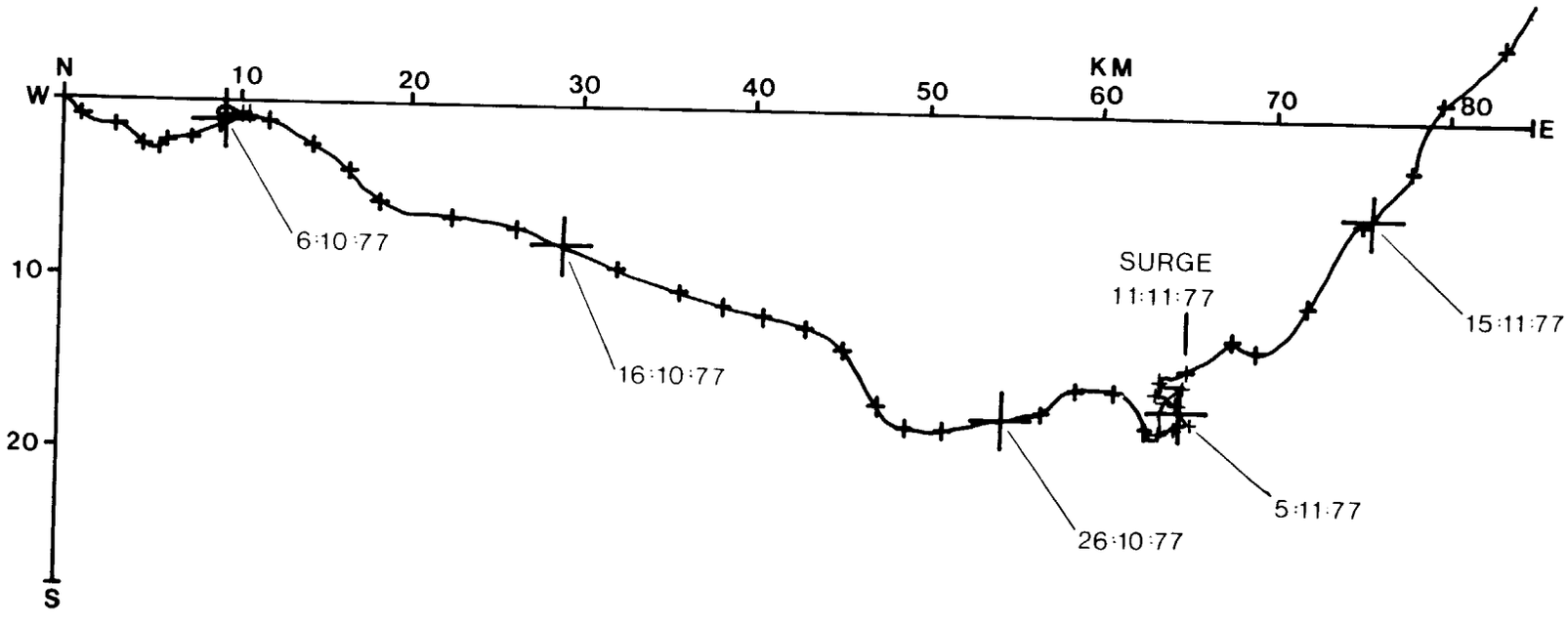

B = 68·08 %

Fig.19

FIGURE 20

A progressive vector plot of the residual water movements at 2 m above the seabed, at Station A in Swansea Bay, before, during, and after the November 1977 storm surge

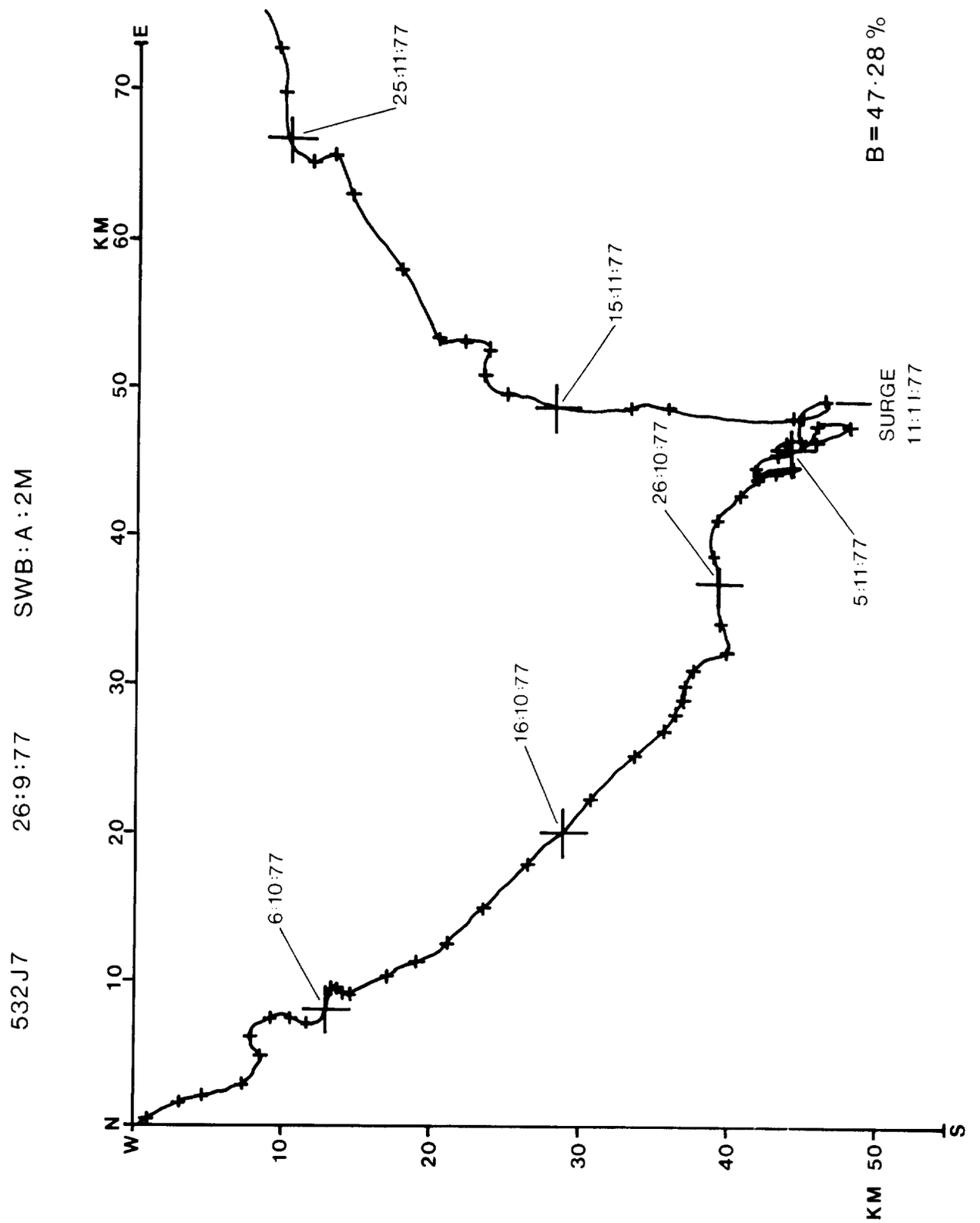
532J7
26:9:77
SWB:A:2M
B=47·28 %
N
W
E
S
KM
10
20
30
40
50
60
70
6:10:77
16:10:77
26:10:77
5:11:77
15:11:77
25:11:77
SURGE
11:11:77

Fig.20

FIGURE 21

The location of surface salinity measurements and salinity and temperature profiles in Swansea Bay (data obtained by the Welsh National Water Development Authority)

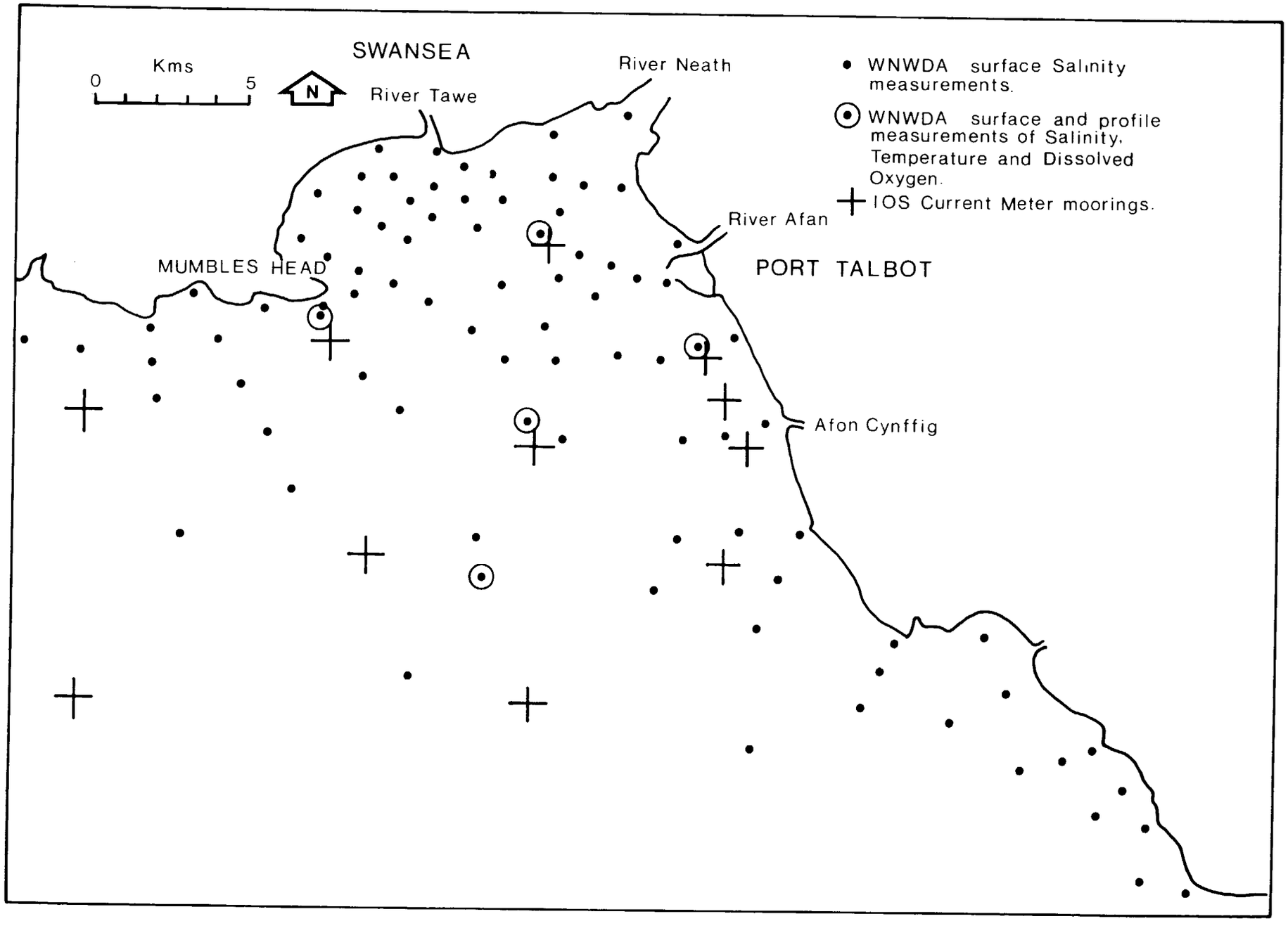
SWANSEA
Kms
0
5
N
River Tawe
River Neath
River Afan
MUMBLES HEAD
PORT TALBOT
Afon Cynffig
WNWDA surface Salinity measurements.
WNWDA surface and profile measurements of Salinity, Temperature and Dissolved Oxygen.
IOS Current Meter moorings.

Fig. 21

FIGURE 22

Summer surface salinity distributions, in parts per thousand (0/00), for (a) HW, (b) Ebb, (c) LW and (d) Flood stages of the tidal cycle illustrating the effects of freshwater discharges at the head of the Bay

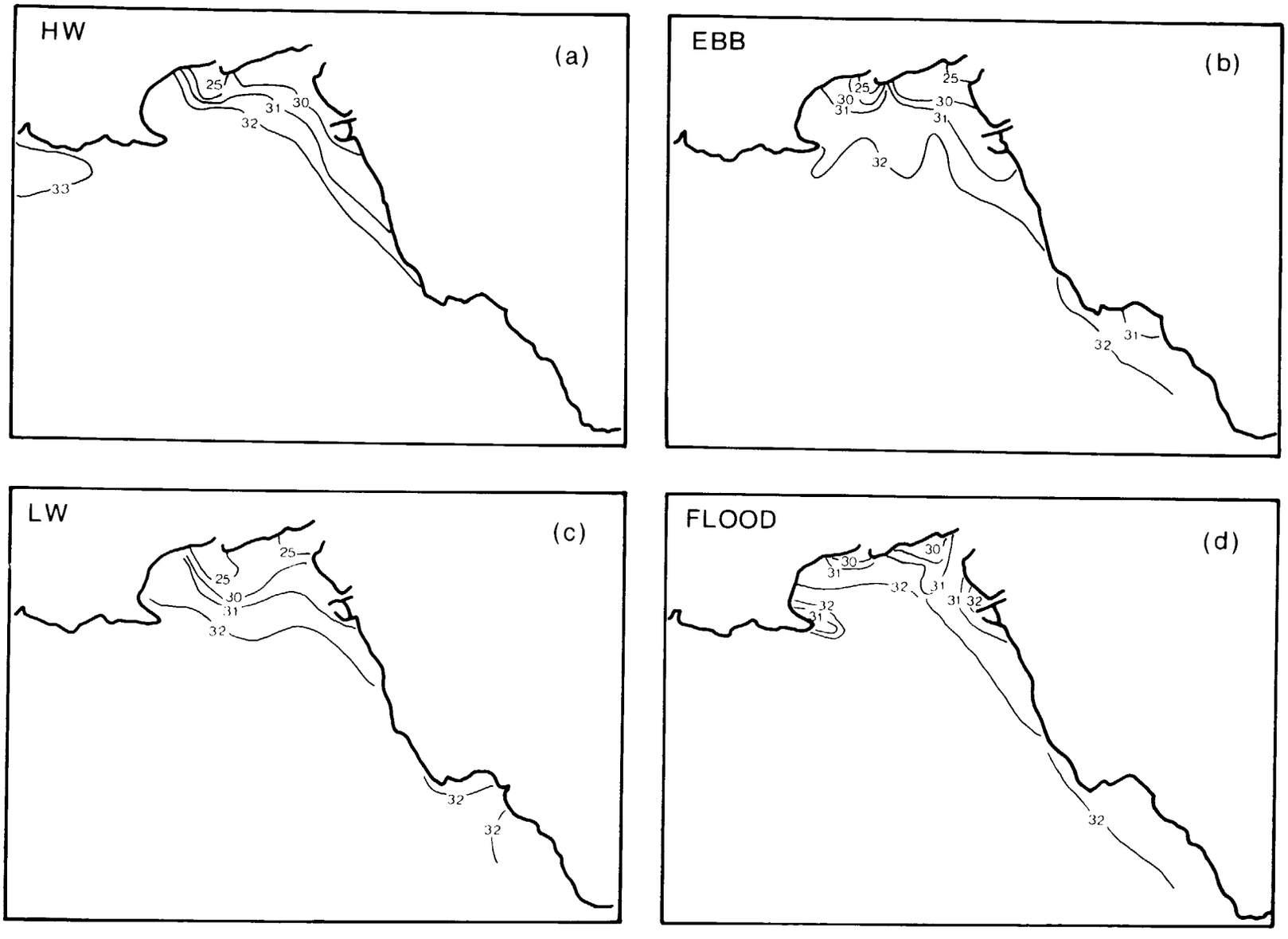
HW
(a)
25
30
31
32
33
EBB
(b)
25
25
30
30
31
31
32
32
31
LW
(c)
25
25
30
31
32
32
32
FLOOD
(d)
30
30
31
32
31
31
32
32
31
32

Fig.22

FIGURE 23

Winter surface salinity distributions, in parts per thousand (0/00), for (a) HW, (b) Ebb, (c) LW and (d) Flood stages of the tidal cycle illustrating the intrusion of more saline oceanic water (see the 33 0/00 isohaline) into the area

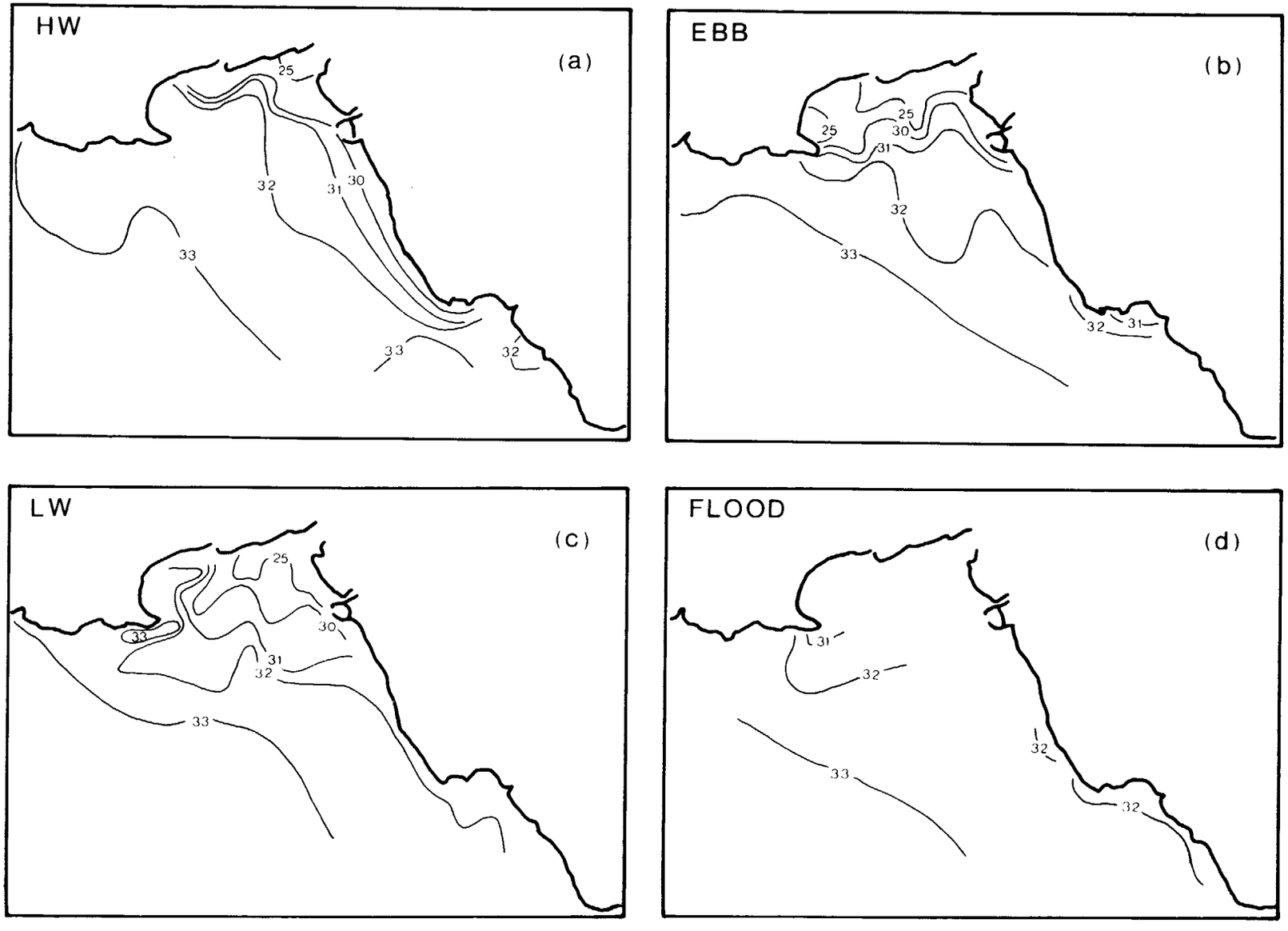
HW
(a)
25
32
31
30
33
33
32
EBB
(b)
25
25
30
31
32
33
32
31
LW
(c)
25
30
33
31
32
33
FLOOD
(d)
31
32
32
33
32

Fig. 23

FIGURE 24

Salinity in parts per thousand (0/00), time series at Stations A, B and G illustrating horizontal and vertical stratification effects

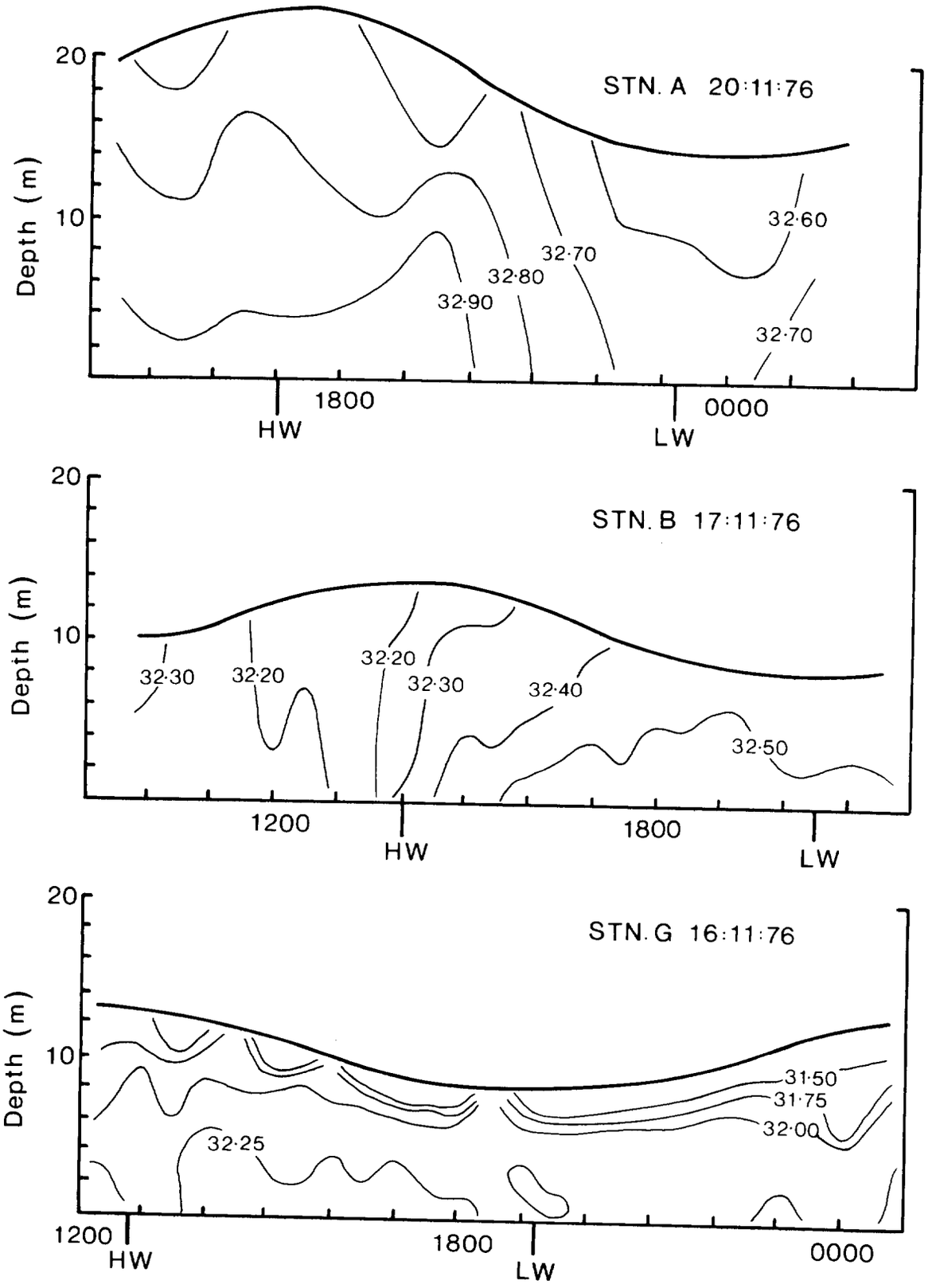
STN. A 20:11:76
Depth (m)
20
10
32·60
32·70
32·80
32·90
32·70
1800
HW
0000
LW
STN. B 17:11:76
Depth (m)
20
10
32·30
32·20
32·20
32·30
32·40
32·50
1200
HW
1800
LW
STN. G 16:11:76
Depth (m)
20
10
31·50
31·75
32·00
32·25
1200
HW
1800
LW
0000

Fig. 24

FIGURE 25

Isopycnal (σ_t) spacing and orientation determined from salinity and temperature measurements at Stations, A, B and G.
$X_1 X_2$ is the section along which density currents have been calculated

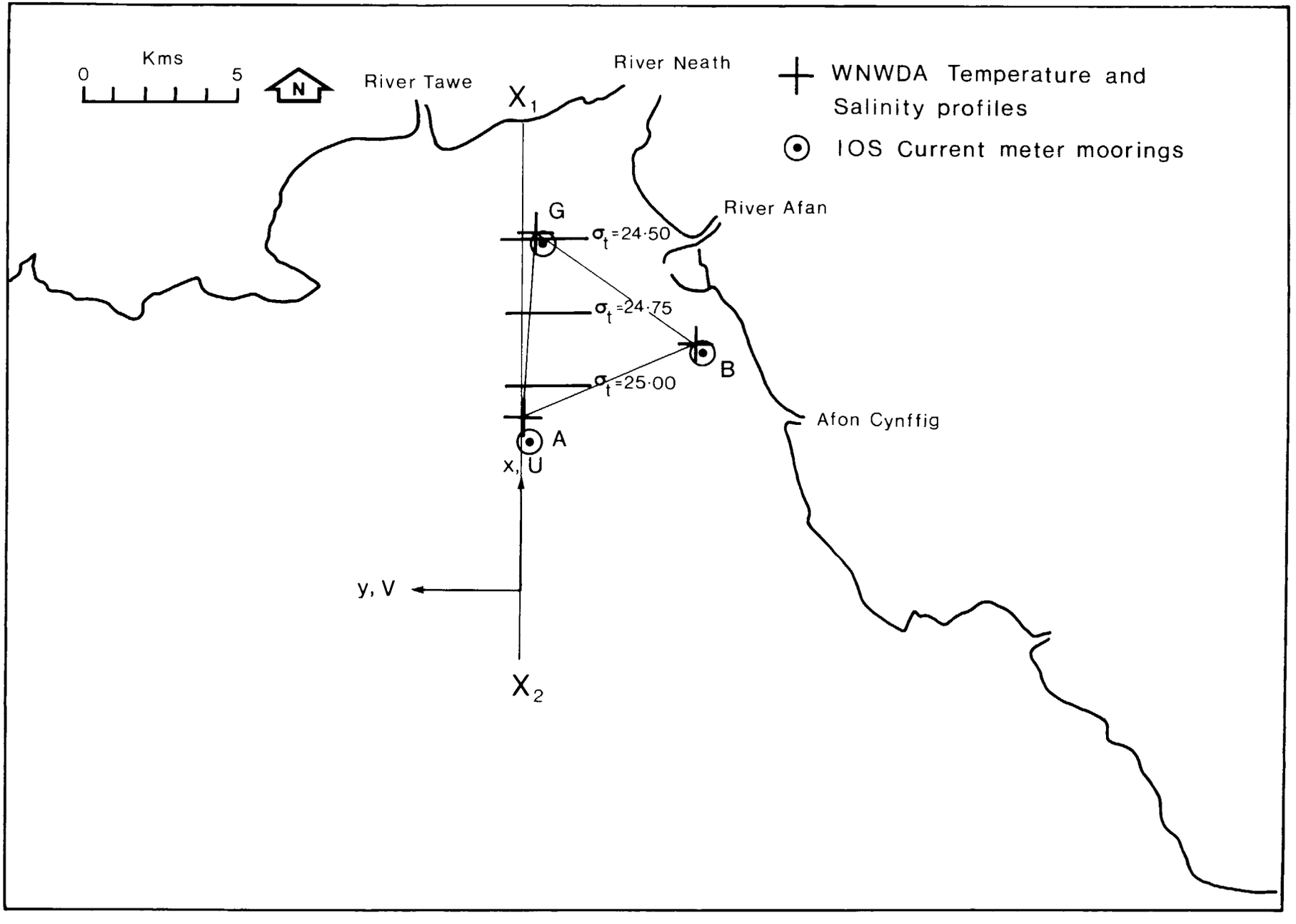
Kms
0
5
N
River Tawe
River Neath
River Afan
Afon Cynffig
WNWDA Temperature and Salinity profiles
IOS Current meter moorings
X1
X2
G
B
A
σt=24·50
σt=24·75
σt=25·00
x, U
y, V

Fig. 25

FIGURE 26

Details of the bathymetry along section $X_1 X_2$ showing the positions of temperature and salinity measurements and current meter moorings. x, y, z, u and v are defined as shown, q is the river discharge parameter, h the mean depth and ζ the tidal elevation

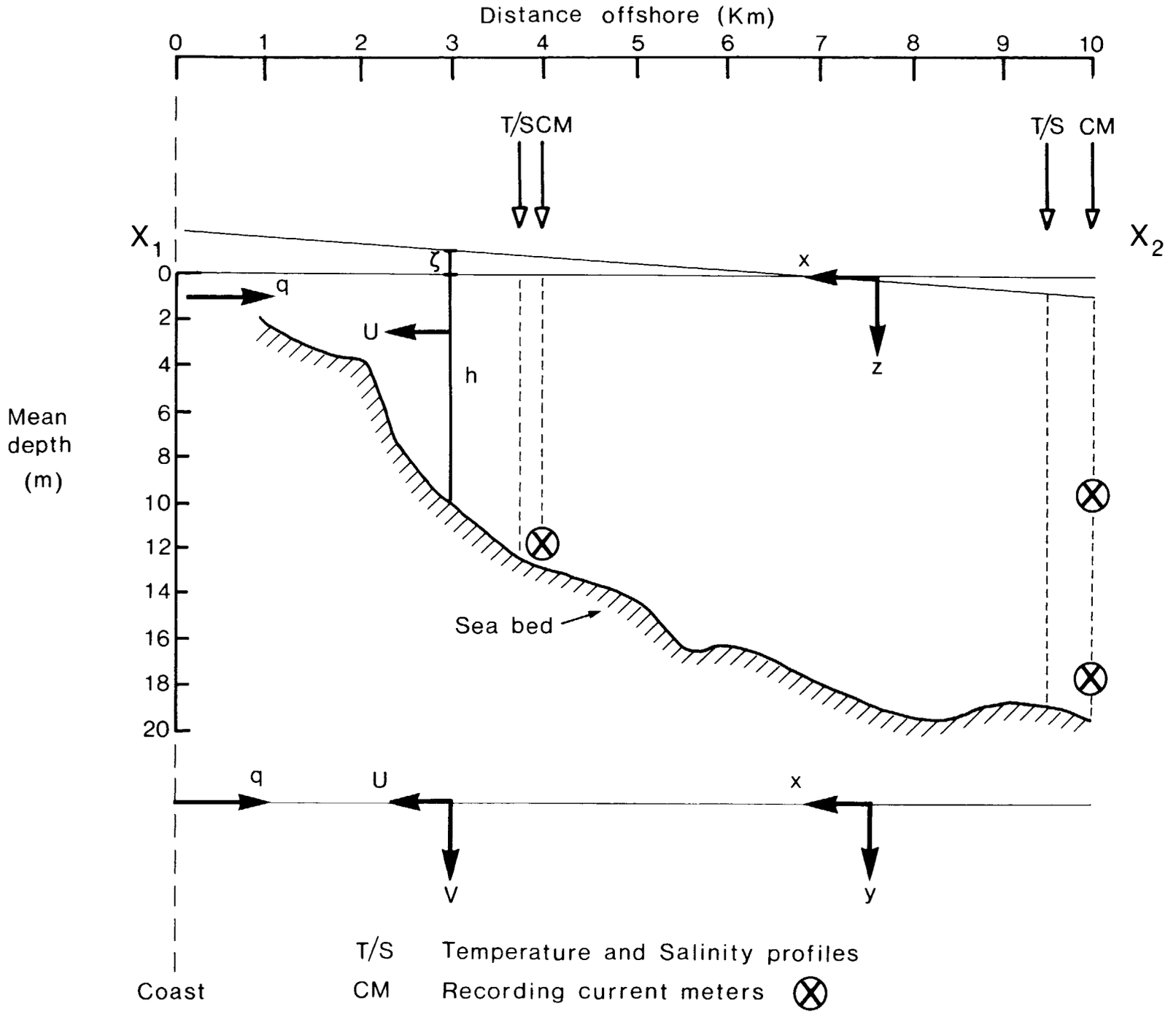
Distance offshore (Km)
0
1
2
3
4
5
6
7
8
9
10
T/SCM
T/S CM
X1
X2
ζ
x
q
U
h
z
Mean depth (m)
0
2
4
6
8
10
12
14
16
18
20
Sea bed
q
U
x
V
y
Coast
T/S Temperature and Salinity profiles
CM Recording current meters

Fig.26

FIGURE 27

The distribution of resultant surface (V_s) and bottom (V_b) density currents along section X_1X_2 for values of Λ = 1, 2 and 4. The directions θ_s and θ_b of the resultant currents are measured anti-clockwise from the x axis in Figures 25 and 26

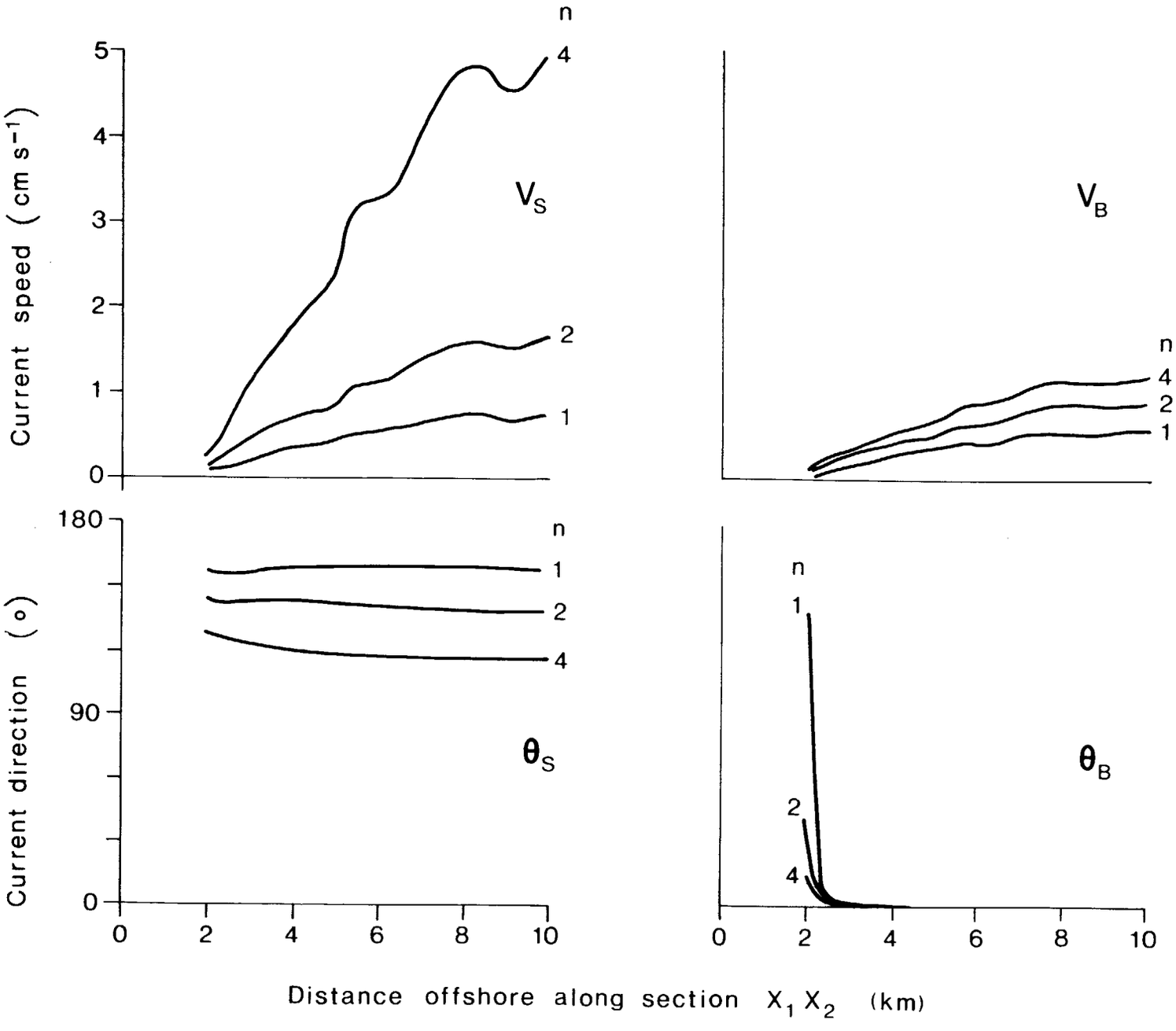
n
4
2
1
5
4
3
2
1
0
Current speed (cm s⁻¹)
V_S
V_B
n
4
2
1
180
90
0
Current direction (o)
n
1
2
4
θ_S
n
1
2
4
θ_B
0
2
4
6
8
10
Distance offshore along section $X_1 X_2$ (km)

Fig.27

FIGURE 28

Profiles of the density current components u and v for $\Lambda = 4$, mid-way along section $X_1 X_2$ showing a shoreward flowing (u) bottom current of about 1 cm s^{-1} and an alongshore current (v) flowing towards the W at about 2 cm s^{-1}. η is the dimensionless depth.

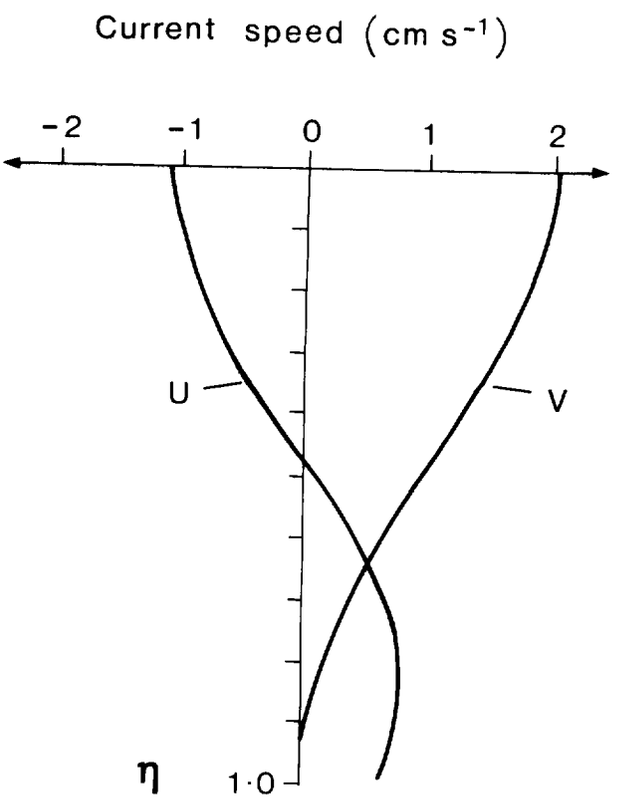

Fig. 28

FIGURE 29

A schematic diagram showing the major features of the mean tidal, or residual, circulation in Swansea Bay. Note: (a) an area of divergence to the S of Port Talbot; (b) an area of possible upwelling in a clockwise eddy over the Scarweather Sands; (c) an area of mean flow reversal off Mumbles Head; (d) an area to the SW of the River Neath where the mean circulation may be influenced by density currents. Upper arrows (where shown) indicate mid-depth residuals otherwise arrows indicate near-bottom residuals with flow speeds shown in arrow heads in cm s^{-1} (see Figure 14 for further details)

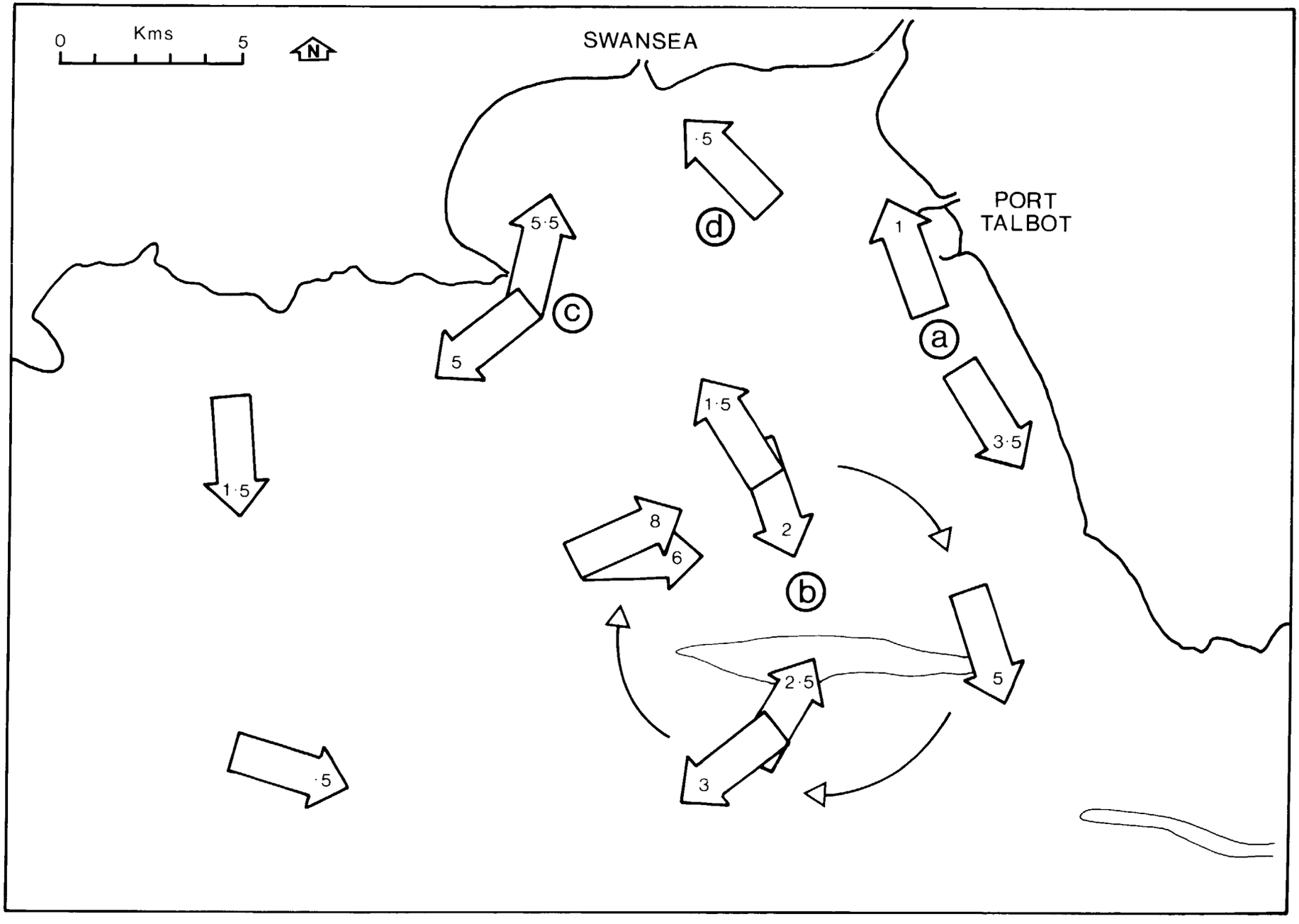

Fig. 29

APPENDIX A

EKMAN'S THEORIES OF WIND DRIVEN CURRENTS

A.1 Unbounded infinite depth case

The case of pure drift currents in an unbounded homogeneous ocean of infinite depth, over which the wind field is uniform, was first studied in detail by Ekman (1905).

Pure drift currents are those which arise from the action of applied wind stress at the sea surface with frictional coupling between the lower and successively slower moving layers of fluid. Horizontal pressure gradients within the water column do not occur.

The equations of motion for a fluid element are simplified to include only the local acceleration, the Coriolis force and the frictional terms. Writing these for convenience in a left hand rectangular co-ordinate system with x and y in the sea surface and z positive downwards, gives:

$$\frac{\partial u}{\partial t} = f v + N_z \frac{\partial^2 u}{\partial z^2}$$
$$\frac{\partial v}{\partial t} = f u + N_z \frac{\partial^2 v}{\partial z^2} \qquad \text{(A1)}$$

where $f = 2\Omega \sin \phi$ is the Coriolis parameter and N_z is the vertical eddy viscosity coefficient. Ω is the Earth's angular velocity and ϕ of the latitude.

Ekman (1905) first considered non-accelerated or stationary drift currents in an idealized ocean and thus the equations in (A1) become

$$-f v = N_z \frac{\partial^2 u}{\partial z^2}$$
$$f u = N_z \frac{\partial^2 v}{\partial z^2} \qquad \text{(A2)}$$

At the upper boundary a constant wind stress (τ_x , τ_y) is applied, and if for simplicity the wind blows in the y direction only, this leads to the upper boundary conditions

$$\tau_x = -N_z \frac{\partial u}{\partial z}\Big|_{z=0} = 0 \quad \text{and} \quad \tau_y = -N_z \frac{\partial v}{\partial z}\Big|_{z=0} = 0 \qquad \text{(A3)}$$

where since u and v depend on z only, we may employ total differentials. The equations in (A3) imply that the stress must be continuous across the surface.

A lower boundary condition may be taken as

$$u|_{z=\infty} = 0 \quad \text{and} \quad v|_{z=\infty} = 0 \qquad \text{(A4)}$$

that is the current at infinite depth vanishes everywhere.

With these conditions and the assumption of a constant eddy viscosity (N_z) it may be shown (see for example Neumann and Pierson, 1966), that the solution of the equations in (A2) is

$$\left.\begin{aligned} u &= V_0 e^{-(\pi/D)z} \cos\left(\frac{\pi}{4} - \frac{\pi z}{D}\right) \\ v &= V_0 e^{-(\pi/D)z} \sin\left(\frac{\pi}{4} - \frac{\pi z}{D}\right) \end{aligned}\right] \qquad \text{(A5)}$$

where

$$D = \pi\left(\frac{2N_z}{f}\right)^{1/2} \qquad \text{(A6)}$$

and V_0 is the velocity of the wind driven current at the surface. The variation of u and v with depth in equations (A5) describes the well known Ekman spiral and it can be seen that at the surface the current V_0 is directed at 45° to the right of the wind in the Northern Hemisphere, decreasing exponentially in strength and rotating clockwise in direction with increasing depth. Equations (A5) show that at depth D the current has decreased to $e^{-\pi}$ (about 1/23) of its value at the surface and is in the opposite direction. Although the current approaches zero asymptotically for $z \to \infty$ by far the most important currents occur above depth D and for this reason Ekman (1905) referred to D as the "depth of frictional influence".

The magnitude of a pure drift current is proportional to the wind stress and given by

$$V_0 = \frac{\tau}{\rho(N_z f)^{1/2}} \qquad \text{(A7)}$$

At the equator $f \to 0$ and V_0, theoretically, becomes infinitely large. However the assumptions made in deriving equation (A7) do not hold at the equator since with $D \to \infty$ the lower boundary condition, $u = v = 0$ at $z \to \infty$, cannot be achieved.

Although D has been used in this report to determine the likelihood of the water responding to an applied wind stress, by far the most useful solutions of equations(A2) are those for unbounded and bounded oceans of finite depth.

A.2 Unbounded finite depth case

Ekman (1905) solved equations (A2) for the case of an unbounded ocean of finite depth h and constant N_z and obtained solutions of the form

$$u = A \sinh(\xi\pi/D)\cos(\xi\pi/D) - B\cosh(\xi\pi/D)\sin(\xi\pi/D)$$

$$v = A\cosh(\xi\pi/D)\sin(\xi\pi/D) + B\sinh(\xi\pi/D)\cos(\xi\pi/D)$$

where

$$A = \frac{\tau D}{\rho N_z \pi} \cdot \frac{\cosh(\lambda\pi/D)\cos(\lambda\pi/D) + \sinh(\lambda\pi/D)\sin(\lambda\pi/D)}{\cosh(2\lambda\pi/D) + \cos(2\lambda\pi/D)}$$

$$B = \frac{\tau D}{\rho N_z \pi} \cdot \frac{\cosh(\lambda\pi/D)\cos(\lambda\pi/D) - \sinh(\lambda\pi/D)\sin(\lambda\pi/D)}{\cosh(2\lambda\pi/D) + \cos(2\lambda\pi/D)} \qquad \text{(A8)}$$

and $D = \pi(2N_z/f)^{1/2}$. $\xi = h - z$ is the height above the sea-bed.

The angle between the wind and the current (α) in the case of finite depth is different from $\frac{\pi}{4}$ and given by

$$\tan\alpha = \frac{\sinh\left(\frac{2\pi\lambda}{D}\right) - \sin\left(\frac{2\pi\lambda}{D}\right)}{\sinh\left(\frac{2\pi\lambda}{D}\right) + \sin\left(\frac{2\pi\lambda}{D}\right)} \qquad \text{(A9)}$$

The ratio λ/D is important in Ekman's theory. For $\lambda/D > 1$ the solutions (A8) approximate the infinite depth case. As the ratio λ/D becomes smaller, the surface current decreases and flows at smaller and smaller angles to the right of the wind (in the Northern Hemisphere). The variation of α with λ/D is illustrated in the table below (after Neumann and Pierson, 1966):

λ/D	0.25	0.50	0.75	1.00
α	21.5°	45°	45.5°	45°

A.3 Bounded finite depth case

Ekman also examined the current system off a straight coastline. A wind blowing onshore will pile water against the coast, leading to an increase in sea level. The slope thus acquired by the sea surface leads to a horizontal pressure gradient in the water column and a modified current system, consisting of the shoreward wind driven current and a return flow or slope current in a bottom boundary layer.

The solutions given by Ekman (1905) for these slope currents have the form:

$$u = g\frac{\sin\gamma}{f}\left[1 - \frac{\cosh\frac{\pi}{D^*}(\lambda+z)\cos\frac{\pi}{D^*}(\lambda-z) + \cosh\frac{\pi}{D^*}(\lambda-z)\cos\frac{\pi}{D^*}(\lambda+z)}{\cosh\frac{2\pi\lambda}{D^*} + \cos\frac{2\pi\lambda}{D^*}}\right]$$

$$v = g\frac{\sin\gamma}{f}\left[\frac{\sinh\frac{\pi}{D^*}(\lambda+z)\sin\frac{\pi}{D^*}(\lambda-z) + \sinh\frac{\pi}{D^*}(\lambda-z)\sin\frac{\pi}{D^*}(\lambda+z)}{\cosh\frac{2\pi\lambda}{D^*} + \cos\frac{2\pi\lambda}{D^*}}\right] \qquad \text{(A10)}$$

where $\sin\gamma$ is the sea-surface slope.

Similarly to the wind driven shear current at the surface (see equations A5) we can calculate a thickness for the bottom layer of frictional influence given by

$$D^* = \pi\left(\frac{2N_z}{f}\right)^{1/2}. \qquad \text{(A11)}$$

D and D^* are of the same order and for water depths $\lambda > D + D^*$ equations (A8) and A10 describe Ekman's elementary current system with a purely geostrophic current flowing between the upper and lower layers of frictional influence (see Neumann and Pierson, 1966, for a full discussion).

A.4 Eddy viscosity parameterization

There are of course fundamental limitations in the application of Ekman's theory to a real current system. Foremost amongst these is the assumption of N_z constant with depth and secondly the calculation of actual drift currents is hindered by the uncertain knowledge of N_z and its strong dependence on wind speed (W). Furthermore, complications arise in shallow seas with appreciable tidal currents due to the combinations of shear arising in the surface mixed layer and in the bottom boundary layer. Additionally, stratification may modify the resulting current system (for discussion see Section 5 and Appendix F).

However some calculations are possible and these enable us to make a qualitative assessment of the influence of the wind on the water circulation in Swansea Bay.

Ekman's theory assumes a value of N_z which remains constant with increasing depth. However in the case of a wind stress being applied at the sea surface it is clear that the downward mixing of momentum will be greatest at the sea's surface and become less with increasing depth. If there is appreciable wave activity at the surface the downward flux of momentum will be even greater. Neumann (1952) gives values of N_z which vary with the square or even the cube

of wind speed, ie $N_z \propto W^2$ or W^3, and which for a fully developed sea lie in the range .005 $m^2 s^{-1}$ for a wind speed of 4 m s^{-1}, to .25 $m^2 s^{-1}$ at a wind speed of 18 m s^{-1}. These values were derived from estimates of the energy balance in fully developed wind generated seas.

Various attempts have been made to determine an empirical relationship between the eddy viscosity N_z and the wind speed. Thorade (1914), using carefully selected current observations, obtained

$$N_z = .995 \times 10^{-3} W^3 \ m^2 s^{-1} \text{ for } W < 6 \ m s^{-1} \qquad \text{(A12)}$$

and

$$N_z = .420 \times 10^{-3} W^2 \ m^2 s^{-1} \text{ for } W > 6 \ m s^{-1} \qquad \text{(A13)}$$

where W is the wind speed in m s^{-1} at a height of 10 m above the sea surface. These results give reasonable agreement with the energy balance values reported by Neumann (1952). Values calculated by both these methods are shown in Table A1.

However as previously remarked the amount of mixing which takes place in shallow tidal currents will be some combination of that which occurs due to surface layer mixing and that which originates in the bottom boundary layer and varies in some manner throughout the water column to the surface (linear and parabolic parameterizations of N_z are frequently employed - eg Bowden et al, 1959: Johns, 1969).

For a shallow tidal current with u_0 of order 50 cm s^{-1}, Bowden et al (1959) give a value of N_z of the order 250 $cm^2 s^{-1}$. While this is greater than the wind mixed surface layer value of N_z at low wind speeds ($W <$ 10 m s^{-1}) it is apparent that at the higher wind speeds (W of order 20 m s^{-1} say) wind induced mixing may be at least a factor of five times larger than that due to current shear alone. However, in a tidal current N_z will vary with tidal stream amplitude and depth and in an earlier paper Bowden (1953) suggests on dimensional grounds that N_z should be given by

$$N_z = M u_0 h, \qquad \text{(A14)}$$

where $M \simeq 2.5 \times 10^{-3}$,

u_0 is the amplitude of the tidal stream,

h is the depth.

We may therefore also examine, on an order of magnitude basis, the variation of N_z which occurs with changes in tidal stream amplitude and water depth.

In Table A1 values of N_z for surface layer mixing have been calculated at different wind speeds (W) using Thorade's (1914) relation (equations A12 and A13). Values of N_z due to vertical turbulent shear originating in the bottom boundary layer (and calculated using equation A14) are also shown in Table A1 for different tidal stream amplitudes and for a mean depth (typical of Swansea Bay) of h = 20 m.

Thus it can be shown that the value of N_z due to the wind does not exceed that due to turbulent shear until a wind speed of about 10 m s^{-1} is reached. However at a wind speed of 35 m s^{-1} the value of N_z is of the order .5 $m^2 s^{-1}$, that is an order of magnitude larger than N_z due to turbulent shear alone in a tidal stream of 1.0 m s^{-1} which is fairly typical of Swansea Bay.

A.5 Validity of Ekman's theory

Various attempts have been made to test Ekman's theory and, in particular, estimates of D and V_0, the surface drift, have given general agreement with oceanographic observations. In middle latitudes (see Neumann and Pierson, 1966) D is of order 50 m and V_0 (from equation A7) is about .35 m s^{-1} for a wind speed of 10 m s^{-1}.

Early measurements, eg Thorade (1914), Durst (1924) and Palmen (1931) indicated that V_0 was of the order of 1–3% of the wind speed. More recent Eulerian and Lagrangian measurements in coastal waters, of depth of order 50 m and less, suggest that these were probably realistic estimates. For example Carruthers et al (1949) gives 1.5%, Lee and Ramster (1968) give 2–3%, Dooley and Steele (1969) give 1.4%, Booth et al (1978) gives 1%.

Various theoretical studies of wind driven currents in coastal waters have been carried out. For example Bretschneider (1968) with an appropriate choice of upper and lower boundary conditions obtained V_0/W ratios in the range 2.8 to 4.2% for depths from 6–60 m and for winds parallel to the coast. However it is beyond the scope of this report to describe these theoretical developments and for an up-to-date assessment reference should be made, for example, to the work of Csanady (1972), Murray (1975) and Farmer (1976).

The results of recent laboratory experiments for contained bodies of water have been summarised by Spillane and Hess (1978). Those of Kondo (1976) suggest that V_0/W is strongly depth dependent but that if W is measured at a height above the surface which is a fixed proportion of the water depth the ratio V_0/W approaches a constant value of 3.3% which is independent of the surface roughness, ie whether waves are present or not, provided that the stress across the air-water interface is continuous.

In addition Wu (1973, 1975) has shown some dependence of the ratio v_0/w on fetch, although for very long fetches it approaches a constant value of about 3.5%.

TABLE A1

Values of the vertical eddy viscosity coefficient (N_z) in wind mixed surface layers and tidal currents as a function of wind speed (W) and tidal stream amplitude (U_0).

Values calculated using Thorade's (1914) relationships and Bowden's (1953) formula (equations A12, A13 & A14) for a total depth of h = 20m.

W ($m\ s^{-1}$)	N_z ($m^2\ s^{-1}$)
2	.000080
4	.00064
6	-
8	.027
10	.042
12	.060
14	.082
16	.11
18	.14
20	.17

U_0 ($m\ s^{-1}$)	N_z ($m^2 s^{-1}$)
.2	.01
.4	.02
.6	.03
.8	.04
1.0	.05
1.2	.06
1.4	.07
1.6	.08
1.3	.09
2.0	.10

Values given by Neumann's (1952) energy balance for fully developed wind generated seas.

W ($m\ s^{-1}$)	N_z ($m^2\ s^{-1}$)
4	.0057
6	.0157
8	.0324
10	.0563
14	.1317
18	.2459

APPENDIX B

STOKES DRIFT: MOTION IN THE INTERIOR OF THE FLUID

By including the effects of viscosity in Stokes' (1847) original solution for the drift velocity (see equation 10), Longuet-Higgins (1953) obtained an expression for the drift velocity in the interior of the fluid of the form

$$u_s\big|_{0<z<h} = \frac{a^2\sigma k}{4\sinh^2 kh}\Big[2\cosh\{2kh(\mu-1)+3 + kh\sinh 2kh(3\mu^2-4\mu+1) + 3\Big(\frac{\sinh 2kh}{2kh}+\frac{3}{2}\Big)(\mu^2-1)\Big]\Big] \qquad (B1)$$

where h is fluid depth and $\mu = z/h$. Here z is the distance measured positive downwards from the surface. This solution, which is essentially for laminar flow, reduces to the usual expression for the Stokes drift velocity near the bed which is given by equation (13). This may also be applied (see Longuet-Higgins, 1957) to a turbulent boundary layer. Equation B1 has been used here to calculate the Stokes drift velocities which are shown in Table 3.

Experimental observations (eg Russell and Osario, 1957) suggest that good estimates of the Stokes drift at the surface are probably given by Stokes' original irrotational flow solution (equation 10) but that in the interior of the fluid, and particularly at the bed, the effects of viscosity may well lead to Stokes drift velocity profiles of the form predicted by equation (B1).

In reality of course, the situation is far more complex than this with the total wave induced mass transport velocity being the resultant effect of a superposition of waves having a random distribution of heights, periods and phases.

It should be noted that considerable controversy still surrounds the relative magnitude of the wind driven shear current and the wave induced mass transport velocity. Wu (1975) has shown in laboratory experiments that the wave-induced Stokes transport may only be 3-15% of the surface dirft and this would not seem an unreasonable estimate in the light of our own calculations. However, as suggested by Wu (1975), the situation is far from being clear with, for example, Shemdin (1972) claiming, on the basis of laboratory data, that the surface drift is essentially a wind-induced shear current, whereas Bye (1967) and Kenyon (1972) concluded from a study of oceanic wave data that the surface drift is primarily a wave induced mass transport.

APPENDIC C

ROTARY ANALYSIS AND THE CONSTRUCTION OF TIDAL ELLIPSES

The following description of the method is based upon that given by Maddock and Pingree (1978).

Any vector time series may be expressed in terms of two orthogonal components each of which can in turn be expressed as a Fourier series. Therefore by resolving the measured currents into east and north flowing components u and v we may express the velocity components at a particular frequency, ω , as

$$u_\omega = a_u \cos\omega t + b_u \sin\omega t \qquad (C1)$$

$$v_\omega = a_v \cos\omega t + b_v \sin\omega t \qquad (C2)$$

where a_u , b_u , a_v and b_v are Fourier coefficients.
In complex notation the vector describing the ellipse for a constituent having frequency ω is given by

$$\underset{\sim}{u}_\omega = u_\omega + i v_\omega \qquad (C3)$$

It can be shown that by substituting (C1) and (C2) in (C3) and expanding $\cos\omega t$ as $(e^{i\omega t} + e^{-i\omega t})/2$ and $\sin\omega t$ as $(e^{i\omega t} - e^{-i\omega t})/2i$, the complex quantity $\underset{\sim}{u}_\omega$ is given by

$$\underset{\sim}{u}_\omega = \tfrac{1}{2}[(a_u + b_v) + i(a_v - b_u)]\, e^{i\omega t} + \tfrac{1}{2}[(a_u - b_v) + i(a_v + b_u)]\, e^{-i\omega t} \qquad (C4)$$

which may be written as

$$\underset{\sim}{u}_\omega = \underset{\sim}{u}_+ e^{i\omega t} + \underset{\sim}{u}_- e^{-i\omega t}. \qquad (C5)$$

Thus the vector describing the tidal ellipse for a constituent having a frequency ω is described by two contra-rotating vectors, $\underset{\sim}{u}_+$ and $\underset{\sim}{u}_-$, having constant amplitudes and rotating anticlockwise and clockwise respectively with frequencies ω and $-\omega$. The maximum value of the current for this particular constituent occurs when $\underset{\sim}{u}_+$ and $\underset{\sim}{u}_-$ lie in the same direction. The semi-major and semi-minor areas of the ellipse are given respectively by

$$\left.\begin{aligned} a &= |\mathcal{U}_+| + |\mathcal{U}_-| \\ b &= |\mathcal{U}_+| - |\mathcal{U}_-| \end{aligned}\right] \qquad (C6)$$

The phases of the anticlockwise and clockwise components are given respectively by

$$\left.\begin{aligned} \theta_+ &= \tan^{-1}\left(\frac{a_v - b_u}{a_u + b_v}\right) \\ \theta_- &= \tan^{-1}\left(\frac{a_v + b_u}{a_u - b_v}\right) \end{aligned}\right] \qquad (C7)$$

which gives the phase of constituent with frequency ω as

$$g_\omega = \frac{\theta_+ - \theta_-}{2} \qquad (C8)$$

and the orientation of the major axis of the ellipse as

$$\phi_\omega = \frac{\theta_+ + \theta_-}{2} \quad . \qquad (C9)$$

From the harmonic analysis of the u and v time series we obtain sets of amplitudes, H_u and H_v, and phases, g_u and g_v, for the required tidal constituents. From this information it is possible to calculate the Fourier coefficients a_u, b_u, a_v and b_v and so construct the tidal ellipses.

APPENDIX D

DOODSON'S X_0 FILTER

Doodson's X_0 filter can only be applied to hourly values of the tidal currents. It has therefore been necessary in this study to reduce the original data sets by averaging the 10 minute values of speed and direction to give hourly values.

The 10 minute values of current speed were first resolved into an orthogonal frame of reference, having arbitrary orientation, and then arithmetically meaned to give hourly values. The two components of the original vector time series were then operated on separately by the X_0 filter to give residual currents in the x and y direction of the chosen frame of reference. A variable frame of reference was chosen so that an x or y filter product might correspond, for example, to an alongshore current adjacent to a coastline of any particular orientation.

For the calculation of the residuals shown in Tables 13 and 14 the y direction has been taken as true north. However in the meteorological application the y direction has been taken as 325(^{o}T) this direction corresponding to the orientation of the coast on the east side of Swansea Bay.

Thus Doodson's X_0 filter generates residual currents in the x and y direction given by:

$$\overline{u}_x(t) = \sum_{i=-N}^{N} w_i u_x(t+t_i) \qquad \text{(D1)}$$

$$\overline{u}_y(t) = \sum_{i=-N}^{N} w_i u_y(t+t_i) \qquad \text{(D2)}$$

where the constant coefficients and times w_i and t_i have the properties $w_{-i} = w_i$ and $t_{-i} = t_i$. The values of the coefficients w_i (taken from Groves, 1955) are given in Table D1. As previously stated the times t_i are constant and equal to 1 hour.

TABLE D1

Values of coefficients used in Doodsons X_0 filter (see equations D1 and D2)

i	w_i
0	0
1	.067
2	.033
3	.033
4	.067
5	0
6	.033
7	.033
8	0
9	.067
10	0
11	.033
12	.033
13	0
14	.033
15	0
16	0
17	.033
18	0
19	.033

APPENDIX E

Smoothed progressive vector diagrams for residual water movements in Swansea Bay. β is the steadiness factor expressed as a percentage.

Figure	Station
E 1.1 - E 1.8	A
E 2.1 - E 2.2	B
E 3.1 - E 3.2	C
E 4.1 - E 4.2	D
E 5.1 - E 5.3	E
E 6.1 - E 6.3	F
E 7.1	G
E 8.1 - E 8.2	H
E 9.1	I
E10.1	K
E11.1	K

Note : The header code on each progressive vector diagram indicates the following:

eg 669G6	:	File name
27:7:76	:	Date record starts
SWB	:	Area (eg Swansea Bay)
A	:	Station
2M	:	Height above sea bed in metres

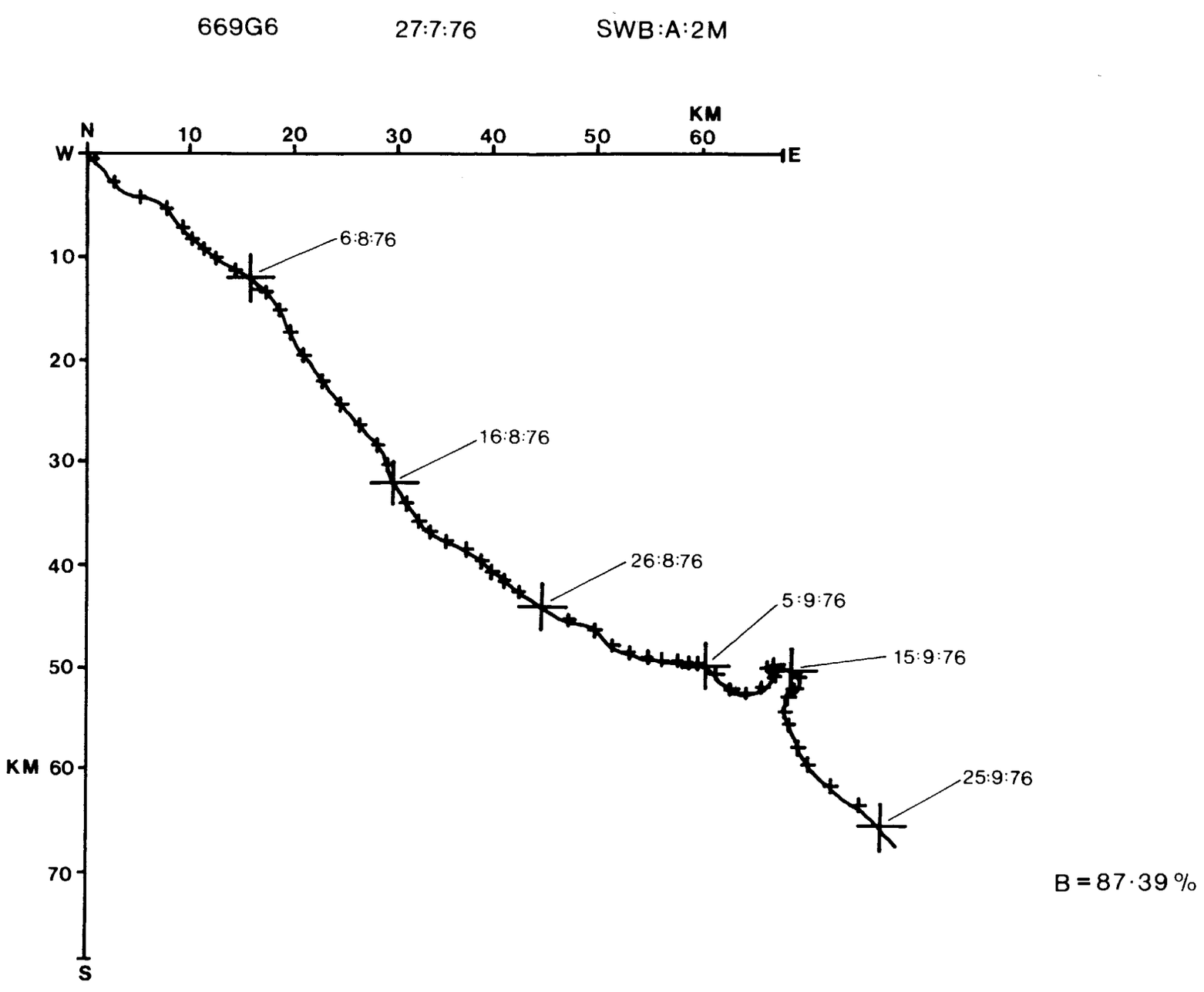
669G6
27:7:76
SWB:A:2M
N
10
20
30
40
50
KM
60
W
E
6:8:76
16:8:76
26:8:76
5:9:76
15:9:76
25:9:76
KM
S
B = 87·39 %

Fig. E 1.1

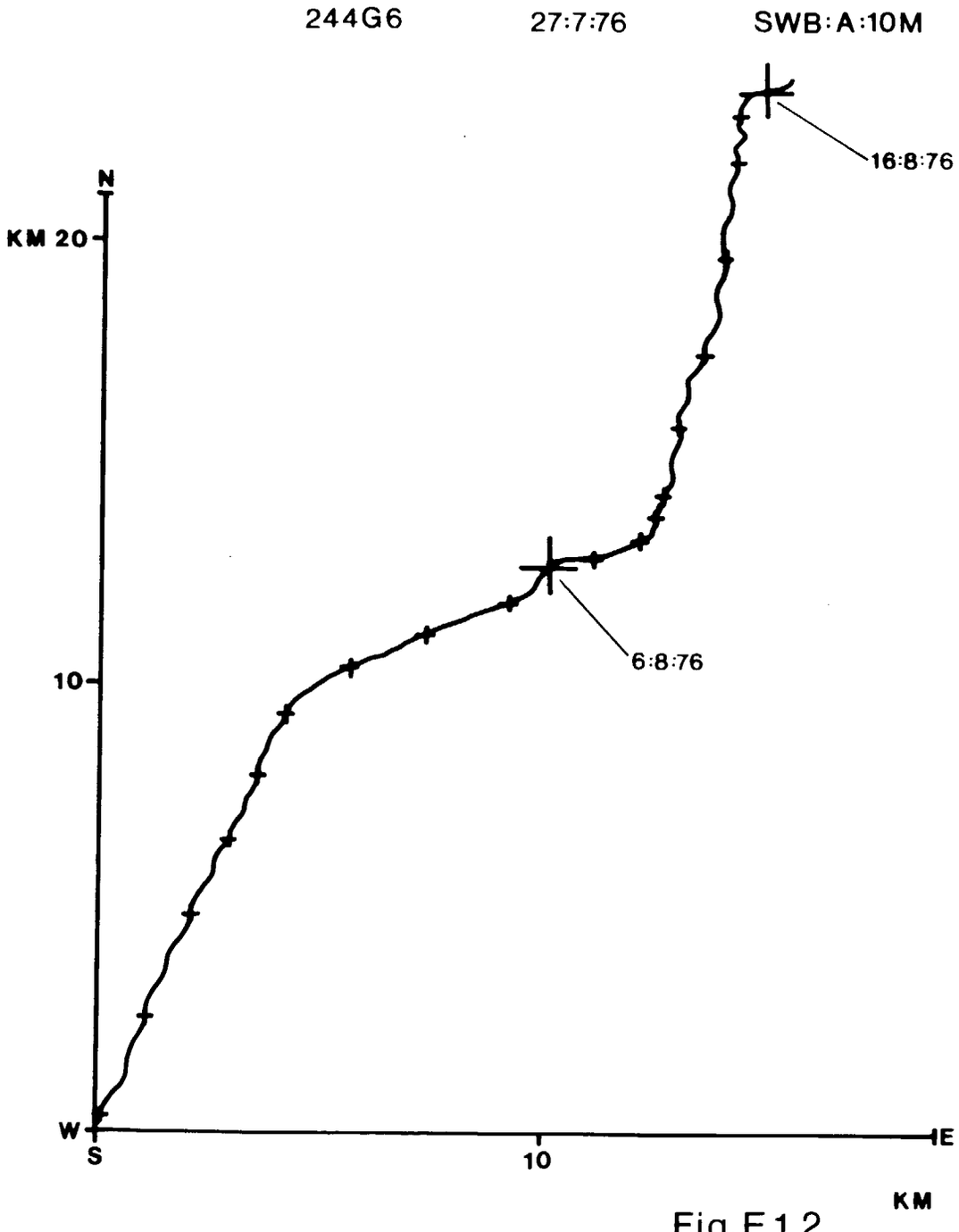

Fig. E 1.2

B = 87·89%

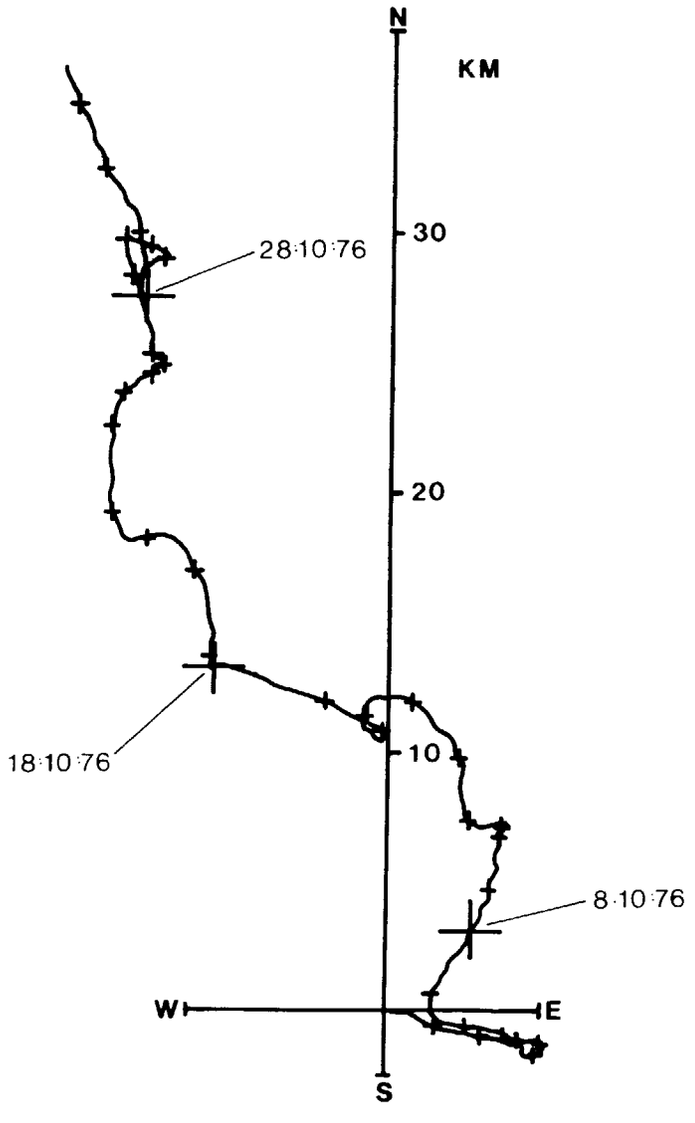

B = 52·61%

Fig. E 1.3

680M6 4:12:76 SWB:A:2M

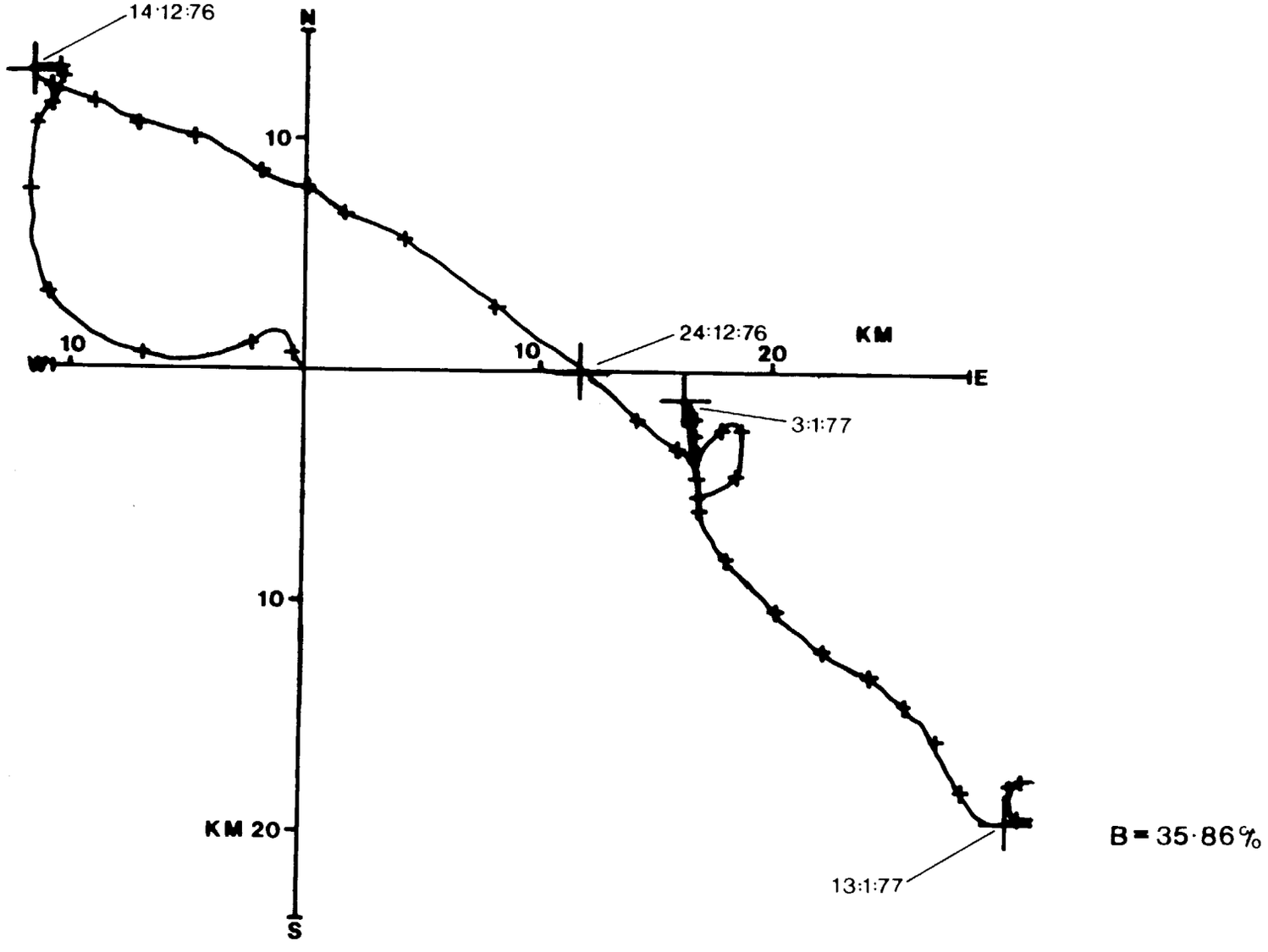

Fig. E 1.4

669G7 26:7:77 SWB:A:10M

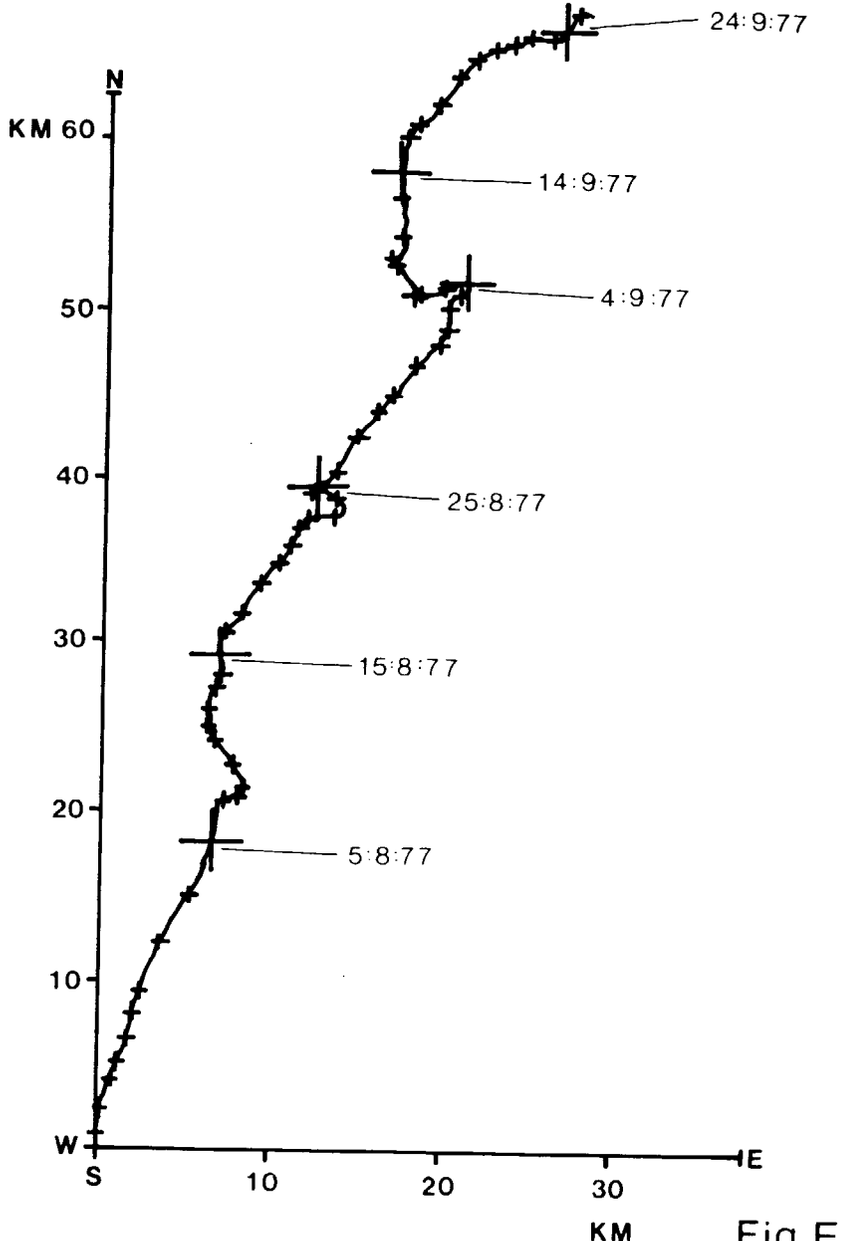

Fig.E 1.5

B= 73·01 %

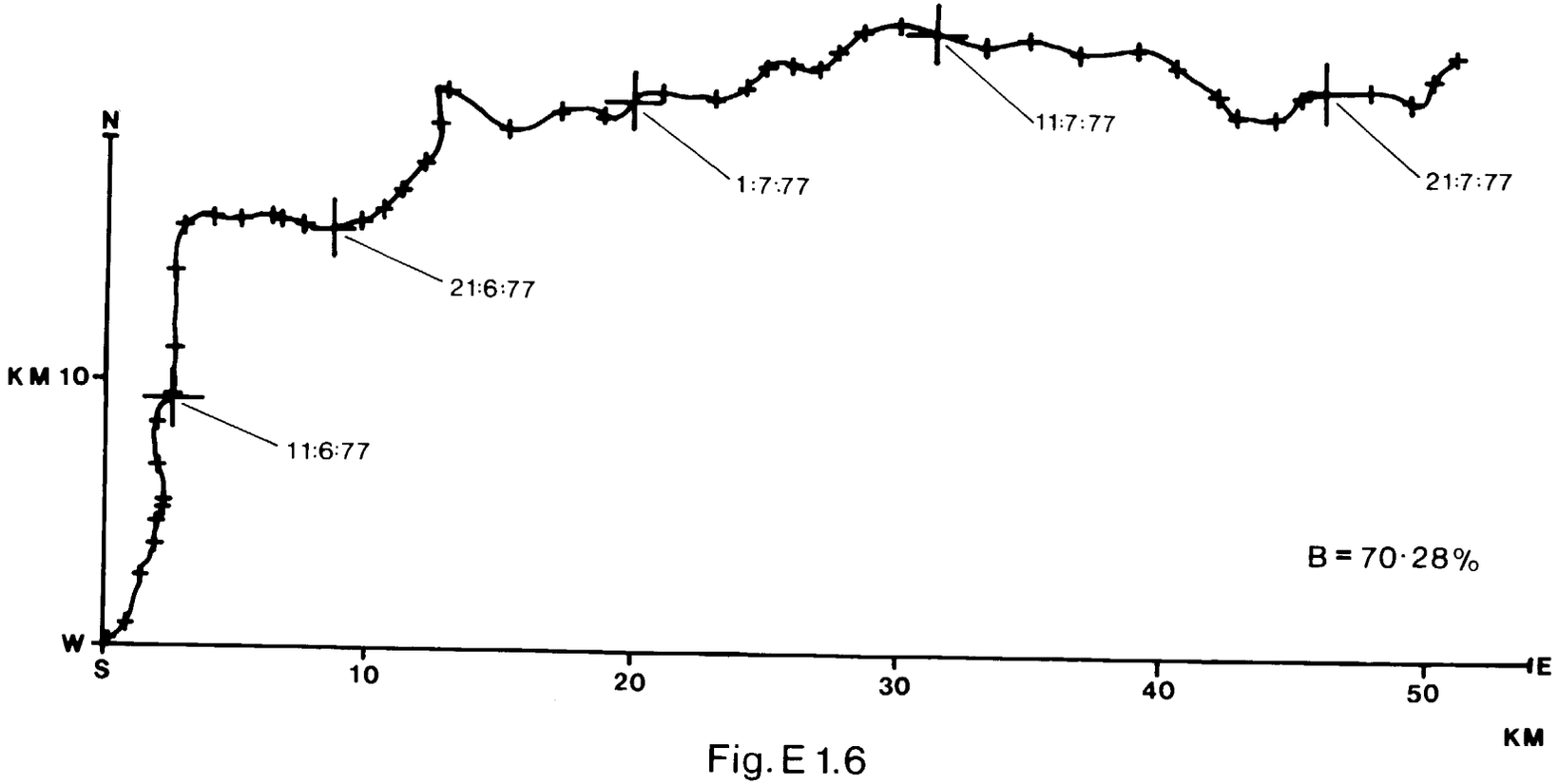

Fig. E 1.6

532F7 1:6:77 SWB:A:2M

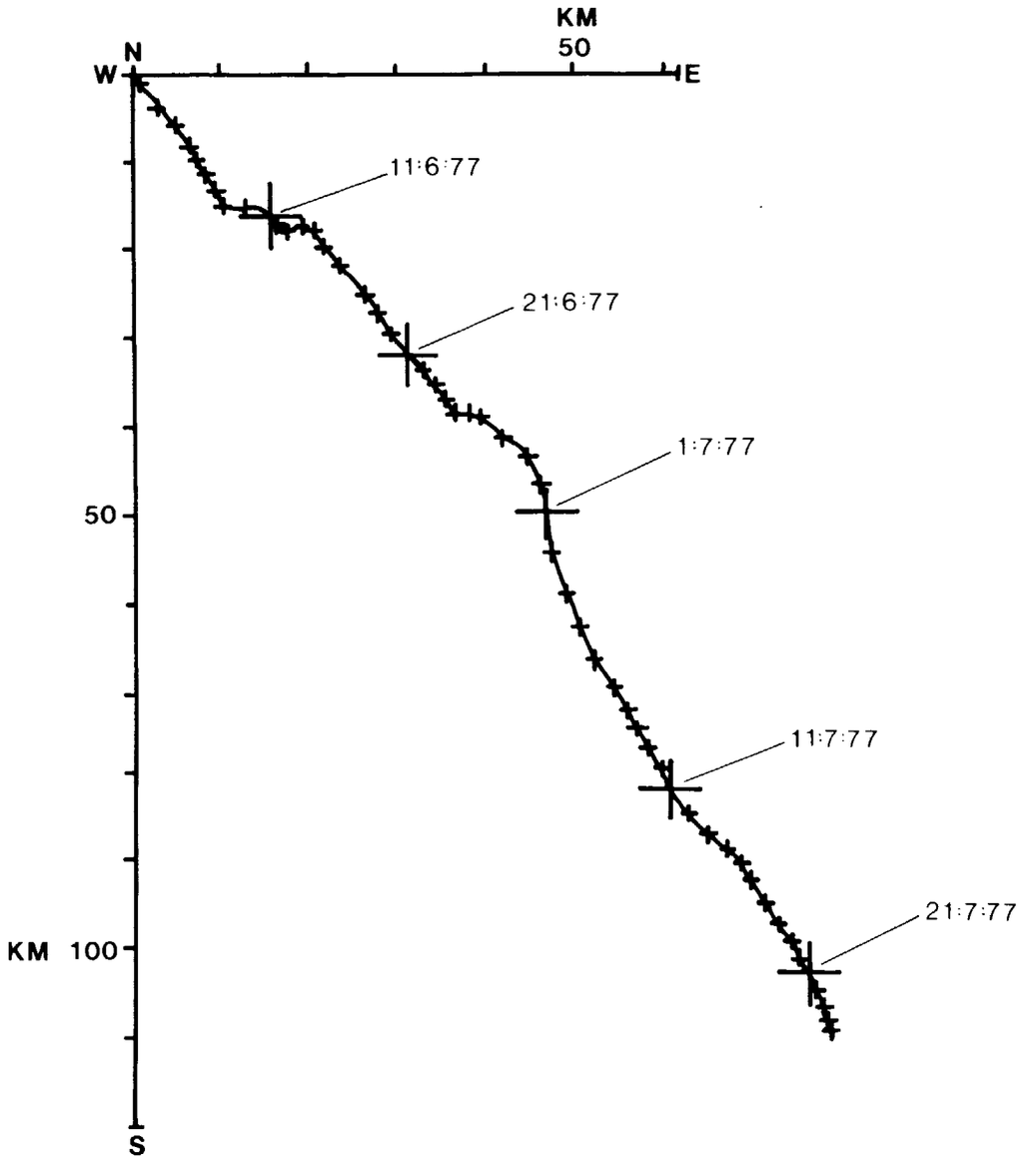

B = 95·08%

Fig. E 1.7

594G7 26:7:77 SWB:A:2M

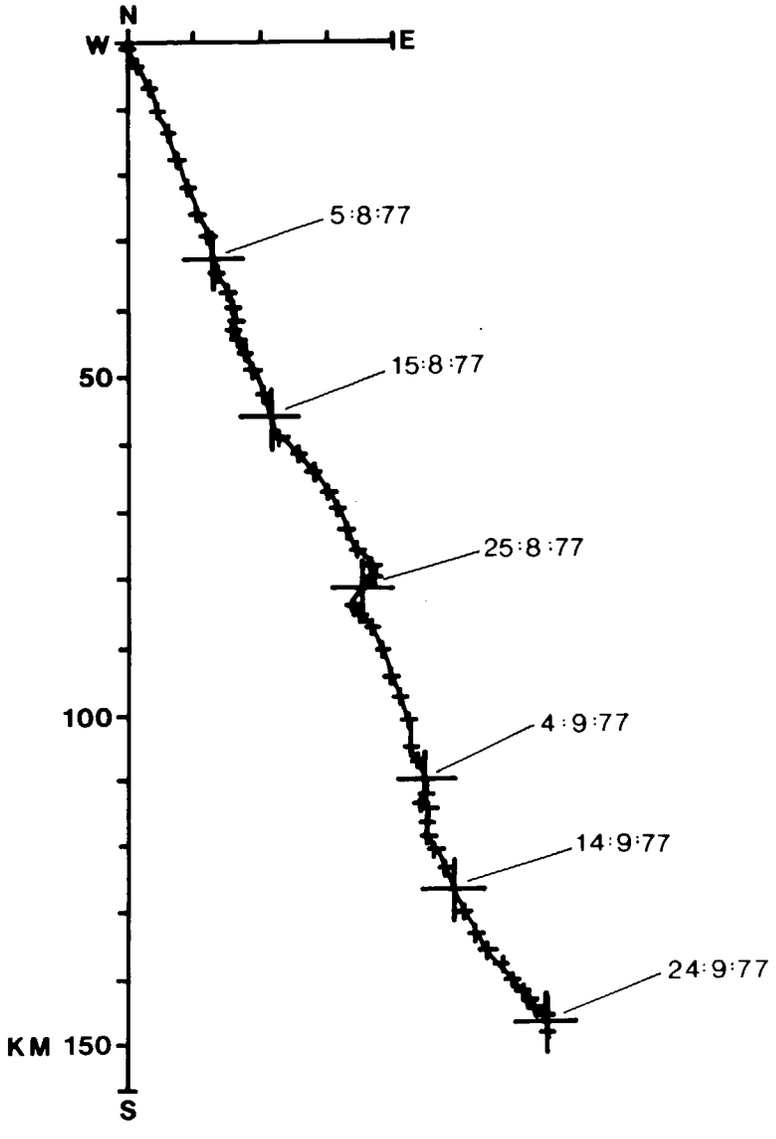

B= 95·14%

Fig. E 1.8

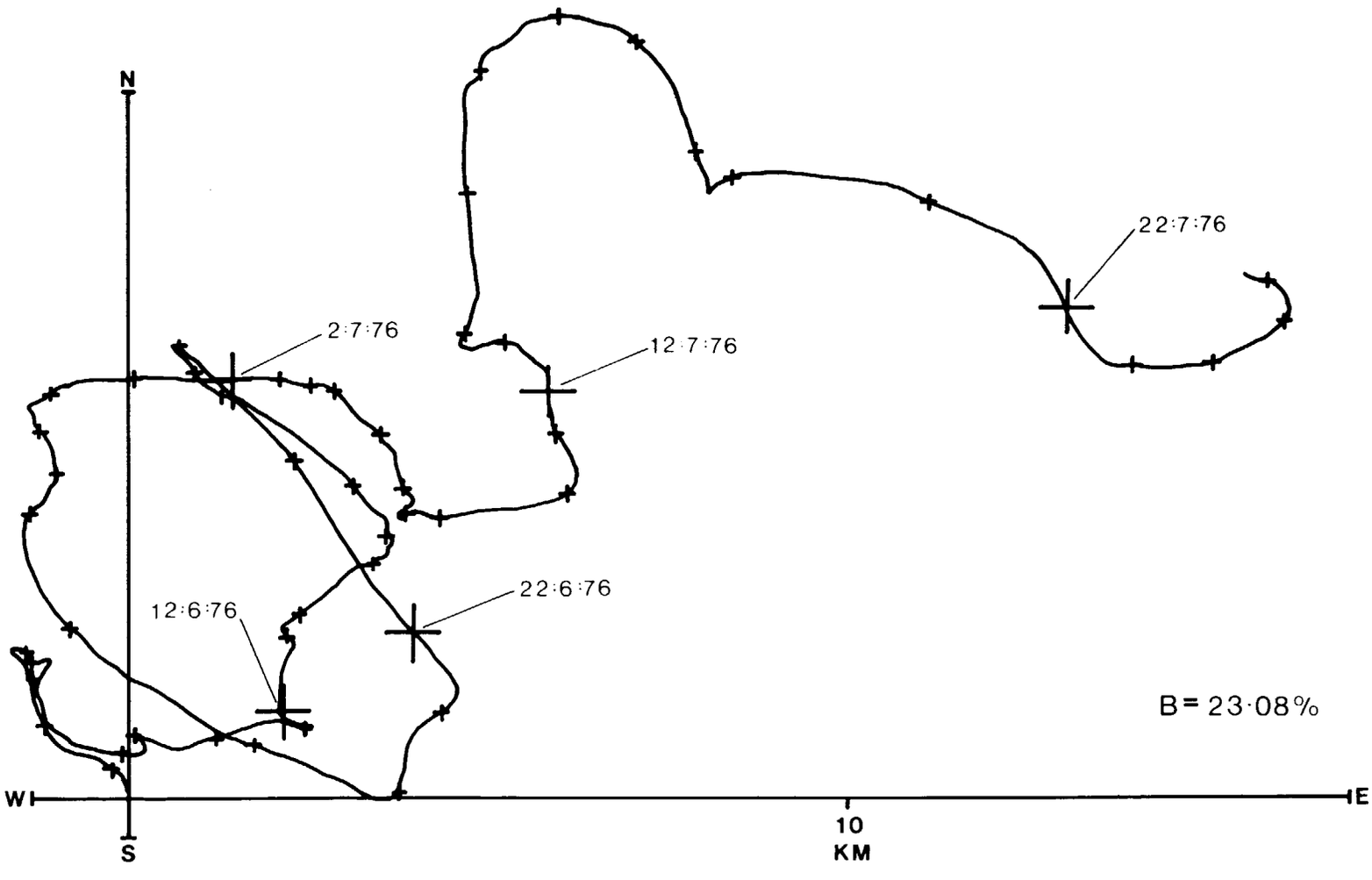
594F6 2:6:76 SWB:B:2M
N
S
W
E
2:7:76
12:7:76
22:7:76
12:6:76
22:6:76
B= 23·08%
10
KM

Fig. E 2.1

680K6 29:10:76 SWB:B:2M

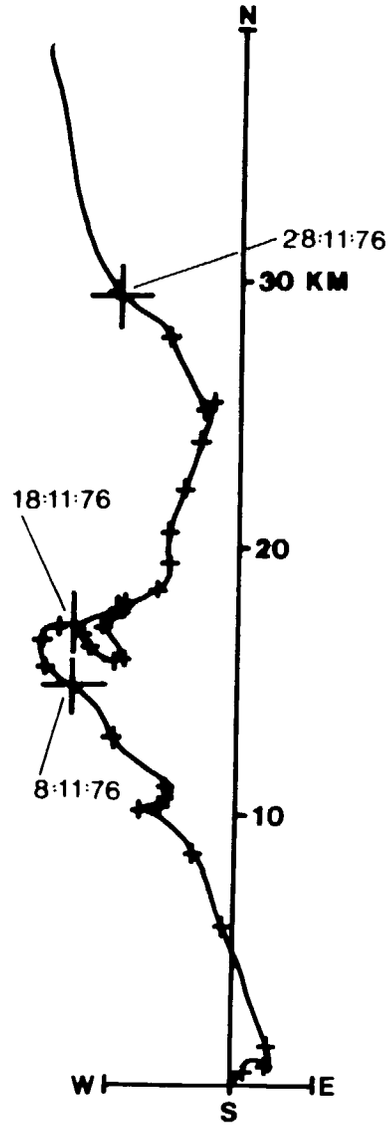

B= 65·19%

Fig. E 2.2

667F6 6:6:76 SWB:C:2M

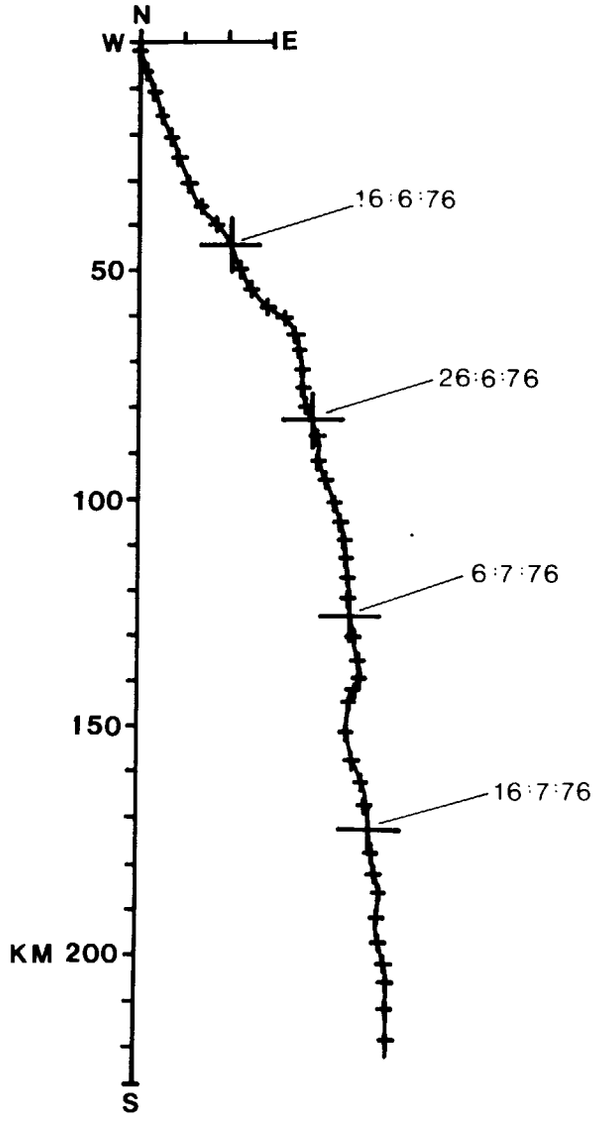

B= 95·60%

Fig. E 3.1

594K6 29:10:76 SWB:C:2M

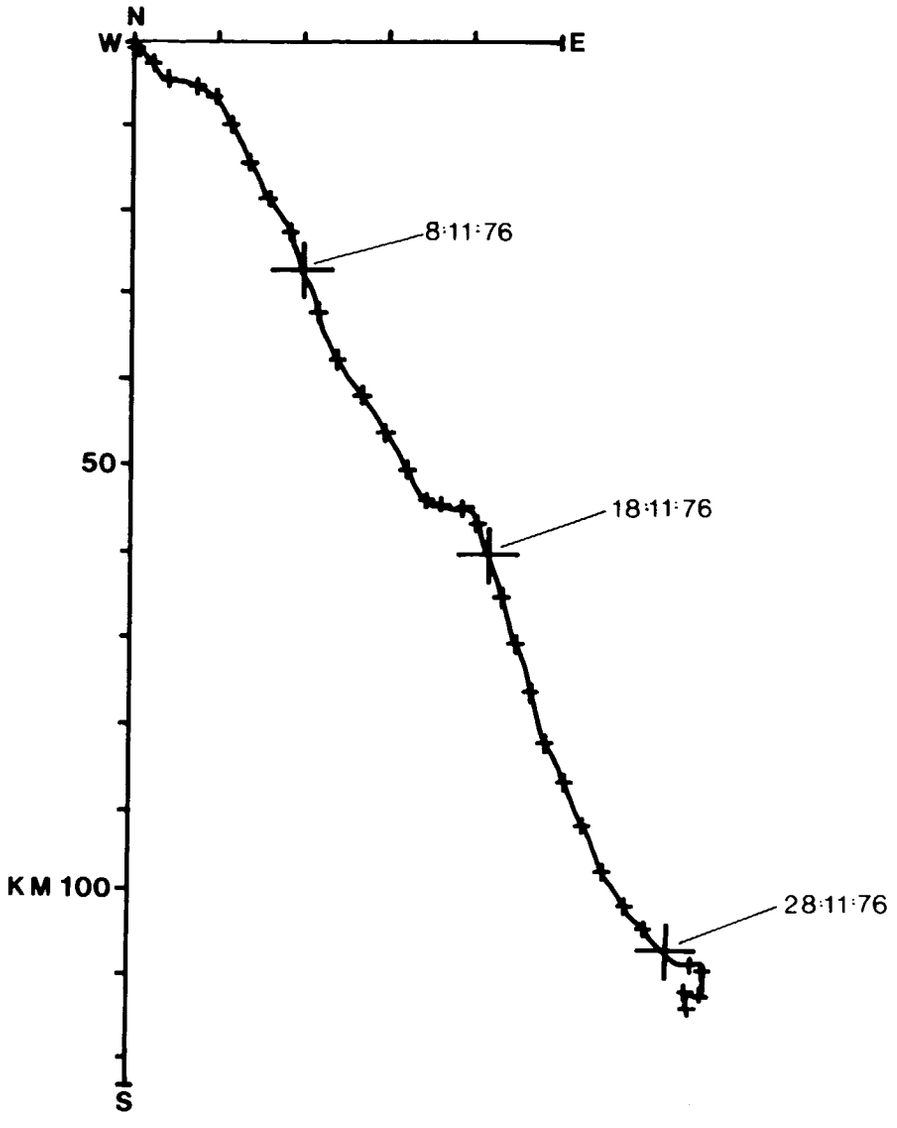

B = 93·14 %

Fig.E 3.2

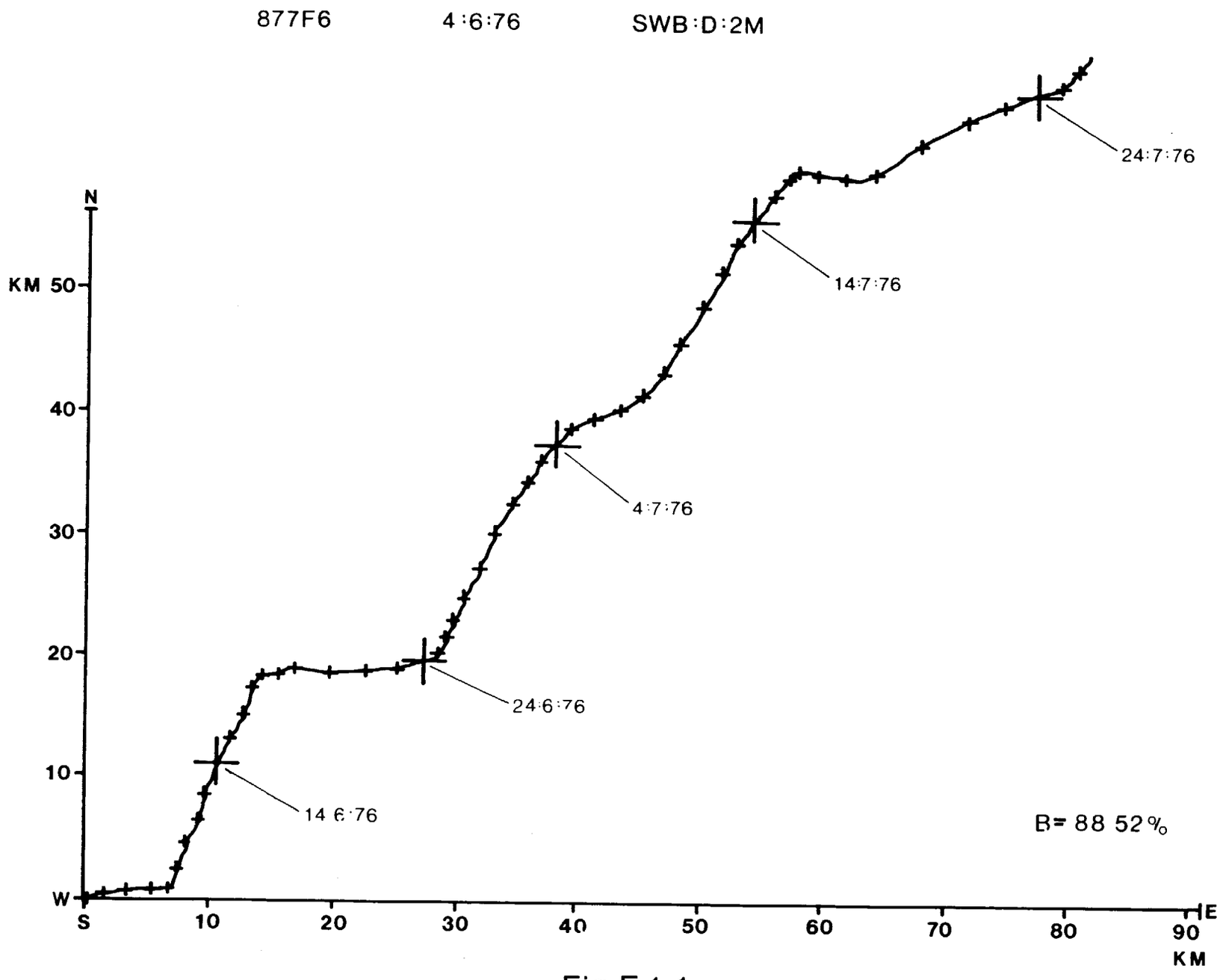
877F6
4:6:76
SWB:D:2M
N
KM 50
40
30
20
10
W
S
10
20
30
40
50
60
70
80
90
E
KM
14:6:76
24:6:76
4:7:76
14:7:76
24:7:76
B= 88 52%

Fig.E4.1

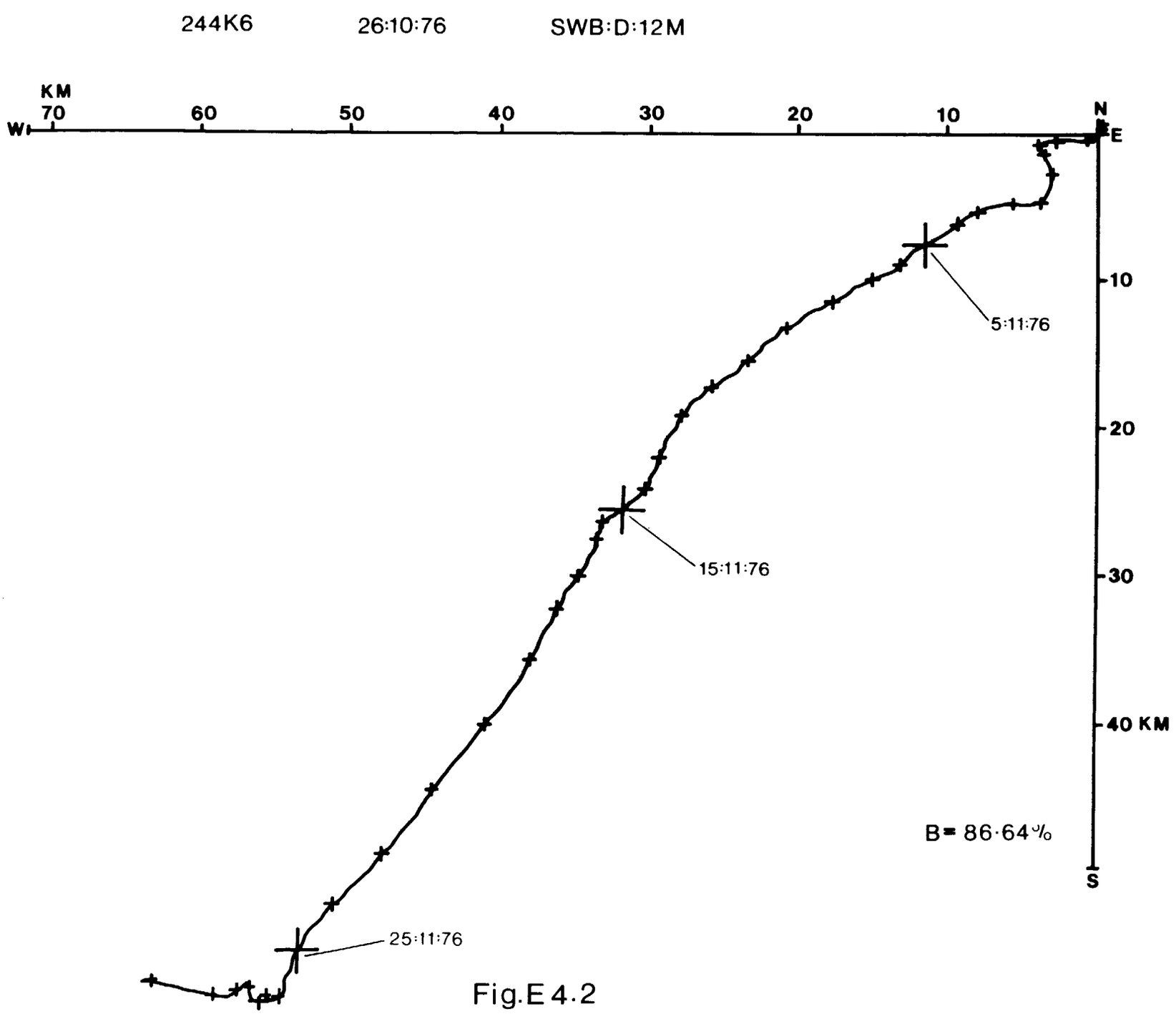
244K6
26:10:76
SWB:D:12M
KM
70
60
50
40
30
20
10
W
N
E
10
20
30
40 KM
S
5:11:76
15:11:76
25:11:76
B= 86·64%

Fig.E 4.2

878F6 4:6:76 SWB:E:2M

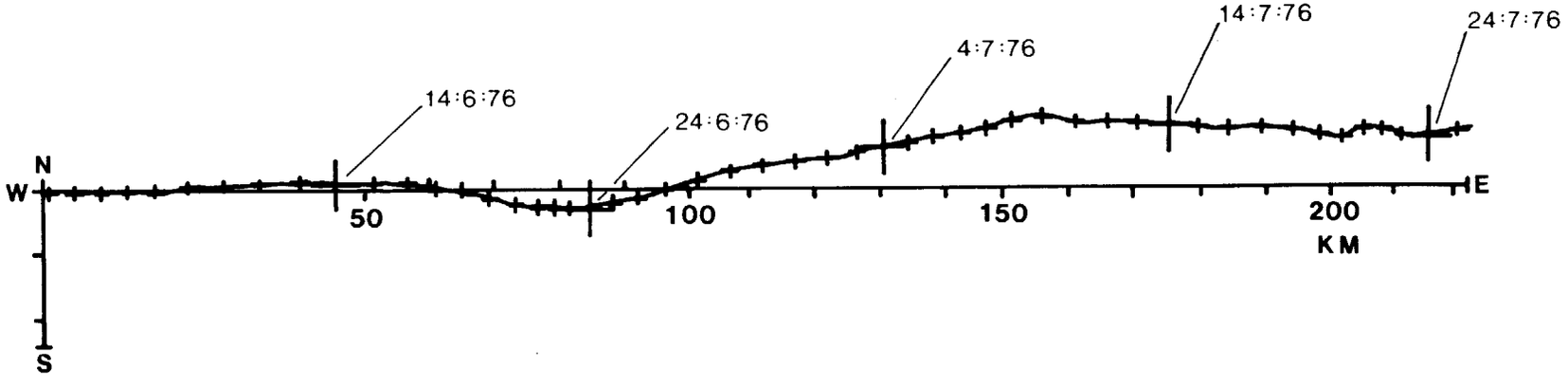

B = 98·69%

Fig.E5.1

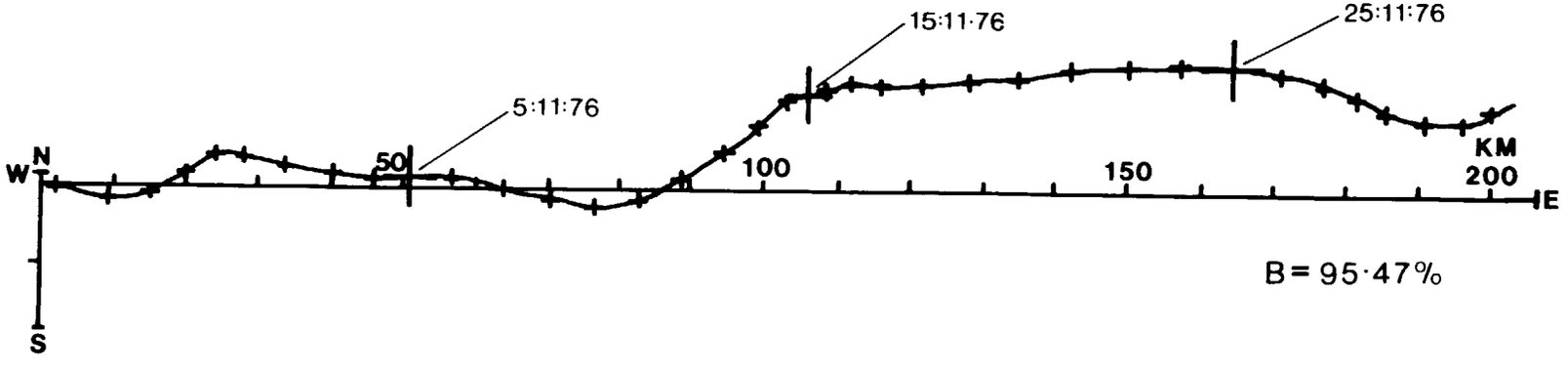

Fig.E5.2

269K6 26:10:76 SWB:E:12M

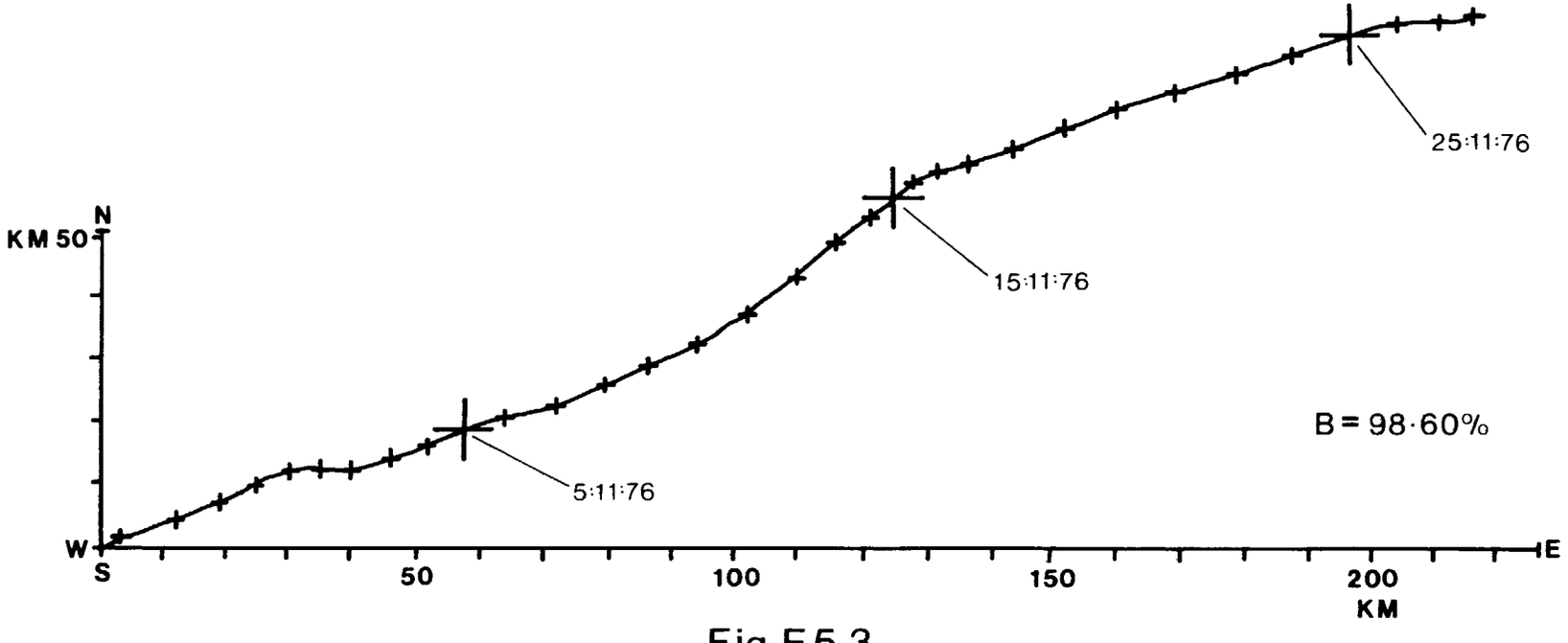

Fig.E5.3

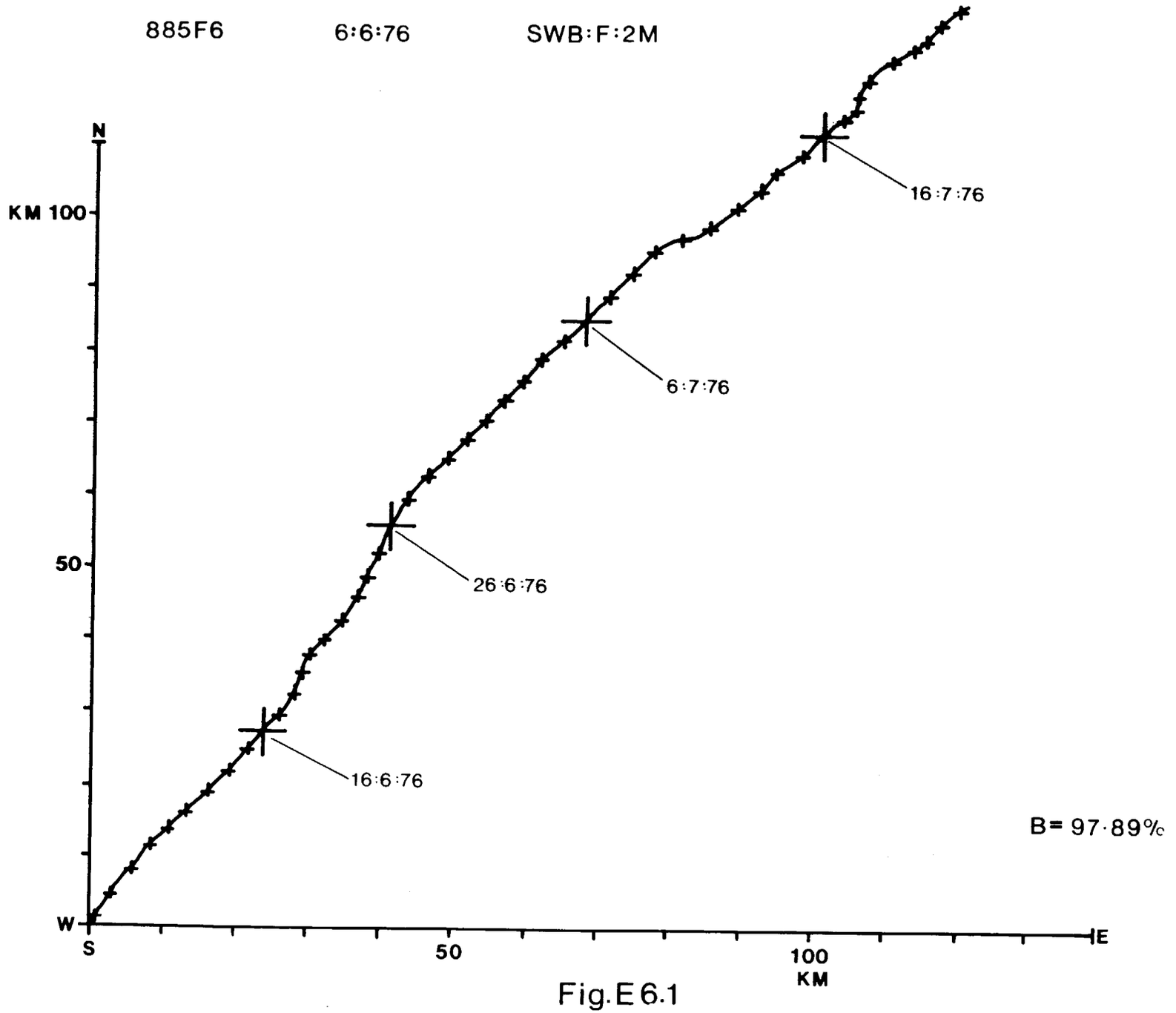
885F6
6:6:76
SWB:F:2M
N
KM 100
50
W
S
50
100
KM
E
16:6:76
26:6:76
6:7:76
16:7:76
B= 97·89%

Fig.E 6.1

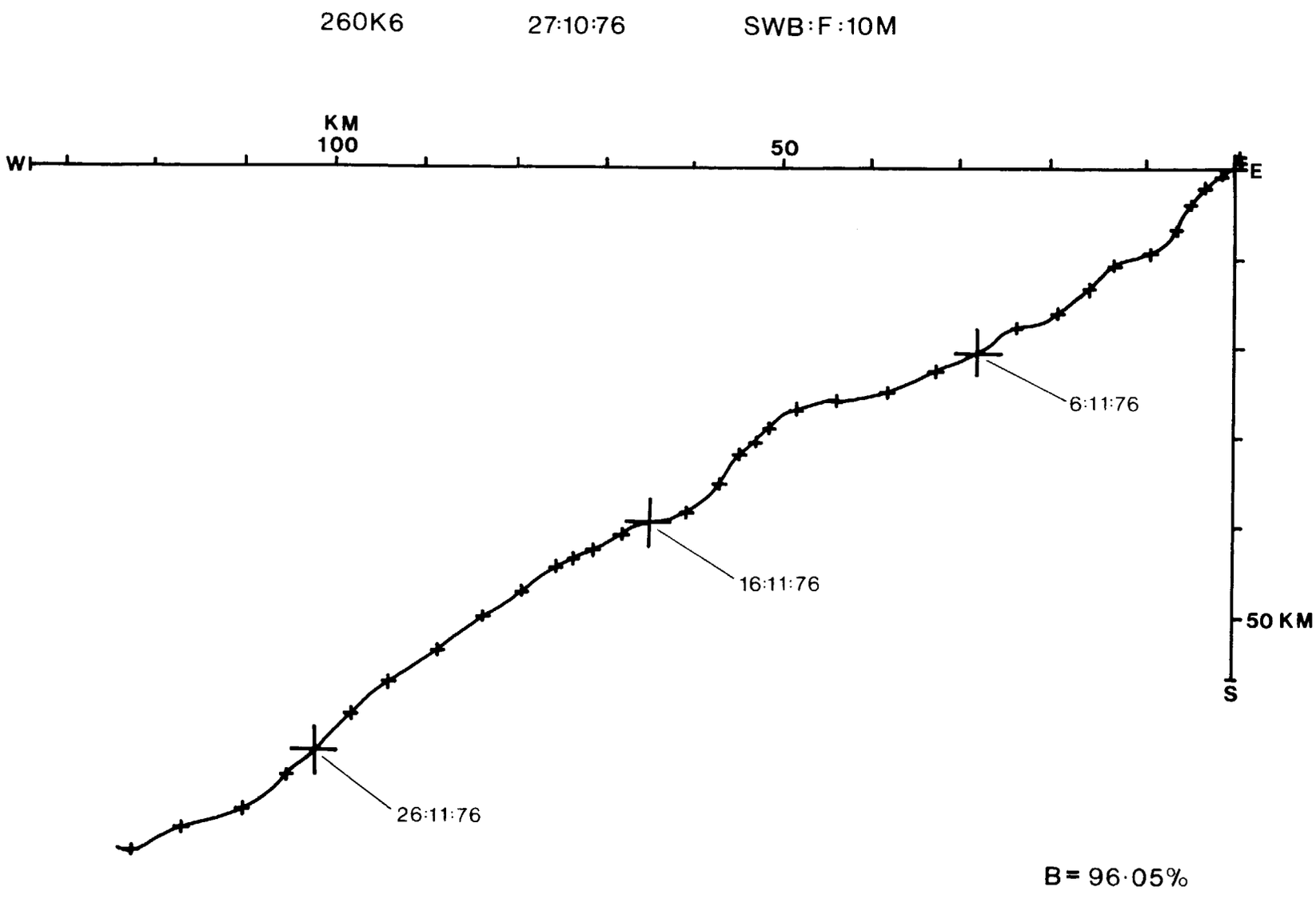
260K6
27:10:76
SWB:F:10M
KM
100
50
W
E
6:11:76
16:11:76
26:11:76
50 KM
S
B= 96·05%

Fig.E6.2

560L6 8:11:76 SWB:F:2M

B= 97·38%

Fig.E6.3

573K5 16:10:75 SWB:G:1M

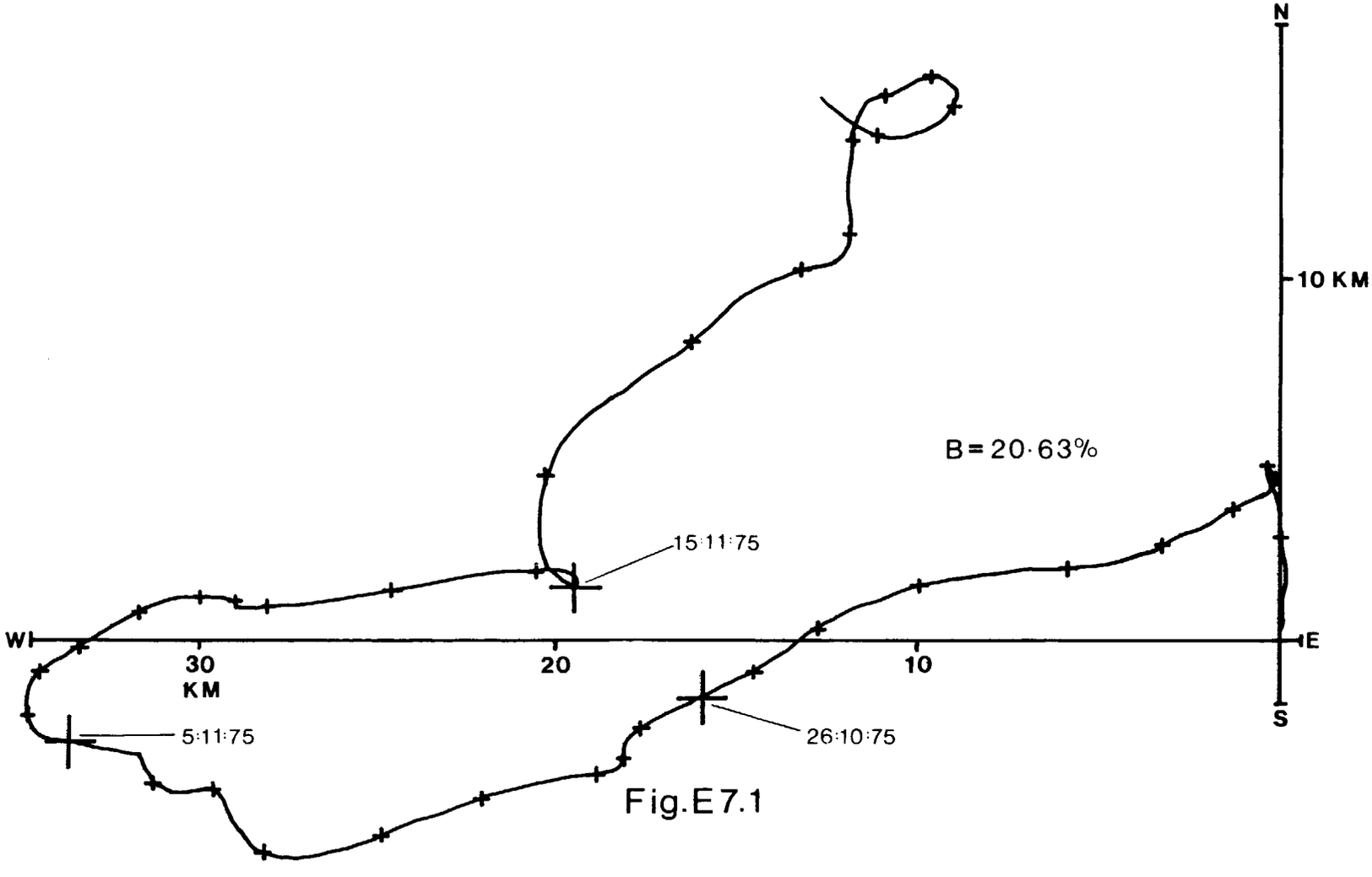

Fig.E7.1

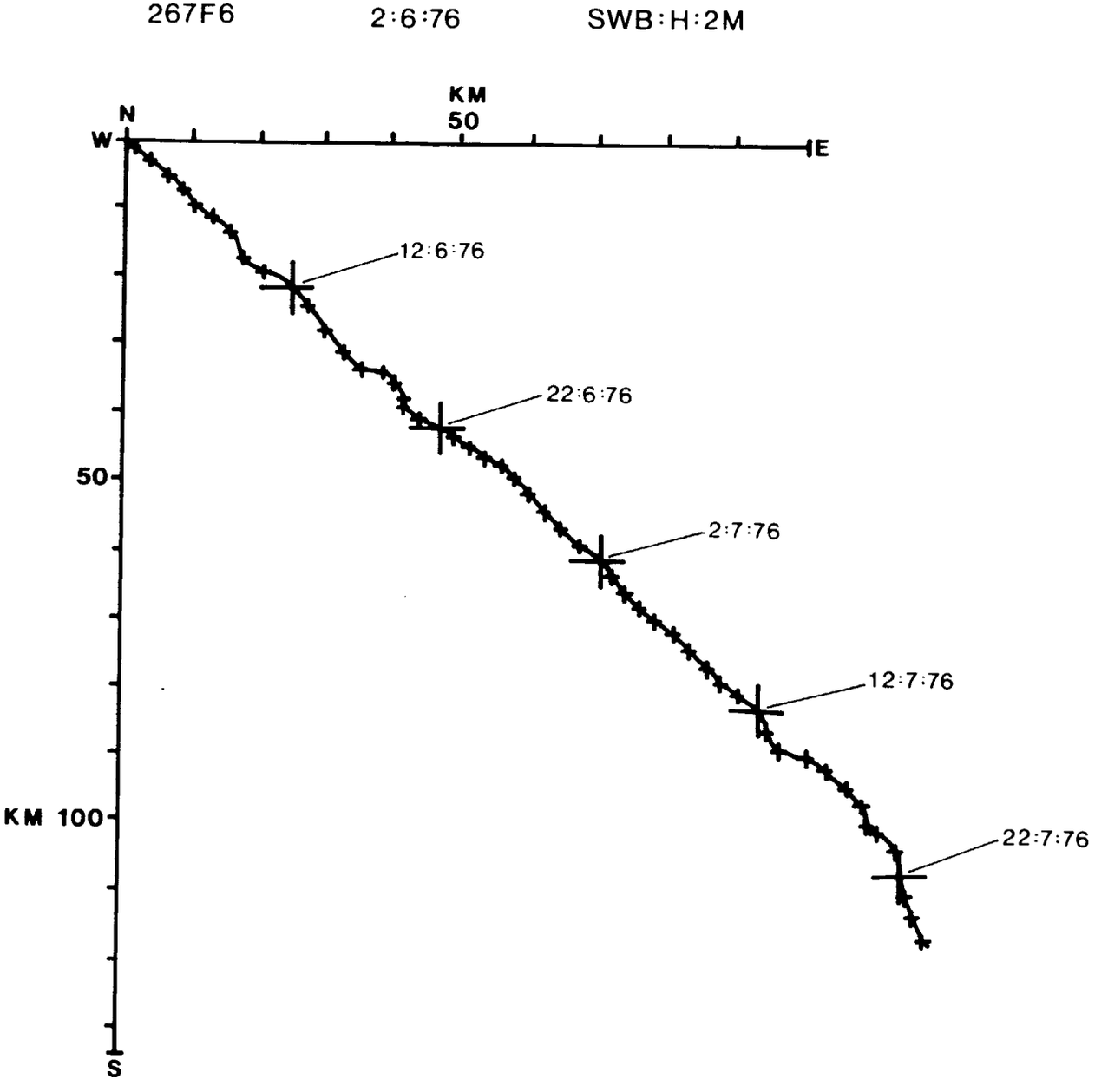

B= 93·90%

Fig.E8.1

534K6 29:10:76 SWB:H:2M

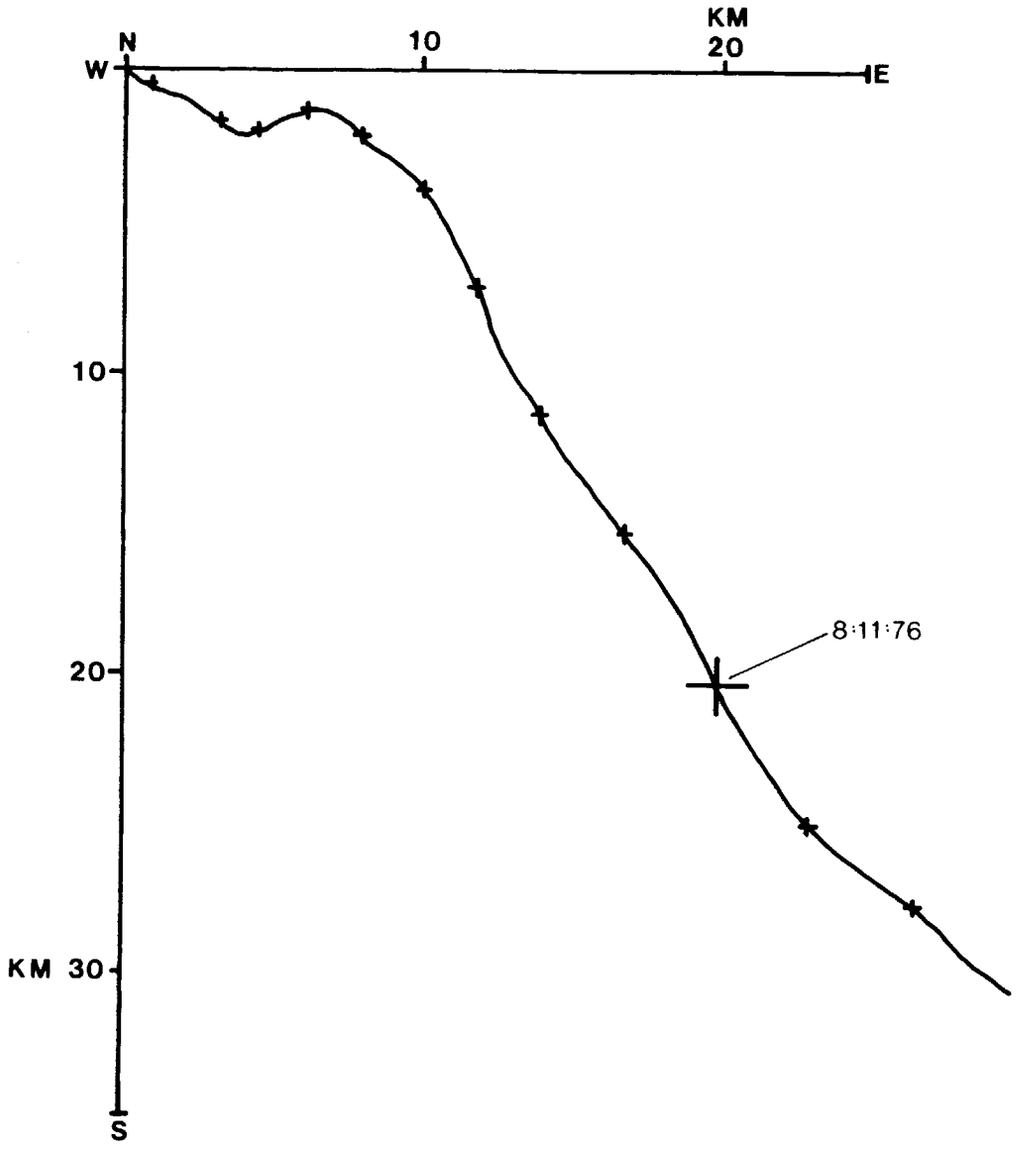

B = 92·20%

Fig. E8.2

534F6 7:6:76 SWB:1:2M

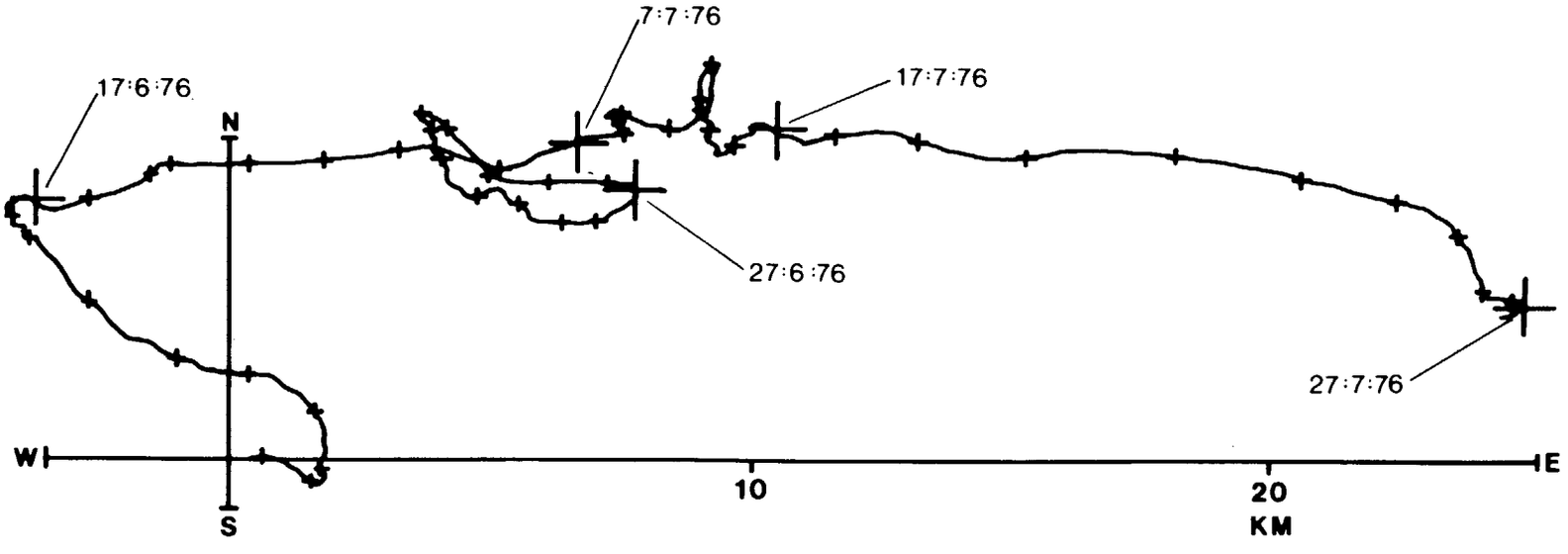

B= 41·76%

Fig.E9.1

532F6 11:6:76 SWB:J:2M

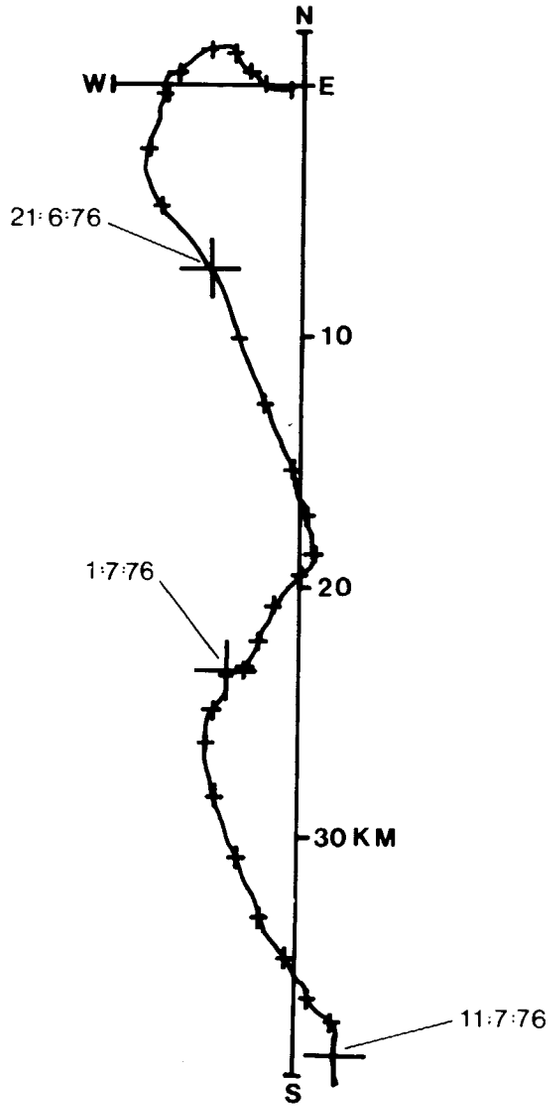

B= 77·30%

Fig. E 10.1

669C7 29:3:77 SWB:K:2M

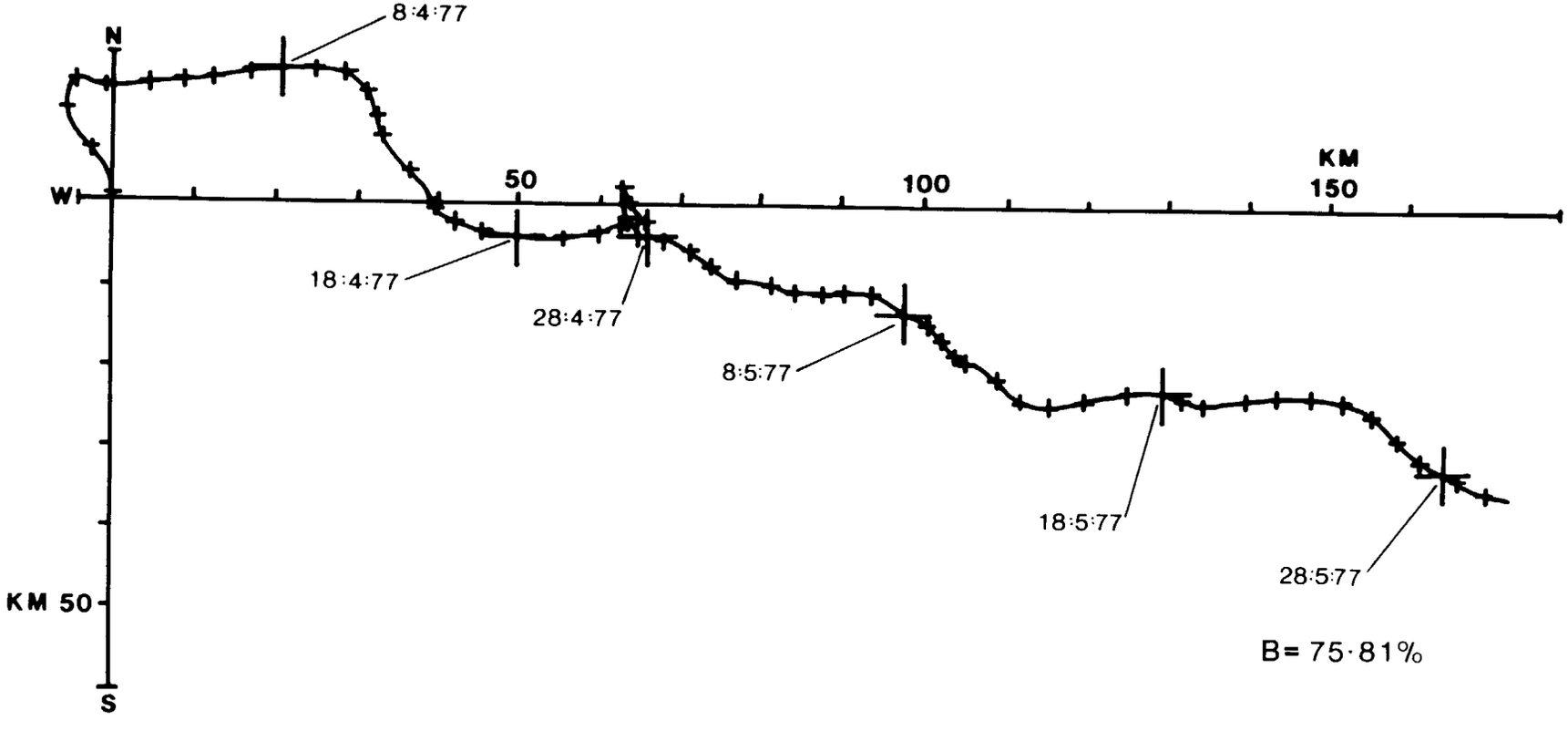

Fig. E 11.1

APPENDIX F

THE CALCULATION OF DENSITY CURRENTS

Consider the steady state motion of a fluid particle adjacent to an infinitely long straight coastline and in the vicinity of one or more river discharges, then the depth integrated equation of continuity and motion are given (See Heaps, 1972) by

$$\int_{-\zeta}^{h} u \, dz = -q \,, \tag{F1}$$

$$N_z \frac{\partial^2 v}{\partial z^2} = -fv + g(z+\zeta)\frac{1}{\rho}\frac{\partial \rho}{\partial x} + g\frac{\partial \zeta}{\partial x} \,, \tag{F2}$$

$$N_z \frac{\partial^2 v}{\partial z^2} = -fu \,, \tag{F3}$$

where u and v are now density currents flowing in a left handed system of cartesian co-ordinates with z positive downwards (see Figures 25 and 26). N_z is a depth mean eddy viscosity, f the Coriolis parameter, g the acceleration due to gravity, ρ the fluid density and ζ the displacement of the sea surface from its undisturbed level. q is a constant which denotes the rate of seaward discharge of water per unit length of coastline, representing the fresh water flows from the rivers.

Introducing the complex variable

$$w_0 = u + iv \tag{F4}$$

and combining (F2) and (F3) gives

$$\frac{\partial^2 w_0}{\partial z^2} = \alpha_D^2 w_0 + \frac{g}{N_z}\left\{(z+\zeta)\frac{1}{\rho}\frac{\partial \rho}{\partial x} + \frac{\partial \zeta}{\partial x}\right\} \,, \tag{F5}$$

where $$\alpha_D = (1+i)\pi/D \,, \tag{F6}$$

and $$D = \pi(2N_z/f)^{1/2} \tag{F7}$$

the latter being the depth of frictional influence which here has a different physical meaning to that described in Appendix A.

Assuming zero tangential stress at the surface and a linear bottom friction law gives a general solution to (F5) of the form

$$w_D = Ae^{\alpha_2(z+\zeta)} + Be^{-\alpha_2(z+\zeta)} + \frac{ig}{f}\left\{(z+\zeta)\frac{1}{\rho}\frac{\partial \rho}{\partial x} + \frac{\partial \zeta}{\partial x}\right\}, \qquad \text{(F8)}$$

where A and B denote arbitrary constants. A and B may be determined (see Heaps, 1972) from the boundary conditions and $\partial\zeta/\partial x$ eliminated from the solutions for u and v in terms of discharge parameter q. Thus from (F8)

$$u = \frac{gH}{f}(XQ - YP)\frac{1}{\rho}\frac{\partial \rho}{\partial x} + \frac{fq}{c}(TP - LQ)/S \qquad \text{(F9)}$$

and

$$v = \frac{gH}{f}(XP + YQ + \Lambda + \eta)\frac{1}{\rho}\frac{\partial \rho}{\partial x} + \frac{fq}{c}(1 - LP - TQ)/S, \qquad \text{(F10)}$$

where c is a linear friction coefficient. The terms in (F9) and (F10) are defined as follows:

$$\begin{aligned}
&Z = z + \zeta, \quad H = h + \zeta, \quad \eta = Z/H \\
&a_0 = \pi H/D, \quad a_1 = a_0(1-\eta), \quad a_2 = a_0\eta, \quad \Lambda = CH/N_z \\
&G = a_0(\sinh a_0 \cos a_0 - \cosh a_0 \sin a_0) + \Lambda(\cosh a_0 \cos a_0) \\
&E = a_0(\sinh a_0 \cos a_0 + \cosh a_0 \sin a_0) + \Lambda(\sinh a_0 \sin a_0) \\
&L = \Lambda \cosh a_2 \cos a_2, \quad T = \Lambda \sinh a_2 \sin a_2 \\
&P = G/(G^2+E^2), \quad Q = E/(G^2+E^2) \\
&R = P \cosh a_0 \cos a_0 + Q \sinh a_0 \sin a_0, \quad S = 1 - R\Lambda \\
&\Lambda = (R - P - S)/S, \quad \lambda_0 = 1 + \Lambda + \Lambda\Lambda \\
&X = \cosh a_1 \cos a_1 + (\Lambda/2a_0)(\sinh a_1 \cos a_1 + \cosh a_1 \sin a_1) \\
&\qquad - \lambda_0(\cosh a_2 \cos a_2) \\
&Y = \sinh a_1 \sin a_1 + (\Lambda/2a_0)(\cosh a_1 \sin a_1 - \sinh a_1 \cos a_1) \\
&\qquad - \lambda_0(\sinh a_2 \sin a_2).
\end{aligned} \qquad \text{(F11)}$$

Given an appropriate parameterisation of the eddy viscosity the above sequence of equations may be used to evaluate the density current components u and v at different depths (z) provided that the terms $\frac{1}{\rho}\frac{\partial \rho}{\partial x}$ and $\frac{fq}{C}$ are known. The first term $1/\rho \cdot (d\rho/dx)$ may be evaluated from the isopycnal spacing if this is known and the second term fq/C from river discharge data. Taking

$$\begin{aligned}
f &= 1.1410 \times 10^{-4}\ \text{s}^{-1}, \\
C &= .2\ \text{cm s}^{-1}, \\
\rho &= 1.025\ \text{gm cm}^{-3}
\end{aligned}$$

and the salinity data shown in Figure 24 and isopycnal spacing in Figure 25, gives $1/\rho \cdot (d\rho/dx) \simeq 1.1 \times 10^{-9}\ \text{cm}^{-1}$.

Taking a river discharge of 30 $m^3 s^{-1}$ (Stoner, 1977) over a representative length of coastline of 20 km in the head of the Bay, gives $q \simeq 1.5\ m^3 s^{-1}/km$ and thus $fq/C \simeq 8.5 \times 10^{-3}\ cm\ s^{-1}$. Similarly to Heaps (197?), therefore, we find that the direct effect of the river discharges is small.